THE USE OF THE SCANNING ELECTRON MICROSCOPE IN THE ANALYSIS OF SEMICONDUCTOR DEVICES

by

Robert Philippe Beaulieu

(January, 1971)

Submitted to the Department of Electrical Engineering in partial fulfilment of the requirements for the degree of Master of Science.

Department of Electrical Engineering
Faculty of Pure and Applied Science

University of Ottawa

Ottawa, Canada

1971

© Robert Philippe Beaulieu 1971

ABSTRACT

In addition to the study of surface topography, the Scanning Electron Microscope is proving to be a powerful tool for measurement of the microproperties of semiconductor devices and materials. This thesis is primarily concerned with the information which can be obtained from the correlation of results of the microscope used in several modes. Particular emphasis is given to the conductive mode of operation.

An analysis based on the photovoltage generation, which applies for low generation rates, shows that the signal is proportional to the derivative of the resistivity variation in the sample. An applied electric field results in a decreased amplitude and a shift in the phase of the signal relative to the resistivity variation.

Experimental results do not agree well with the analysis and three possibilities exist. Relevant bulk properties may have been overlooked, surface properties may be responsible for the observed results, or because of the high resolution of electron beam measurements, the theory based on bulk phenomena may not be valid. More work is required to determine which of the above three possibilities apply.

ACKNOWLEDGEMENTS

I wish to express my appreciation to Professor P. M. Thompson, University of Ottawa, for his guidance in this work. His enthusiasm and discussions on many aspects of the research contributed significantly towards the completion of this work.

Thanks are also due to Dr. P. R. Thornton, formerly of the Communications Research Centre, and Dr. C. D. Cox, C.R.C., who suggested the topic. I am particularly indebted to Dr. D. V. Sulway, C.R.C., for the many worthwhile discussions throughout the duration of the experimental work.

I should also like to thank the Royal Radar Establishment and Fairchild Semiconductor for the experimental devices from which the results were obtained.

The encouragement and assistance provided by my colleagues at the Communications Research Centre and at the University of Ottawa are gratefully acknowledged.

The work was supported jointly by the Defence Research Board, the National Research Council, and the Northern Electric Company. The experimental work was performed at the Communications Research Centre.

LIST OF SYMBOLS

A	Area irradiated by the electron beam
b	μ_n/μ_p, the ratio of electron to hole mobility
D_n, D_p	Electron, hole diffusion constant
E	Electric field intensity
E'	Electric field due to a variation in impurity concentration.
e	Electronic charge, 1.6×10^{-19} Coul.
E_{F_n}, E_{F_p}	Quasi fermi levels for electrons and holes
E_i	Ionization energy for the creation of electron-hole pairs
E_o	Electron beam energy
Δf	System bandwidth
g	Generation rate of electron-hole pairs
ΔI, ΔV	Beam-induced current and voltage respectively
I_p	Primary electron beam current
I_s	Secondary electron current
I_{rp}	Reflected primary electron current
k	Boltzmann's constant, 8.63×10^{-5} eV/°K
L	The irradiated length along the specimen
L'	The diffusion length of generated carriers in the semiconductor
L''	The diffusion length in the metal contacts
ℓ	The specimen length
ℓ_d	The diffusion length of the minority carriers
ℓ_e	The drift length of the minority carriers

N	Concentration of impurities
N_c, N_v	Effective density of states in the conduction and valence band
Δn	Generated carrier density
n_i	Intrinsic carrier density
n_o	Equilibrium electron density
Δn_o	Maximum value of generated carrier density
p_o	Equilibrium hole density
$Q(I)$	Distribution of minority carriers
R	Range of penetration of electrons in the irradiated specimen
ΔR	Beam-induced resistance change
R_s	Equilibrium specimen resistance
T	Absolute temperature
V_c	Chemical emf
V_d	Dember emf
V_{eff}	Effective beam accelerating voltage
V_o	Accelerating voltage
V_{ph}	Photovoltage
V_s	Surface potential
x_o	Coordinate defining the position of the electron beam
λ	The period of resistivity variation
μ_n, μ_p	Mobility of electrons and holes
ξ_n, ξ_p	Chemical potential of electrons and hole ensembles
ξ_{n_o}, ξ_{p_o}	Equilibrium chemical potential of electron and hole ensembles

ρ_1	The average value of specimen resistivity
$\Delta\rho$	The amplitude of the resistivity variation
ρ_o	Equilibrium specimen resistivity
σ_y	Secondary electron yield
σ	Conductivity
$\Delta\sigma$	Beam-induced change in conductivity
σ_o	Equilibrium conductivity
τ_c	Chopping period
τ	Excess carrier lifetime
τ_s	Signal period

CONTENTS

I ABSTRACT

II ACKNOWLEDGMENTS

III LIST OF SYMBOLS

		PAGE
INTRODUCTION	--	1
CHAPTER I:	THE SCANNING ELECTRON MICROSCOPE -----	5
1.1	The Instrument ----------------------	5
1.1.1	The Emissive Mode -------------------	7
1.1.2	The Conductive Mode -----------------	8
1.1.3	The Luminescent Mode ----------------	10
1.2	Display Techniques ------------------	10
1.2.1	The Contoured Display ---------------	11
1.2.2	The Deflection Modulation Display ----	12
1.2.3	Modulated Beam and Modulated Bias Operation ------------------------	12
1.3	Applications of the Scanning Electron Microscope -----------------------	13
1.3.1	Biological Sciences -----------------	14
1.3.2	Analysis of Materials and Devices ----	14
1.3.3	Pattern Generation ------------------	16
1.3.4	Registration ------------------------	17

		PAGE
1.3.5	Machining	17
1.3.6	Failure Analysis	17
CHAPTER II:	THEORY OF THE BEAM INDUCED VOLTAGE	19
2.1	The Beam-Induced Current	19
2.2	The Beam-Induced Voltage	20
2.2.1	The Continuity Equation	23
2.2.2	Solution for an Infinite Bar	25
2.2.3	Solution for a Finite Bar with $E = 0$	28
2.2.4	Solution for a Finite Bar with $E \neq 0$	31
2.2.5	Conductivity Variations	34
2.2.6	Photovoltage Calculations	35
2.2.7	Conditions for Negligible Internal Field	38
2.3	Condition for Equivalence of Current and Voltage Information	40
2.4	Sources of Error	44
2.4.1	Effect of Electron Emission on the Photovoltage	44
2.4.2	Effect of Contacts on the Photovoltage	47

		PAGE
2.5	The Case of Small Impurity Concentrations --------------------	52
CHAPTER III:	MEASUREMENT TECHNIQUES AND RESULTS ---	54
3.1	Measurement Techniques ---------------	54
3.1.1	Emissive Mode Measurements -----------	54
3.1.2	Luminescent Mode Measurements --------	56
3.1.3	Conductive Mode Measurements ---------	56
3.1.4	Contoured Conductive Measurements ----	58
3.1.5	Phase Sensitive Detection ------------	60
3.1.5.1	Capacitively Coupled Measurements ----	64
3.1.5.2	Line Scan Measurements ---------------	66
3.1.6	Calibration Techniques ---------------	68
3.2	Experimental Results -----------------	69
3.2.1	Devices Investigated -----------------	69
3.2.2	Measurement Results ------------------	70
3.2.2.1	The Use of Multiple Modes to Examine Semiconductor Devices --------------	72
3.2.2.2	The R-450 Devices -------------------	76
3.2.2.3	The F-216 Devices -------------------	80
3.3	Results of Computer Analysis ---------	85

PAGE

CONCLUSION -- 89

APPENDIX 1 Photovoltage Generation in Semiconductors --------------------- 93

APPENDIX 2 The Computer Program ----------------- 101

REFERENCES -- 107

INTRODUCTION

The present trend in microelectronics is the size reduction of components to allow large packing densities. The benefits are reduced costs and increased reliability. The reduction in size results in problems of material evaluation before device manufacture and device assessment after manufacture. The need to examine microscopic phenomena over the substrate suggests the use of a Scanning Electron Microscope.

Proposals have been presented to incorporate the Scanning Microscope (SEM) in an integrated manufacturing processor. Two such proposals will be outlined below, the first is by K.R. Shoulders[1], and the second is by G. Glinski[2].

In Shoulders' system an electron-beam and an ion-beam machine are enclosed in a three chamber vacuum system where the following procedures can be carried out.

1. Material deposition by evaporation from an electron-beam heated source.
2. Resist deposition followed by exposure with an electron beam.
3. Etching the unprotected layer with a molecular beam which forms a volatile compound of the material being machined.
4. Examination with a Scanning Electron Microscope.

The deposition of the various layers is carried out in an ultra-high vacuum chamber. The electron beam machine is located outside of this chamber and the substrate must be moved to the electron-beam machine for

exposure of the resist and for examination. This system involves a registration problem and a mechanical problem of transferring the substrate from one chamber to the other.

In Glinski's system called the Multipurpose Microelectronic Processor an electron-beam machine and an ion-beam machine are incorporated into a single high vacuum chamber. The substrate is fixed throughout the various operations required to produce a microcircuit. The electron source is mounted along the specimen axis and the ion source is mounted normal to this axis. The ion beam is directed to the surface of the specimen by a magnetic field[3,4]. The main advantage of this system is the reduction of the registration problem.

In order to implement the MMP concept, many areas must be investigated. Some work has already begun, but some areas are still open for future work. Some of the aspects of the MMP project that need to be considered are listed below.

1. The bending of ion-beams including pulsed ion-beams.
2. The development of ion sources.
3. The study of high resolution ion doping of semiconductors.
4. Methods of identifying compositional variations.
5. The use of the ion-beam for machining.
6. The use of the electron beam for qualitative and quantitative study of materials and devices.
7. Chemical analysis by the use of Auger electron and X-ray spectroscopy.

Studies have begun on a number of these topics. Samaroo[3,4] has designed magnetic circuits to bend an ion-beam. Development work on high

current density ion sources was begun by Jirafe[5], and continued by Tsai[6]. A study of solid state detectors to be used in pairs for the detection of compositional variation has been conducted by Ramana[7]. Hayes[8] has begun a study of high resolution ion beam inplantation, and Caloia[9] has studied the limiting packing density of active devices from the point of view of maximum allowable heat dissipation.

The Scanning Electron Microscope can be used as a tool for analysing semiconductor devices in different modes of operation depending which signal is detected. These modes are:

1. Emissive Mode

    Primary reflected electron detection

    Secondary electron detection

2. Conductive Mode

    Beam induced conductivity

    Specimen neutralizing current

3. Cathodoluminescent Mode

In the emissive mode of operation, either primary or secondary electrons are detected and amplified. In the conductive mode of operation, the variation of current flowing in an external circuit is detected and amplified. The specimen current is the charging current which flows into the specimen due to the difference between the incident beam current and the back-scattered current. In the cathodoluminescent mode of operation, light emitted from the specimen during electron bombardment is detected and amplified. In each case, these amplified signals intensity modulate the display.

All the modes of operation can be used to obtain the most information possible in the analysis of material or device quality. The standard emissive mode of operation gives information about surfaces only. This may be important in the evaluation of device quality by showing faults in the metallization, bonds and oxide layers. The conductive mode gives the resistivity variation and hence, the impurity concentration variations in the specimen. The cathodoluminescent mode of operation gives an indication of the concentration of bulk impurities and of surface contamination. These last two modes of operation give information which is not evident in the emissive micrographs, which show only surface information.

In the following chapters, the application of the Scanning Microscope to material physics and device technology is discussed. The emphasis is placed on the conductive mode of operation considering in detail, the magnitude of the detected signals.

In the first chapter, a discussion of the Scanning Microscope, its modes of operation and its fields of application is presented. In the second chapter, a theoretical discussion of the conductive signal is presented. The discussion begins from a consideration of the continuity equation and applies the theory of photovoltage generation due to irradiation of the semiconductor specimen. Chapter III is concerned with measurement techniques and results obtained from a series of Gallium Arsenide devices. A discussion of the results obtained is included. The results of the computer analysis are compared with the experimental results, and it is concluded that bulk theory cannot fully explain the observations.

CHAPTER I

THE SCANNING ELECTRON MICROSCOPE

As mentioned in the introduction, the Scanning Electron Microscope can be used to advantage in device technology. It is a high resolution instrument having applications in the manufacturing and analysis of microcircuits. The latter use is the one of interest and will be discussed in the following chapters. The Scanning Microscope will first be described, then the modes of operation will be considered along with some particular display techniques. The discussion in this chapter will be concluded with a review of the applications of the microscope.

1.1 The Instrument

The main functional blocks of the Scanning Electron Microscope are given in Figure 1. The physical basis of operation is the interaction of an electron beam with a solid specimen. A primary beam of electrons from a cathode is directed through a system of condenser lenses to the sample to be studied. The last lens supports the scanning coils or plates which deflect the beam in a raster over the specimen. In its usual form, the signal to be displayed is constructed from the emitted secondary electrons. These are collected and converted to an electrical signal with semiconductor detectors or a scintillator-photomultiplier combination. The magnification is accomplished by varying the deflection ratio of the cathode ray tube and the specimen. This is accomplished by an attenuator network between the scan generator and the deflection coils or plates.

The instrument in the form described, can be used in the life sciences for direct observation of specimens. For application in the physical

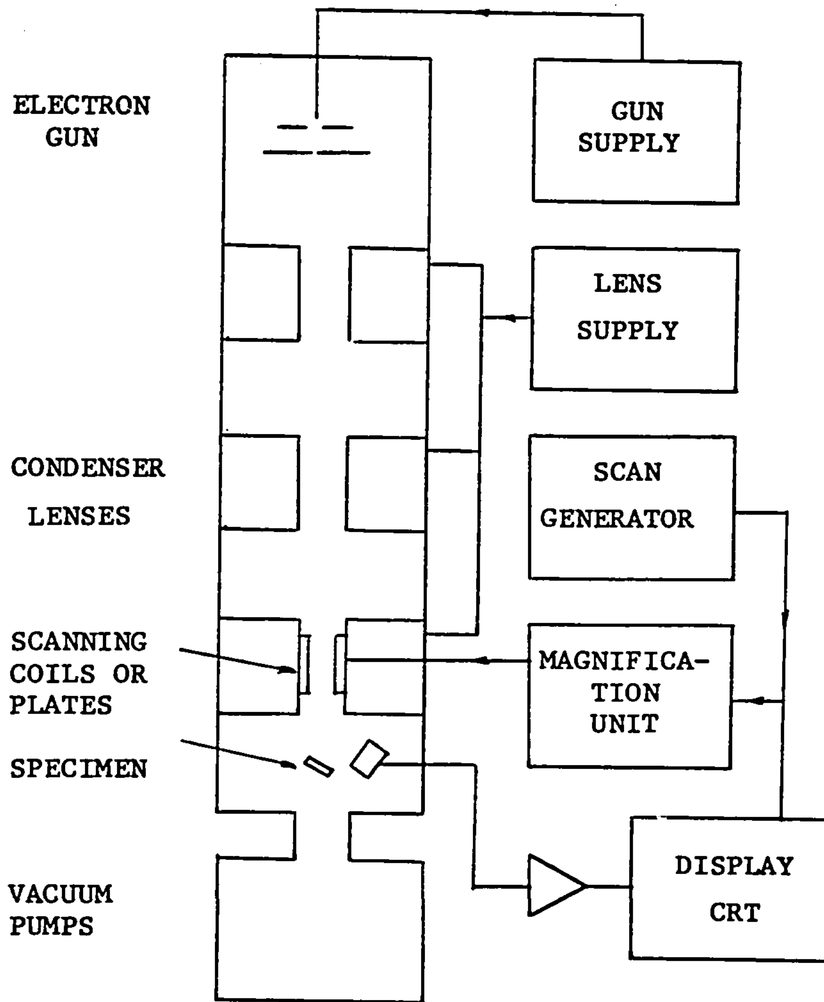

Fig. (1). Functional Block Diagram of a Scanning Electron Microscope

sciences, some modifications are possible. These modifications involve the use of different detection systems for the production of the electrical signal. The modes discussed are:

1. The Emissive Mode
2. The Conductive Mode
3. The Luminescent Mode

The discussion to follow will apply to the particular system used in this work.

1.1.1 The Emissive Mode

In the emissive mode, the primary reflected electrons and the secondary electrons can be collected and the variation of the electron emission with position is converted to a contrast variation on the CRT display. The energy difference between primary reflected and secondary electrons is the basis of selection of the reflected electrons from the total emission. In the instrument used in this work, a scintillator response to high energy electrons is converted to an electric signal by a photomultiplier tube. The secondary electron energy is far lower than the threshold energy for activation of the scintillator. This technique then reproduces only information carried by primary reflected electrons. To select secondary electrons the collector must be placed out of the path of reflected primary electrons. Inside the collector, which takes the form of a Faraday cup, a scintillator is placed at a high potential to give the captured secondary electrons sufficient energy to produce scintillation. The Faraday cup is held at a small positive potential which can easily bend the trajectory of the low energy secondary electrons[10] but not that of the high energy reflected electrons.

The total back-scattering coefficient is defined as the ratio of all emitted and reflected electrons to the number of primary electrons. This coefficient lies between 1 and 1.5 for metals, the maximum occurs at values of primary energy in the range of 300 to 800 eV. For insulators these quantities are larger[11]. Secondary emission does not vary substantially for different materials and cannot be used for measuring compositional variation.. The back-scattering coefficient which is a measure of the reflection efficiency of electrons, depends on the atomic number of the specimen being irradiated. For this reason, the reflected primary signal has been used to detect compositional variations where there is a large difference in atomic number[11,12].

A problem in using the above method, is that the angle of incidence of the beam is an important factor affecting the contrast in the emissive mode[13].

Consider an electron beam which is not normal to the surface. If the surface is not smooth the surface vector varies from point to point. An increase of the angle between the direction of incidence of the electron beam and the surface vector results in an increase of secondary electron emission due to the higher number of scattered electrons reaching the surface of the specimen. The variation in secondary emission is directly related to the variation of the surface angle. In the absence of other mechanisms, the emission of secondary electrons yields information about surface topography.

1.1.2 The Conductive Mode

In the conductive mode of operation, the changes in beam induced conductivity are converted to a contrast variation on the CRT display. It

is convenient to treat the effect of the electron beam in terms of carrier generation. If a specimen is irradiated by an electron beam, electron-hole pairs are created which can drift through the specimen if there is an electric field. This field could be caused by an inhomogeneity such as a p-n junction or by an externally applied potential. The current which flows in the external circuit is called the beam induced current.

At high values of electric field, avalanche can occur. Usually avalanche begins in some localized area since the impurity concentration is not uniform over all of the device. These areas of high electric field have a large generation rate and will be clearly visible in the conductive micrographs[14].

The specimen current is an important effect which can be used to reveal information about the sample. This is a neutralizing current which flows into the specimen to compensate for the net emission of electrons. The specimen current can be written in terms of primary beam current, secondary emission current, and reflected primary current as follows:

$$I_p - (I_s + I_{rp})$$

This current depends on the variation of secondary emission and the reflection coefficient at the surface. This signal is small and is detectable only if the charge collection current is not present or very inefficient. This process is detectable only in specimens not containing p-n junctions.

The importance of the conductive mode of operation lies in its applicability to quantitative measurements. The method of signal retrieval must be modified from the conventional contrast variations on a CRT display in this case. Such modifications will be discussed in a further section.

1.1.3 The Luminescent Mode

Cathodoluminescence is the luminescent phenomenon which results from excitation of electrons in a material by electron-beam bombardment. The electrons and holes which have been excited to the conduction and valence band can recombine directly or via impurity levels in the forbidden band gap. For direct recombination emission of light is the important mechanism, but in the case of indirect transition, phonon emission predominates. The luminescent signal is strongly dependent on carrier lifetime, the probability of a radiative transition increases as the lifetime increases. The luminescent signal is therefore sensitive to the various effects affecting lifetime such as:

1. The presence of trapping centers in the bulk.
2. The presence of dislocations in the bulk.
3. The presence of surface states.

Cathodoluminescence has been studied in the Scanning Electron Microscope as an aid to assess semiconductor material quality. The luminescent information and surface evidence of dislocation structures can be related[15]. The presence of p-n junctions can be detected by a fall in luminescent signals at the junction[16].

This mode of operation, although potentially an important technique, has assumed a role of minor importance.

1.2 Display Techniques

The display described in preceding sections is an analogue technique. The output in the display is a continuous variation of brightness or amplitude. There are some improvements possible in cases where quantitative measurements are required. Two such improvements are:

1. The Contoured Display

2. The Deflection Modulation Display

In addition to these, the signal to noise ratio can be improved with electron beam modulation and signal detection with a phase sensitive detector network.

1.2.1 The Contoured Display

An analogue signal display has an amplitude limitation given by the saturation value of the device. This may be a saturation voltage in the case of an amplifier, or a saturation light intensity in the case of a CRT phosphor or a photographic emulsion. This imposes a limitation on the gain of the system and may render the amplification of some detail impractical. In such a case the contoured display technique is useful.

This technique presents the information in a series of closed contour curves. The signal is amplified and passed through a network digital multilevel which produces a stepwise approximation of the input signal. Adding this signal and the original signal in antiphase, gives a new signal which varies in amplitude by constant value equal to a double step. The step size is chosen to be less than half of the saturation value, and the gain can be made as large as required to reveal the detail sought. As the specimen is scanned in a raster, the positions of the minima and maxima change slightly in position in each successive scan line. In the final micrograph, all these maxima merge to form a contoured display. This technique is useful in the conductive mode of operation[17,18] and will be discussed further in Chapter III.

1.2.2 The Deflection Modulation Display

The second modified technique of signal presentation is the deflection modulation display. This display produces a curve whose amplitude variation with position indicates the signal variation along the scan line. If several line scans are included in one figure, a three dimensional plot results. The line scans can be calibrated and serve as the basis of many measurements. Some applications of this technique are the measurements of:

1. The depletion layer width
2. The lifetime and diffusion lengths[19]

The depletion layer width can also be measured from a beam induced conductivity micrograph[20]. The deflection modulation technique is more accurate but the beam induced current micrograph clearly shows its variation along the specimen.

1.2.3 Modulated Beam and Modulated Bias Operation

As mentioned above, the techniques of contoured display and deflection modulation display can benefit from reduced noise under beam modulation. In devices where bias is applied, the bias can be modulated and thereby obtain a modulated signal. Both techniques of modulation allow a phase sensitive detector to be used and results in an improved signal to noise ratio. The second technique can be used to operate a device under high power operation at a low duty cycle.

In the first case, modulation is applied in order to allow the use of a phase sensitive detector in recovering the signal. In such a system, the modulated signal input is multiplied by a square wave, whose amplitude varies between -1 and +1 and which is of the same frequency and phase as the modulating signal. The resultant waveform is passed through a low pass filter and the output is proportional to the signal amplitude. Noise discrimination is obtained if noise is not modulated with the signal. Of the noise that is multiplied in the modulation process, only that noise falling in the band width of the low pass filter appears at the output.

1.3 Applications of the Scanning Electron Microscope

The Scanning Electron Microscope has been demonstrated to be a versatile instrument with applications in the Biological and Physical Sciences. The instrument evolved to a modern design by 1955. At this time it was applied in the life sciences to observe specimens without having to prepare replicas. Similar uses exist in the textile and in the pulp and paper industries. The SEM is now used as a research tool in the physical sciences and a diagnostic tool in the technology of electronic device fabrication.

A brief outline of the major applications of the instrument will be given below. Review papers have been published on this topic (21,22,18).

The discussion of the applications will be presented under the headings of:

1. The Biological Sciences
2. The Analysis of Materials and Devices
3. Pattern Generation
4. Registration
5. Machining
6. Failure Analysis

1.3.1 Biological Sciences

The first studies conducted with the Scanning Electron Microscope gave topographical detail. This was adequate for biological studies. The transmission microscope requires very thin specimens, therefore replicas of thick specimen must be made. Specimens which are too thick for the transmission microscope and too small for replica techniques can best be studied in the SEM. Irregular surfaces cannot be examined with the reflection microscope because these require a low angle of incidence which results in high distortion and loss of surface detail. Depressions in the surface would be lost. The SEM, when used to detect secondary electrons only, can reveal detail from within the depressions[10]. The usefulness of the scanning microscope in the biological sciences has been established, but the applications of the instrument in the analysis of materials and devices shows its versatility.

1.3.2 Analysis of Materials and Devices

The Scanning Electron Microscope yields different information in each of its different modes of operation when applied to materials

and devices. The three basic modes of operation are listed below with the emissive mode subdivided into three categories.

1. The Emissive Mode
    (a) Primary reflected electrons
    (b) Secondary electron collection
    (c) Voltage contrast detection
2. The Conductive Mode
3. The Luminescent Mode

These modes can be applied to measurements of physical properties of materials and observations of surfaces. The first two categories (a) and (b), are applied to the study of spatial aspects of the sample, such as the surface texture and the geometry. The third category (c), reveals variations in surface potential. Voltage gradients along resistors in microcircuits[22] can be observed and the location of p-n junctions can be accurately determined[23]. The topography and voltage variations are evident even with much of the surface covered with passivating layers. The beam induced conductivity results in the surface of the insulator attaining the same potential as the semiconductor insulator interface[24].

The conductive mode can be employed to obtain a measure of the carrier diffusion length and to measure the thickness of the oxide and aluminum layers on integrated circuits[23]. A pulsed beam technique can be used to measure carrier lifetime. Complications arise because of excess charge introduced by the electron beam, and charging

effects on the passivating layer or a contamination layer. These problems must be taken into account when making lifetime measurements.

1.3.3 Pattern Generation

A promising application of the Scanning Electron Microscope is the exposure of a photoresist with an electron beam. This technique could increase resolution over the current masking and photographic techniques. It is possible to produce isolated lines with edge sharpness of 0.14μm[22], taking into account the minimum practical photoresist film thickness and the effect of exposure by backscattered electrons. Optical techniques can produce edges of 1.5μm sharpness. This implies an improvement of edge resolution by one order of magnitude. The importance of this improvement is well illustrated in the case of an insulated gate device[22]. The optical method has an edge definition of 1.5μm or an uncertainty of ±0.75μm. If another uncertainty of ±0.1μm due to lateral diffusion of the source and drain region is added, the channel will have an uncertainty of ±0.85μm on either edge. The channel length uncertainty is then ±1.7μm, and if a 10% variation is allowable, the total length must be 17μm. For the electron beam method the edge uncertainty is ±0.075μm. With the additional ±0.1μm lateral diffusion margin, the channel length uncertainty is 3.5μm. A five time reduction in device size appears feasible with this technique.

1.3.4 Registration

The problem of registration in device manufacture can be facilitated with the use of the SEM. The electron beam induced photovoltage at a p-n junction can be used as a bench mark during all stages of fabrication. In the example stated above, a fraction of the resist polymerizing electrons penetrate into the bulk and create electron-hole pairs. A photovoltage results as these diffuse across a p-n junction. This photoresponse can be used to locate the beam at the centre of the gate and the beam scan range limited to the required gate length using the central point as a reference. The disadvantage of this system is that leads are required to detect the photovoltage. Tarui et al.[25] have used a reflected primary electron signal to establish beam position. A reference mark must be made which will not be destroyed by evaporated thin films deposited over the surface.

1.3.5 Machining

The Scanning Electron Microscope can be used for micro-machining if it is modified to produce a high power density electron beam. El-Kareh[26] designed such a machine with a beam diameter of 0.001 inch, a beam current of 5ma at 100 kV to give a power density of 100 megawatts/ cm^2.

1.3.6 Failure Analysis

In the above discussion, some applications of the SEM in microcircuit inspection has been mentioned. This topic is usually termed,

failure analysis and has been discussed by Thornton et al.[18,27]. In failure analysis, the SEM must be equipped with facilities to heat or cool the specimen. The application of the heat sink arises when a device must be studied at rated output. A heated stage may be required to study anealing effects.

The next chapter will be devoted to a more complete description of the conductive mode of operation. Particular emphasis will be placed on the application of this mode to the measurement of resistivity variations and variations in impurity concentration of a semiconductor specimen.

CHAPTER II

THEORY OF THE BEAM INDUCED VOLTAGE

In Chapter I, a brief discussion of the Scanning Electron Microscope, its various modes of operation and its areas of application was presented. It was pointed out that the conductive mode of operation is important in obtaining quantitative information. The conductive mode implies a beam-induced current. However, a beam-induced voltage also exists which can be equally important. In this chapter a discussion of the beam induced voltage will be presented, and its applicability in the measurement of resistivity will be discussed.

2.1 The Beam-Induced Current

The conductive mode of operation is based on the change in conductance which results in a change in current. This change in current is called the beam-induced current and occurs when an electron beam scans the specimen. This current change can be obtained from Ohm's Law and is given by the following expression.

$$\Delta I = \frac{\Delta V}{R} - \frac{V}{R^2}\Delta R \qquad (1)$$

where:

ΔI, ΔV are the beam induced current and voltage

R is the equilibrium specimen resistance

ΔR is the change in R upon irradiation

V is the specimen bias voltage

From the above expression, it can be seen that the beam-induced voltage plays a role in the generation of the beam-induced current. In the case that the change in specimen resistance is small, compared to R, then the beam-induced current and voltage are directly proportional. In the sections that follow, the beam-induced voltage will be considered in detail. A criterion will be developed which will allow a determination of the magnitude of $\frac{\Delta R}{R^2}$ and hence the importance of the second term in equation 1.

2.2 The Beam-Induced Voltage

In the preceding section, the beam-induced current was found to consist of two terms. One term depends on the bias voltage and resistance variation upon irradiation with the electron beam. The other term is a voltage variation. This beam-induced voltage is the basis of the technique to be discussed below. The beam-induced voltage can be important in itself as a means of analysis whenever the ratio $\Delta R/R^2$ is small making the second term negligible.

If a light beam impinges on a semiconductor specimen, and a voltage appears across the contacts, this effect is known as the photovoltage generation[28,29]. A similar process occurs upon irradiation with an electron beam. The photovoltage is proportional to the gradient of specimen resistivity, and hence, the resistivity

variation or the variation in impurity concentration along the specimen can be found from the photovoltage.

The photovoltage in an inhomogeneous semiconductor can be written as the sum of two terms.

$$V_{ph} = V_c + V_d$$

where:

V_c is a chemical emf due to variations of the chemical potential of electron and hole ensembles along the sample.

V_d is a Dember voltage due to the differences in the mobility of electrons and holes.

It can be shown that for an n-type semiconductor, the above emf's can be written as follows (see Appendix I).

$$V_c = \frac{kT}{e} \int \Delta\sigma \frac{d\rho_o}{dx} dx \tag{2}$$

$$V_d = -\frac{kT}{e} \frac{\mu_n - \mu_p}{\mu_n + \mu_p} \int \Delta\sigma \frac{d\rho_o}{dx} dx \tag{3}$$

The photovoltage becomes

$$V_{ph} = \frac{kT}{e} \frac{2}{1 + b} \int \Delta\sigma \frac{d\rho_o(x)}{dx} dx \tag{4}$$

where:

$$b = \frac{\mu_n}{\mu_p}$$, the ratio of electron and hole mobilities.

$\Delta\sigma = (\mu_n + \mu_p)\Delta n$, Δn is the density of injected carriers, and is a function of beam position.

$\rho_o(x)$ = the equilibrium resistivity as a function of x.

These equations apply for the one dimensional case where all variables are functions of one coordinate only.

The above equation of photovoltage is applicable to the case of electron beam irradiation of the sample. The only requirement is for a radiation-induced change in conductivity. This conductivity modulation can be obtained by evaluating the density of generated carriers as the integral of the distribution of carriers obtained from a solution of the continuity equation, and multiplying by the sum of the electron and hole mobilities. The photovoltage can then be obtained from equation 4, if the resistivity function $\rho_o(x)$ is known. In this discussion, the photovoltage will be evaluated for arbitrary functions $\rho_o(x)$. A comparison of the functions of resistivity with position and of photovoltage with position will then be possible. This procedure will illustrate the usefulness of the technique of photovoltage detection in the analysis of resistivity variation.

2.2.1 The Continuity Equation

The calculation of photovoltage was discussed in the above section. It was shown that both the variation of equilibrium resistivity and the conductivity variation as a function of electron beam position are required in the calculation of photovoltage. The solution of the continuity equation will give the distribution of minority carriers Δp, from which the conductivity variation can be found.

The continuity equation is the relation giving the time rate of change of the quantity of charge per unit volume and is written as follows.

$$\frac{\partial}{\partial t} \Delta p = g - \frac{\Delta p}{\tau} + D \frac{d^2}{dx^2} \Delta p - \mu E \frac{d}{dx} \Delta p \qquad (5)$$

This equation holds for the ambipolar case where both electron and hole conduction takes place.

g = the generation rate of electron-hole pairs

τ = the excess carrier lifetime

$D = \dfrac{p + n}{n/D_p + p/D_n}$ is the ambipolar diffusivity

$\mu = \dfrac{n - p}{p/\mu_n + n/\mu_p}$ is the ambipolar mobility

E = the component of the electric field in the x direction

For an n-type semiconductor, the constants D and μ become D_p and μ_p, the diffusion constant for holes and the hole mobility. Equation 5 becomes:

$$\frac{\partial}{\partial t} \Delta p = g - \frac{\Delta p}{\tau} + D_p \frac{d^2}{dx^2} \Delta p - \mu_p E \frac{d}{dx} \Delta p \qquad (6)$$

The generation term can be written as follows:

$$g = \frac{I_p}{AeR} \frac{E_o}{E_i}$$

and gives the number of carriers generated per unit volume per second.

I_p is the beam current

A is the area of the specimen which is irradiated

E_o is the beam energy

E_i is the ionization energy for the specimen

R is the range of the electrons in the specimen

Equation 6 can be reduced further by making the following substitutions.

$\ell_d = \sqrt{D\tau}$ Diffusion length

$\ell_e = \tau\mu E$ Drift length

The continuity equation becomes:

$$\frac{d^2}{dx^2} \Delta p - \frac{\ell_e}{\ell_d^2} \frac{d}{dx} \Delta p - \frac{\Delta p}{\ell_d^2} = -g \frac{\tau}{\ell_d^2} \qquad (7)$$

This is the equation to be solved to obtain the distribution of minority carriers in the specimen. In the following section, the solution of this equation is obtained for different boundary conditions.

2.2.2 Solution for an Infinite Bar

The solution of the continuity equation will be obtained for a specimen having an externally applied electric field[30]. A specimen shaped as a narrow bar of infinite length is first considered in this section. An electron beam irradiates a small region of width L. The specimen can then be divided into three regions for analysis, as shown in Figure 2.

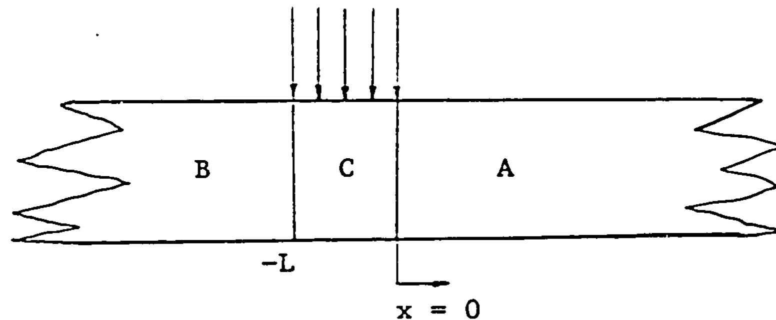

Fig. 2 Infinite Bar Specimen

The generation rate is non-zero in region C and zero in A and B.

$$g = \begin{cases} 0 \quad , & -L > x > 0 \\ \dfrac{I_p}{AeR} \dfrac{E_o}{E_i} \quad , & 0 \geq x \geq -L \end{cases}$$

In region A the equation to be solved is

$$(D^2 - \frac{\ell_e}{\ell_d{}^2} D - \frac{1}{\ell_d{}^2}) \Delta p = 0 \tag{8}$$

This is a linear homogeneous differential equation of order two with a solution of the form:

$$\Delta p_1 = c_1 e^{x/\ell_1} + c_2 e^{-x/\ell_2} \tag{9}$$

where:

$$\ell_1 = \frac{2\ell_d{}^2}{\ell_e + (\ell_e{}^2 + 4\ell_d{}^2)^{\frac{1}{2}}} \tag{10}$$

$$\ell_2 = \frac{2\ell_d{}^2}{-\ell_e + (\ell_e{}^2 + 4\ell_d{}^2)^{\frac{1}{2}}} \tag{11}$$

In region B the solution is of the same form:

$$\Delta p_2 = c_3 e^{x/\ell_1} + c_4 e^{-x/\ell_2} \tag{12}$$

In region C, the generation term must be taken into account; this results in a non-homogeneous equation. The particular solution is:

$$\Delta p_p = g\tau$$

Therefore, the solution in region C becomes:

$$\Delta p_3 = c_5 e^{x/\ell_1} + c_6 e^{-x/\ell_2} + g\tau \qquad (13)$$

The solutions are subject to the following boundary conditions.

$$\begin{aligned}
\Delta p_1(0) &= \Delta p_3(0) \\
\Delta p_2(-L) &= \Delta p_3(-L) \\
\frac{\partial}{\partial x}\Delta p_1(0) &= \frac{\partial}{\partial x}\Delta p_3(0) \\
\frac{\partial}{\partial x}\Delta p_2(-L) &= \frac{\partial}{\partial x}\Delta p_3(-L) \\
\Delta p_1(+\infty) &= \Delta p_2(-\infty) = 0
\end{aligned} \qquad (14)$$

Applying the boundary conditions 14 to the equations 9, 12, and 13, a system of six equations in c_1 to c_6 is obtained. The values of c_1 to c_6 are then found and substituted in equations 9, 12, and 13. The following equations are then obtained for the distribution of minority carriers. In region A, the solution is:

$$\Delta p_1 = g\tau \frac{\ell_2}{\ell_1 + \ell_2} [1 - e^{-L/\ell_2}] e^{-x/\ell_2} \qquad (15)$$

In the region B, the solution is:

$$\Delta p_2 = - g\tau \frac{\ell_1}{\ell_1 + \ell_2} [1 - e^{L/\ell_1}] e^{x/\ell_1} \qquad (16)$$

In the region C, the solution is:

$$\Delta p_3 = g\tau \frac{1}{\ell_1 + \ell_2} \{ \ell_2 [1 - e^{(-L + x)/\ell_2}] + \ell_1 (1 - e^{x/\ell_1}) \} \qquad (17)$$

This analysis applies for the case of an infinite specimen with an applied field. The approximation of an infinite bar is valid in cases where the diffusion and drift lengths are small with respect to the specimen length and the electron beam does not approach the contacts.

2.2.3 Solution for a Finite Bar with $E = 0$

In cases where the previous approximation based upon a solution for an infinite bar is not valid, a solution for a finite bar must be considered[31,32]. In this case, the electric field is assumed to be zero. The electron beam irradiates a region about a point x_o as shown in Figure 3.

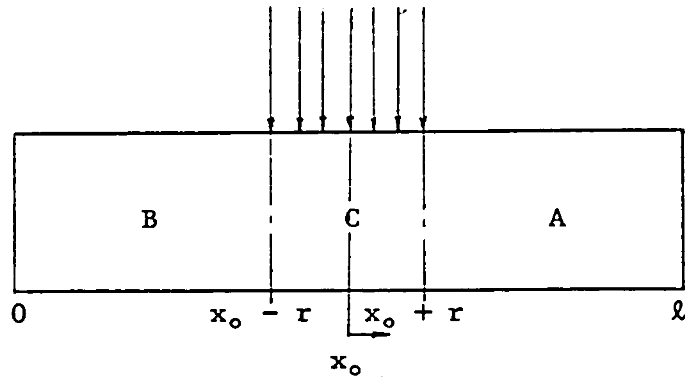

Fig. 3 Finite Bar Specimen

The specimen length is ℓ and the spot position is x_o. Since there is no applied electric field $\ell_e = 0$, and the continuity equation becomes:

$$(D^2 - \frac{1}{\ell_d{}^2}) \Delta p = - g \frac{T}{\ell_d{}^2} \tag{18}$$

where:

$$g = \begin{cases} 0 & , \quad -r > x > r \\ \frac{I_p}{AeR} \frac{E_o}{E_i} & , \quad -r \geq x \geq r \end{cases}$$

The solutions in this case are of the form:

$$\Delta p_1 = c_1 e^{x/\ell_d} + c_2 e^{-x/\ell_d}$$

$$\Delta p_2 = c_3 e^{x/\ell_d} + c_4 e^{-x/\ell_d} \tag{19}$$

$$\Delta p_3 = c_5 e^{x/\ell_d} + c_6 e^{-x/\ell_d} + g\tau_p$$

The boundary conditions are similar to the previous case and are given below.

$$x = 0 \qquad \Delta p_2(0) = 0$$

$$x = x_o - r \qquad \Delta p_2(x_o - r) = \Delta p_3(x_o - r)$$

$$\frac{\partial}{\partial x}\Delta p_2(x_o - r) = \frac{\partial}{\partial x}\Delta p_3(x_o + r) \tag{20}$$

$$x = x_o + r \qquad \Delta p_3(x_o + r) = \Delta p_1(x_o + r)$$

$$\frac{\partial}{\partial x}\Delta p_3(x_o + r) = \frac{\partial}{\partial x}\Delta p_1(x_o + r)$$

$$x = \ell \qquad \Delta p_1(\ell) = 0$$

Substituting the boundary conditions 20 into the solutions 19, the constants C_1 to C_6 are evaluated and the solutions become:

In region A

$$\Delta p_1 = g\tau_p \frac{2}{\text{Sin h }(\frac{\ell}{\ell_d})} \text{ Sin h }(\frac{r}{\ell_d}) \text{ Sin h }(\frac{\ell - x_o}{\ell_d}) \text{ Sin h }(\frac{x}{\ell_d}) \tag{21}$$

In region B

$$\Delta p_2 = g\tau_p \frac{2}{\mathrm{Sin\,h}\,(\frac{\ell}{\ell_d})} \mathrm{Sin\,h}\,(\frac{r}{\ell_d})\ \mathrm{Sin\,h}\,(\frac{x_o}{\ell_d})\ \mathrm{Sin\,h}\,(\frac{\ell - x}{\ell_d}) \tag{22}$$

In region C

$$\Delta p_3 = g\tau_p \{1 - \frac{1}{\mathrm{Sin\,h}\,(\frac{\ell}{\ell_d})} [\mathrm{Sin\,h}\,(\frac{x}{\ell_d})\ \mathrm{Cos\,h}\,(\frac{\ell - x_o - r}{\ell_d})$$

$$+ \mathrm{Sin\,h}\,(\frac{\ell - x}{\ell_d})\ \mathrm{Cos\,h}\,(\frac{x_o - r}{\ell_d})]\} \tag{23}$$

These solutions apply to a finite bar with no externally applied electric field.

2.2.4 Solution for a Finite Bar with $E \neq 0$

In the previous case, a finite bar was assumed, but with no applied electric field. In order to generalize the solution, an electric field will be considered in this section. The specimen is irradiated in a region of width L as shown in Figure 4.

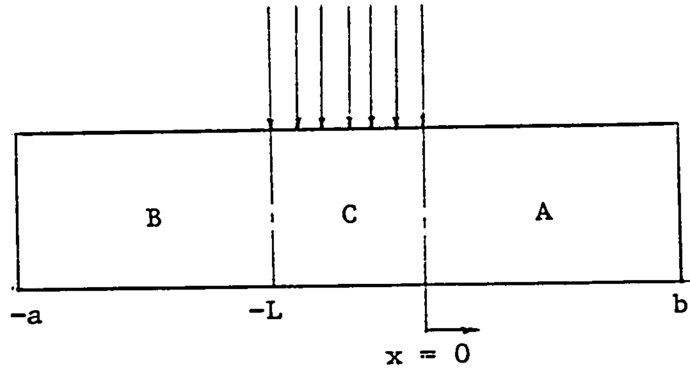

Fig. 4 Finite Bar Specimen

The concentration of minority carriers is zero at $x = -a$, and $x = b$ to satisfy the condition for ohmic contacts. The solutions are given by equations 9, 12, and 13, and must satisfy the following boundary conditions.

$$
\begin{aligned}
x = 0 \qquad & \Delta p_1(0) = \Delta p_3(0) \\
& \frac{\partial}{\partial x}\Delta p_1(0) = \frac{\partial}{\partial x}\Delta p_3(0) \\
x = -L \qquad & \Delta p_2(-L) = \Delta p_3(-L) \\
& \frac{\partial}{\partial x}\Delta p_2(-L) = \frac{\partial}{\partial x}\Delta p_3(-L) \\
-a,\ b \qquad & \Delta p_1(b) = \Delta p_2(-a) = 0
\end{aligned}
\tag{24}
$$

Substituting the boundary conditions 24 in the equations 9, 12, and 13, the following system of equations is found.

$$\begin{bmatrix} e^{b/\ell_1} & e^{-b/\ell_2} & 0 & 0 & 0 & 0 \\ 0 & 0 & e^{a/\ell_1} & e^{-a/\ell_2} & 0 & 0 \\ 1 & 1 & 0 & 0 & -1 & -1 \\ 0 & 0 & e^{-L/\ell_1} & e^{L/\ell_2} & -e^{-L/\ell_1} & -e^{L/\ell_2} \\ 1/\ell_1 & 1/\ell_2 & 0 & 0 & -1/\ell_1 & -1/\ell_2 \\ 0 & 0 & 1/\ell_1 e^{-L/\ell_1} & -1/\ell_2 e^{L/\ell_2} & -1/\ell_1 e^{-L/\ell_2} & 1/\ell_2 e^{L/\ell_2} \end{bmatrix} \begin{bmatrix} C_1 \\ C_2 \\ C_3 \\ C_4 \\ C_5 \\ C_6 \end{bmatrix} = \begin{bmatrix} 0 \\ 0 \\ g\tau \\ g\tau \\ 0 \\ 0 \end{bmatrix}$$

If numerical values are available for a, b, ℓ_1, ℓ_2, and $g\tau$ then the values of C_1 to C_6 can be found by numerical techniques. This can be conveniently solved by computer. The values of C_1 to C_6 are then substituted into the solutions (equations 9, 12, and 13), and the distribution of minority carriers can be plotted.

The following is a list of constants used in the solution. These are based on physical constants of n-type gallium arsenide as used for Gunn-Effect diodes. The gap length of the diode is 100μm.

$a = 5.0 \times 10^{-5}$ meters

$b = 5.0 \times 10^{-5}$ meters

$\mu = 0.045\ m^2/V.Sec$ [33]

$\tau = 2.0 \times 10^{-9}$ Sec [34,35]

$T = 300°K$

$k = 8.63 \times 10^{-5}\ eV/°K$

$$e = 1.6 \times 10^{-19} \text{ Coul}$$

$$E_o = 20 \times 10^{3} \text{ eV}$$

$$E_i = 4.6 \text{ eV}$$ [16]

$$I_p = 1.0 \times 10^{-10} \text{ amps}$$

$$L = 5.0 \times 10^{-7} \text{ meters}$$

$$\text{Area} = 1.963 \times 10^{-13} \text{ meters}$$

$$R = 1.0 \times 10^{-6} \text{ meters}$$

The solution of the minority carrier distribution is obtained for three values of electric field and plotted in Figure 40. The flow chart for the complete program is shown in Appendix II. The subroutine performs a solution of equation 25 to obtain the values of C_1 to C_6.

2.2.5 Conductivity Variations

As was stated in section 2.2.1, the conductivity variation as a function of beam position is required in the calculation of the photovoltage. In the preceding section, a solution of the continuity equation is developed. A minority carrier distribution is then obtained for a given electron beam position. The total change in carrier concentration for this beam position can be obtained by integrating the minority carrier distribution over the specimen length. The conductivity change is then given by:

$$\Delta\sigma = e(\mu_n + \mu_p) \int_{-a}^{b} \Delta p(x)dx \qquad (26)$$

where:

p(x) is the minority carried distribution for a given beam position.

Since the conductivity variation with beam position can be found, the photovoltage can be calculated if the equilibrium resistivity variation with position is known. The photovoltage will be evaluated in the next sections for arbitrary resistivity functions.

2.2.6 Photovoltage Calculations

It was shown in section 2.2 that a beam-induced voltage (photovoltage) is generated when a beam of electrons impinges on a semiconductor. This photovoltage is proportional to the conductivity variation and the derivative with respect to the coordinate x, of equilibrium resistivity of the specimen. The photovoltage is written as follows for an n-type semiconductor.

$$V = \frac{kT}{e} \frac{2}{1+b} \int_{-a}^{b} \Delta\sigma \frac{d\rho_o}{dx} dx \qquad (4)$$

Then substituting for $\Delta\sigma(x)$, and assuming the mobility to be independent of x, this expression becomes:

$$V = \frac{2kT}{e} \mu p \int_{-a}^{b} \Delta p \frac{d\rho_o}{dx} dx \qquad (27)$$

In order to obtain a value for this integral, the variation of equilibrium resistivity ρ_o with x is required. In practice, the function $\rho_o(x)$ must be found from the variation of the photovoltage. The above procedure, however, will allow a comparison of the photovoltage and resistivity functions. A sinusoidal and a step variation of equilibrium resistivity will be assumed.

In the case of sinusoidal resistivity variation, the following relation is assumed.

$$\rho_o = \rho_1 + \Delta\rho \sin (2\pi x/\lambda) \qquad (28)$$

where:

ρ_1 = the average value of resistivity

$\Delta\rho$ = the amplitude of the resistivity variation

λ = the period of the resistivity variation

From the equation 27 and 28 the following expression for photovoltage is obtained.

$$V = \frac{4\pi kT \Delta\rho \mu p}{\lambda} \int_{-a}^{b} \Delta p \cos 2\pi x/\lambda \, dx \qquad (29)$$

In the case of a step variation in resistivity, the following notation can be used.

$$\rho_o = \begin{cases} \rho_1 \; , & -a \le x < c \\ \rho_2 \; , & d < x \le b \\ \rho = \rho_1 + \dfrac{\rho_2 - \rho_1}{c - d} x \; , & c \le x \le d \end{cases} \tag{30}$$

From equations 27 and 30 the expression for photovoltage becomes:

$$V = \frac{2kT}{e} \mu p \int_{-a}^{b} \Delta p \quad K \, dx \tag{31}$$

where:

$$K = \begin{cases} \dfrac{\rho_2 - \rho_1}{c - d} & c \le x \le d \\ 0 \; , & -a \le x < c \\ & d < x \le b \end{cases} \tag{32}$$

These integrals can be evaluated by a numerical quadrature method. For the case of sinusoidal resistivity, a 1.0Ω - cm sample with a 10% resistivity variation is assumed. The amplitude of variation $\Delta\rho_o$ is then 10^{-3} Ω - m. The period of the resistivity variation is taken such that $\ell\lambda^{-1} = 5$. For the case of the step rise in resistivity, a linear rise of resistivity in a distance of 10^{-6} meters is assumed. The increment in resistivity is taken to be from 1.0×10^{-2} Ω - m to 1.1×10^{-2} Ω - m. The slope $\frac{d\rho_o}{dx}$ at the step is then 10^{3} Ω.

The program in Appendix II solves the continuity equation for two hundred beam positions, at each of three values of electric field. The carrier distribution for three values of electric field are then found and the photovoltage variation with beam position is evaluated. The results are plotted in Figures 41 and 42.

2.2.7 Conditions for Negligible Internal Field

In the previous sections the continuity equation was solved, thereby obtaining the distribution of minority carriers. In these solutions it was arbitrarily assumed that the internal electric field due to impurity variations are negligible. In this section a criterion will be derived which will serve as the basis of a decision concerning the importance of the internal field.

The continuity equation given in equation 7 can be written as follows; assuming no externally applied electric field.

$$\frac{d}{dx^2} \Delta n - \frac{e}{kT} E^1 \frac{d\Delta n}{dx} - \frac{\Delta n}{\ell_d^2} = - g \frac{\tau}{\ell_d^2} \qquad (33)$$

where:

E^1 = the electric field due to impurity variations.

The second term in equation 33 is negligible if the following inequality is satisfied.

$$\frac{e/E^1/\ell_d}{kT} \frac{d}{dx} \Delta n << \frac{\Delta n}{d}$$

or

$$/E^1/ << \frac{kT}{e\ell_d} \tag{34}$$

The electric field in a semiconductor due to impurity variations is given by the relation below.

$$E^1 = -\frac{kT}{e} \frac{1}{N} \frac{dN}{dx} \tag{35}$$

where:

N = the impurity concentration as a function of position.

The following linear grading is assumed:

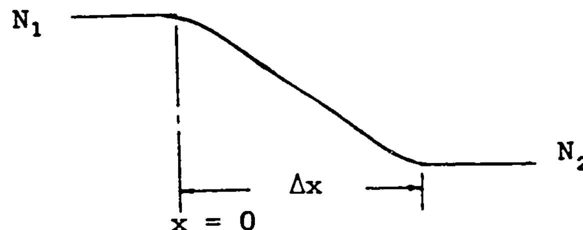

The internal electric field is calculated from equation 35.

The maximum value of electric field occurs at $x/2$ and is given by:

$$E^1_{MAX} = \frac{2kT}{e} \frac{N_1 - N_2}{N_1 + N_2} \cdot \frac{1}{\Delta x} \tag{36}$$

From equation 34 and 36 and assuming $N_1 > N_2$ the following condition for negligible internal field is obtained.

$$\Delta x \gg 2\ell_d$$

The internal electric field is negligible, if the distance over which the variation in impurity concentration occurs, is large with respect to the diffusion length of the minority carriers.

2.3 Condition for Equivalence of Current and Voltage Information

In the previous sections of this chapter, the photovoltage has been considered as a means of acquiring information about the specimen. The photovoltage is related to the specimen equilibrium resistivity and hence is useful to determine the impurity distribution in the semiconductor. It was shown in section 2.1 that the photovoltage is proportional to the beam-induced current, if the ratio of the change in resistance to the equilibrium resistance upon electric beam irradiation is small. In this case, either a voltage or a current can be detected and the information will differ

only by a multiplicative constant, that is, the specimen resistance. The analysis performed in the previous sections is equally valid for a beam-induced current. In this section, a criterion for the applicability of the assumption of a proportionality between the beam-induced current and voltage will be derived.

Consider a specimen of length ℓ irradiated by an electron beam at $x = x_o$. The distribution of generated carriers will be assumed to be exponential and the conductivity variations will be exponential also.

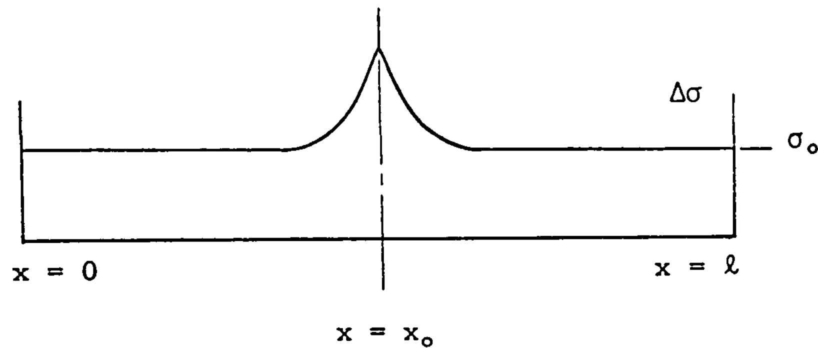

Fig. 5 Conductivity Variation in a Specimen Irradiated by an Electron Beam

The conductivity can be expressed by the relations given below[36].

$$\sigma_1 = \sigma_o[1 + \Delta\sigma \exp(x - x_o)/\ell_d], \quad x_o \geq x \geq 0 \tag{37}$$

$$\sigma_2 = \sigma_o[1 + \Delta\sigma \exp(x_o - x)/\ell_d], \quad \ell \geq x \geq x_o \tag{38}$$

where:

σ_o is the equilibrium conductivity

$\Delta\sigma$ is the maximum conductivity change

If the specimen cross-section area is taken as A then the specimen resistance becomes:

$$r_1 = \frac{1}{A\sigma_o} \int_o^{x_o} \frac{dx}{1 + k \exp(x - x_o)/\ell_d} \tag{39}$$

$$r_2 = \frac{1}{A\sigma_o} \int_{x_o}^{\ell} \frac{dx}{1 + k \exp(x_o - x)/\ell_d} \tag{40}$$

Evaluating these integrals the following expressions are obtained.

$$r_1 = \frac{1}{A\sigma_o} \left\{ x_o - \ell_d \, \ell n\left[\frac{1 + k}{1 + k \exp -x_o/\ell_d}\right] \right\} \tag{41}$$

$$r_2 = \frac{\ell}{A\sigma_o} \left\{ 1 - \frac{x_o}{\ell} - \frac{\ell_d}{\ell} \, \ell n\left[\frac{1 + k}{1 + k \exp - (\ell - x_o)/\ell_d}\right] \right\} \tag{42}$$

The total specimen resistance is obtained by adding 41 and 42. The equilibrium resistance is given by:

$$R = \ell / A\sigma_o$$

The decrease in resistance due to electron beam irradiation is given by the difference between R and $r_1 + r_2$. This resistance decrease can be written as:

$$\Delta r = -\frac{\ell_d}{\ell}\left[\ell n \frac{1 + k}{1 + k \exp - x_o/\ell_d} + \ell n \frac{1 + k}{1 + k \exp - (\ell - x_o)/\ell_d}\right] \quad (43)$$

The maximum value of Δr occurs for $x_o = \ell/2$ and a diffusion length which is small compared to the specimen length ℓ. This value of resistance change is given below.

$$\Delta r \doteq -2\frac{\ell_d}{\ell} \ell n (1 + k) \quad (44)$$

For a specimen with a diffusion length much smaller than the specimen length, the ratio of change in resistance to the equilibrium specimen resistance, is very small. The second term of the equation 1 is therefore negligible and the analysis given in the above sections is applicable to the beam-induced current.

2.4 Sources of Error

In the preceding sections, a discussion of the theory of beam-induced voltages was presented. The assumptions of negligible internal field and of the equivalence of beam-induced current and voltage were also treated. In the sections to follow, some possible sources of error in the photovoltage measurements will be presented. These are:

1. The effect of electron emission on the photovoltage.
2. The effects of contacts on the photovoltage.

2.4.1 Effect of Electron Emission on the Photovoltage

Any factor which causes a specimen potential variation will lead to an error in the photovoltage measurement. One such mechanism arises in the case of electron emission due to specimen bombardment by an electron beam. This case will be considered below.

If a specimen is irradiated by an electron beam, secondary electrons are emitted from the surface. The yield varies with the beam accelerating potential. For most materials, the maximum yield is of the order of 1.5 which occurs at a potential of 500 to 800 volts. The yield is defined as the ratio of the number of emitted electrons per unit time to the incident beam current.

$$\sigma_y = I_s/I_p \tag{45}$$

If the yield σ_y is different from unity, the specimen will acquire a charge. If $\sigma_y > 1$, the surface becomes positive. The yield, however, is a function of the net accelerating voltage and will vary with the specimen potential and can be expressed as follows:

$$\sigma_y = f(V_{eff}) \tag{46}$$

This relation is not well defined mathematically, but is of the form given in Figure 6[37].

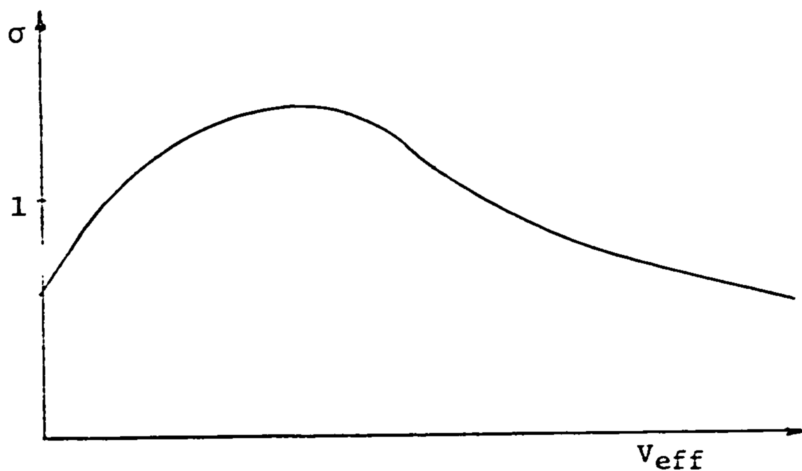

Fig. 6 Yield vs Net Accelerating Potential

The net accelerating potential is:

$$V_{eff} = V_o + V_s$$

where:

V_o is the accelerating potential

V_s is the specimen potential

Assuming a specimen resistance of R ohms to ground, the surface potential can be written in terms of the specimen current $(I_s - I_p)$.

$$V_s = R[I_s - I_p] = V_{eff} - V_o \tag{47}$$

From equation 45 and 47, the expression for yield becomes:

$$\sigma_y = \frac{V_{eff}}{RI_p} - (\frac{V_o}{RI_p} - 1) \tag{48}$$

The effective accelerating potential can be obtained from a solution of equations 46 and 48. The surface voltage can then be obtained.

The surface voltage gives rise to an error in the measurement of the photovoltage. However, under certain conditions, the error can be negligible. From equation 48 a condition for negligible error can be deduced. The equation can be re-written as follows:

$$\left|1 - \sigma_y\right| = \frac{1}{RI_p} \left| V_s \right| \tag{49}$$

The maximum value of $1 - \sigma_y$ is unity then V_s can be taken as negligible if RI_p is sufficiently small.

$$V_s \sim RI_p \tag{50}$$

For a given beam current I_p, the surface voltage is negligible if the specimen resistance is small. For example, if a beam current of 10^{-9} amps gives rise to a 1mv photovoltage, the surface voltage will be negligible if the specimen resistance is less than 10^5 ohms.

2.4.2 Effect of Contacts on the Photovoltage

In the previous section, it was pointed out that any variation in specimen potential will lead to an error in the photovoltage measurement. In a practical case where contacts must be made to the semiconductor, a change in potential occurs when the electron beam scans the region of the junction of the two materials. An error is then produced in the photovoltage measurement.

The voltage produced at the contacts can be calculated from the expressions of the chemical and Dember emf's of equation

7 (Appendix I). In order to apply these relations, the distribution of minority carriers must be known. The Figure 7 illustrates the situation to be considered.

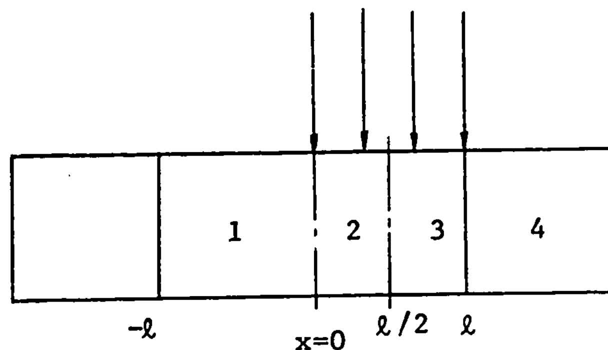

Fig. 7 Finite Bar Specimen with Contacts

For ease of calculation, the specimen length is taken to be twice the beam diameter. The diffusion length in the semiconductor will be taken as L' and in the metal as L'', where $L'' < L'$ (38). At the edges of the irradiated region, the concentration of generated carriers will be different. The distribution of minority carriers can be found from a solution of the continuity equation. For the case of no applied electric field, the continuity equation can be written as follows:

$$D_n \frac{d^2}{dx^2} \Delta n - \frac{\Delta n}{\tau} + g = 0 \tag{51}$$

where:

$$g = \begin{cases} 0, & -\ell < x < 0 \\ K, & 0 < x < \ell \end{cases}$$

The boundary conditions are:

$$\begin{aligned} \Delta n &= 0 , & x &= -\ell \\ \Delta n &= \tfrac{1}{2}\Delta n_o , & x &= 0 \\ \Delta n &= \Delta n_o , & x &\sim \ell/2 \quad \text{where } \ell/2 > L \\ \Delta n &= b\Delta n_o , & x &= \ell \\ \Delta n &= 0 , & x &\to \infty \end{aligned} \tag{52}$$

The following relations also hold

$$\text{at} \quad x = \ell \qquad \begin{aligned} \Delta n_3 &= \Delta n_4 \\ \frac{d}{dx}\Delta n_3 &= \frac{d}{dx}\Delta n_4 \end{aligned} \tag{53}$$

The solutions of equation 51 become:

$$\begin{aligned} \Delta n_1 &= \tfrac{1}{2}\Delta n_o \; e^{x/L'} \\ \Delta n_2 &= \Delta n_o \; (1 - \tfrac{1}{2}e^{-x/L'}) \\ \Delta n_3 &= \Delta n_o \; [1 - ae^{(x - \ell>/L'}] \\ \Delta n_4 &= \Delta n_o b \; \exp[-(x - \ell)/L''] \end{aligned} \tag{54}$$

From equations 53 and 54:

$$a = \frac{L'}{L' + L''} \qquad b = \frac{L''}{L' + L''} \tag{55}$$

The distribution of minority carriers can then be plotted as shown in Figure 8

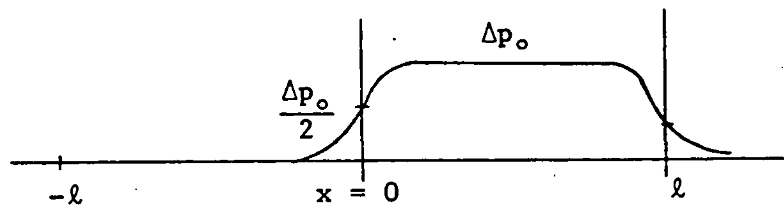

Fig. 8 - Distribution of Minority Carriers in the Specimen Irradiated Over the Right Half.

The generated voltage can be calculated from the expressions of the chemical and Dember emf.

$$V_c = \frac{kT}{e} \int \frac{\mu_n + \mu_p}{\mu_n n + \mu_p p} \frac{\Delta n}{n_o} \frac{dn_o}{dx} dx$$

7 (Appendix I)

$$V_d = -\frac{kT}{e} \int \frac{\mu_n - \mu_p}{\mu_n n + \mu_p p} \frac{d\Delta n}{dx} dx$$

If σ_{n_o} is constant, that is if there is no variation of impurity concentration along the specimen, then $V_c = 0$. The voltage generated is then a Dember emf. The Dember emf can be re-written as follows:

$$V_d = -\frac{kT}{e} \frac{\mu n - \mu p}{\mu n + \mu p} \sigma_{no} \int \frac{1}{(\sigma_{no} + \Delta\sigma)\sigma_{no}} \frac{d\Delta\sigma}{dx} dx \qquad (56)$$

For the case of large generation $\Delta\sigma > \sigma_{no}$. The equation 56 then becomes:

$$V_d = -\frac{kT}{e} \frac{\mu n - \mu p}{\mu n + \mu p} \int \frac{1}{\Delta n} d\Delta n \quad dx \qquad (57)$$

Substituting for Δn from equation 54, the potential becomes:

$$V_d = -\frac{kT}{e} \frac{\mu n - \mu p}{\mu n + \mu p} \left[\frac{\ell}{L'} + \ell_n 2 + \ell_n (1 + \frac{L'}{L''}) \right] \qquad (58)$$

If the analysis is repeated for the beam irradiating the left half of the specimen, the expression of the generated voltage is:

$$V_d = \frac{kT}{e} \frac{\mu_n - \mu_p}{\mu_n + \mu_p} \left[\frac{\ell}{L'} + \ell_n 2 + \ell_n \left(1 + \frac{L'}{L''}\right) \right] \quad (59)$$

The voltage generated at the contacts is negative when the right half of the specimen is irradiated and positive when the left half is irradiated. The expressions 58 and 59 represent error terms in the photovoltage measurements. If these voltages are large with respect to the photovoltage measured, then a more exact analysis must be done in order to apply a correction.

2.5 The Case of Small Impurity Concentrations

In all the previous analysis, it was assumed that the impurity concentration is high and the potentials are determined by ensemble averages of electrons and holes. The variation in photovoltage is then the result of a variation of the ensemble average along the specimen. If the concentration of impurities and the electron beam diameter are sufficiently small, then the photovoltage generated as the beam scans along the specimen, could undergo large random variations. This variation would depend on the random distribution of impurity atoms.

In this chapter, the beam induced voltage was studied. If the change in specimen resistance upon irradiation is small,

compared to the equilibrium resistance of the specimen, then the beam-induced voltage and the beam-induced current are related by a multiplicative constant. When the change in resistance is not negligible, or when the bias voltage is high, the second term of equation 1 must be taken into account. In the analysis, the resistance change was assumed negligible.

In the next chapter, the methods of measurements used to obtain the resistivity variations are given. A list of results are then presented, including the results of the computer analysis.

CHAPTER III

MEASUREMENT TECHNIQUES AND RESULTS

In the previous two chapters, a review of the modes of operation of the SEM and an analysis of the conductive mode of operation were presented. In this chapter, the measurement techniques and the obtained results will be given in order to demonstrate the applications of the SEM in the field of material and device evaluation. All the modes of operation were used to obtain information about the specimen with emphasis on the conductive mode. The following section is a description of the actual system and measuring techniques used in obtaining the measurements. The chapter concludes with a section on computer analysis results.

3.1 Measurement Techniques

The discussion of the measurement techniques will be divided into sub-sections, corresponding to each mode of operation and display technique.

3.1.1 Emissive Mode Measurements

In the emissive mode of operation, either the secondary electrons or the primary reflected electrons are collected. An

electrical signal proportional to the yield of electrons is used to modulate the intensity of a CRT display.

In the apparatus used, the primary beam of electrons strikes the specimen surface at an angle of incidence which can be varied. The emitted electrons are collected by a Faraday cup, held at a positive potential which can also be varied. The Faraday cup encloses a scintillator behind a wire mesh, the scintillator is aluminum plated, and biased at a high positive potential with respect to the Faraday cup. The variation in the number of collected electrons gives rise to a variation of light generated at the scintillator. The light signal is channelled to an S_{11} photomultiplier by a light pipe. The signal is amplified and displayed on a CRT screen as an intensity modulated image.

The apparatus described above allows the variation of the angle of incidence of the primary beam and the collector potential. This allows the collection of either primary electrons or secondary electrons. To collect primary electrons, the wire mesh is biased negatively with respect to the sample and the angle of incidence is adjusted such that the primary reflected electrons enter the Faraday cup. To collect secondary electrons, the wire mesh is biased positively with respect to the sample and the angle of incidence is adjusted such that the reflected primaries are not

captured by the Faraday cup. In this way, secondary or primary reflected electrons can be detected to yield the desired surface detail of rough surfaces, or to increase contrast of smooth surfaces.

3.1.2 Luminescent Mode Measurements

In the luminescent mode of operation, the light emitted by a specimen is converted to an electrical signal which modulates the intensity of a CRT display. In order to collect as much of the emitted light as possible, a large diameter photomultiplier is mounted as close as possible to the specimen, thereby subtending a large solid angle at the specimen. In the apparatus used, an S_1 photomultiplier is mounted in the specimen chamber. The output signal of the photomultiplier is amplified by a d.c. amplifier, having an input impedance of 1000 ohms, a transfer impedance of 10^8 ohms and a bandwidth of 20 Kilohertz. The output of this amplifier is connected to a video amplifier and CRT display.

3.1.3 Conductive Mode Measurements

The conductive mode of operation is one which can be applied in obtaining quantitative information. This mode of

operation is important, and will be discussed in detail. In the conductive mode of operation, the beam-induced current is detected by an amplifier connected to the device in a suitable configuration (Fig. 9). The voltage output from the amplifier modulates the intensity of the CRT display.

The amplifier can be the d.c. amplifier, described above, or an a.c. amplifier. The a.c. amplifier used in the experiments has a transfer impedance of 2×10^7 ohms, and an input impedance of less than 100 ohms. The bandwidth of the amplifier is 1MHz with a lower cutoff frequency of approximately 10Hz.

Line scans of beam-induced signal can be obtained by applying the output of the above amplifier to the Y-axis input of an X-Y recorder. The X-axis signal is obtained from the SEM scan generator, therefore the electron beam and the recorder pen move in synchronism. The scan generator can be triggered externally which allows single line scans to be plotted on the X-Y recorder. The system can be calibrated with the use of a voltage or current source. The calibration procedure will be discussed in section 3.1.6. The measuring system is illustrated below. The amplifiers are transfer impedances.

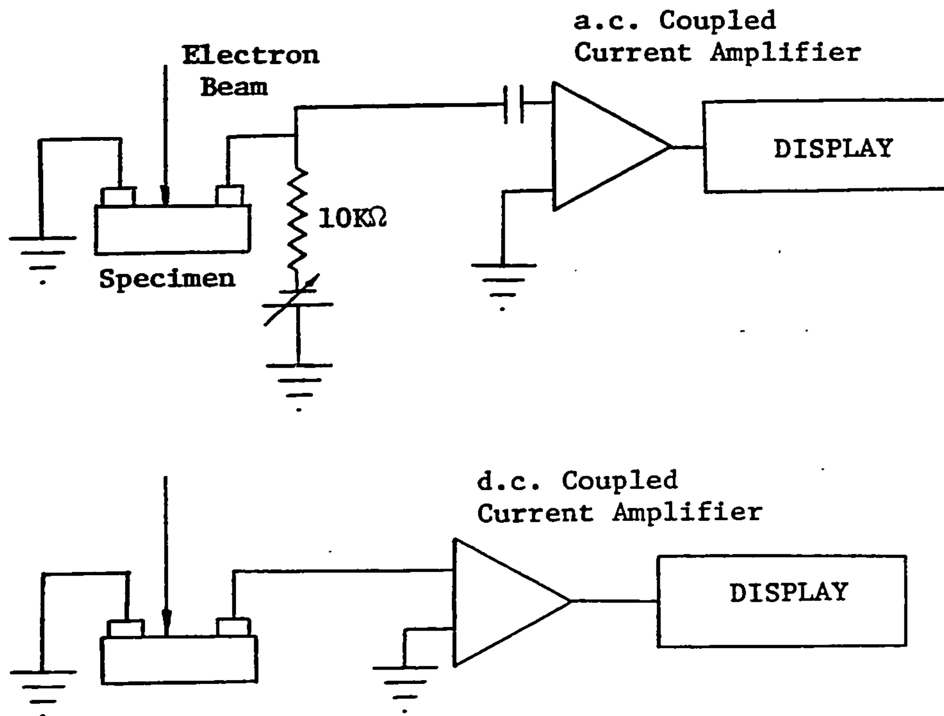

Fig. 9 (a) The measurement circuit for conductive micrographs.

(b) The circuit for specimen current micrographs.

3.1.4 Contoured Conductive Measurements

The signal variation in a two dimensional plane is illustrated as an intensity modulation in the conventional display technique. This technique does not lend itself to

the retrieval of quantitative information. One method of displaying quantitative information in a plane is through the application of the contouring technique described in section 1.2.1.

The contouring network is a circuit which adds a stepwise approximation of the input signal in antiphase with this signal. The resulting signal has the same information as the original signal, but the amplitude is limited to the difference between the upper and lower threshold voltages. An example of a triangular input signal is shown below.

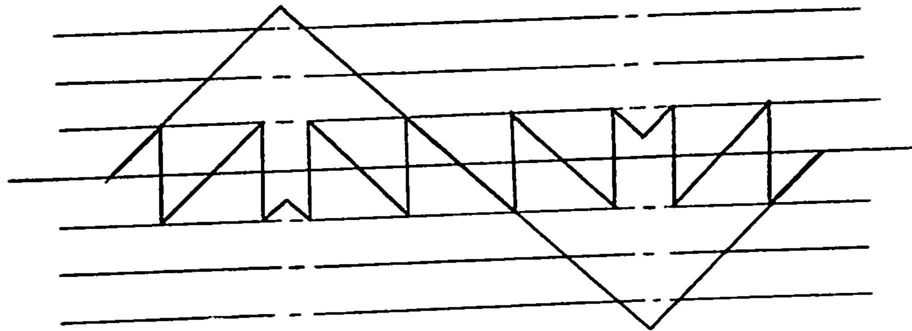

Fig. 10 The output of the contouring network for a triangular input.

When the input voltage reaches the positive threshold, a voltage equal to two threshold intervals is added in anti-phase. The circuit is illustrated in block form in Figure 11[39].

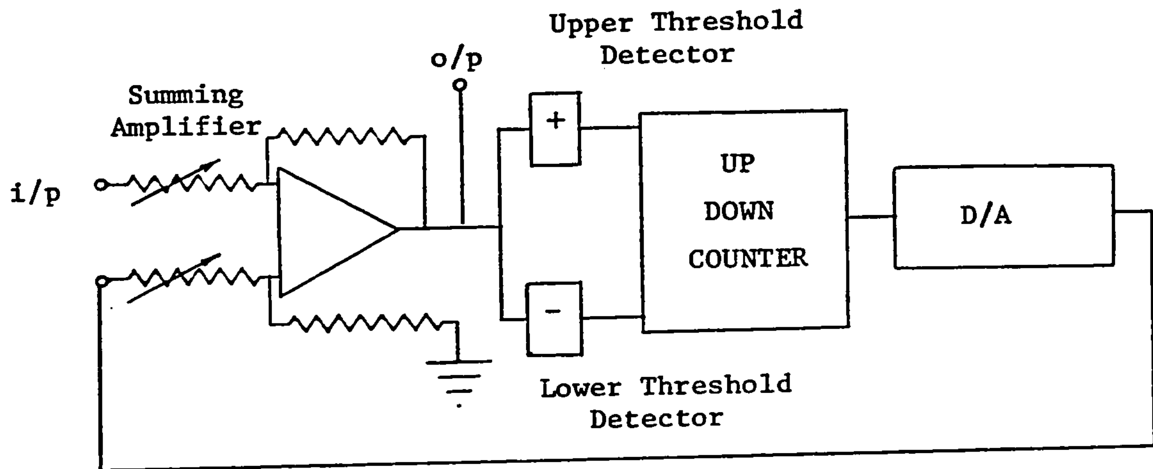

Fig. 11 Block diagram of the Contouring Network

The amplifier in the contouring network has variable gain. Increasing the gain of this amplifier increases the number of contour lines in the output and thereby increases the information content of the micrograph.

3.1.5 Phase Sensitive Detection

When the contouring network is used, a phase sensitive detector can be employed to improve the signal to noise

ratio. The signal must be modulated by a square wave. Then the phase sensitive detection can be obtained by multiplying the modulated input signal by a gating function of the same frequency and phase as the modulating square wave. The output is then obtained from a low pass filter with a cutoff frequency, high enough to let only the signal frequency pass unattenuated. The phase sensitive detector was considered in section 1.2.3.

The system employed in the experimental work is illustrated in Figure 12.

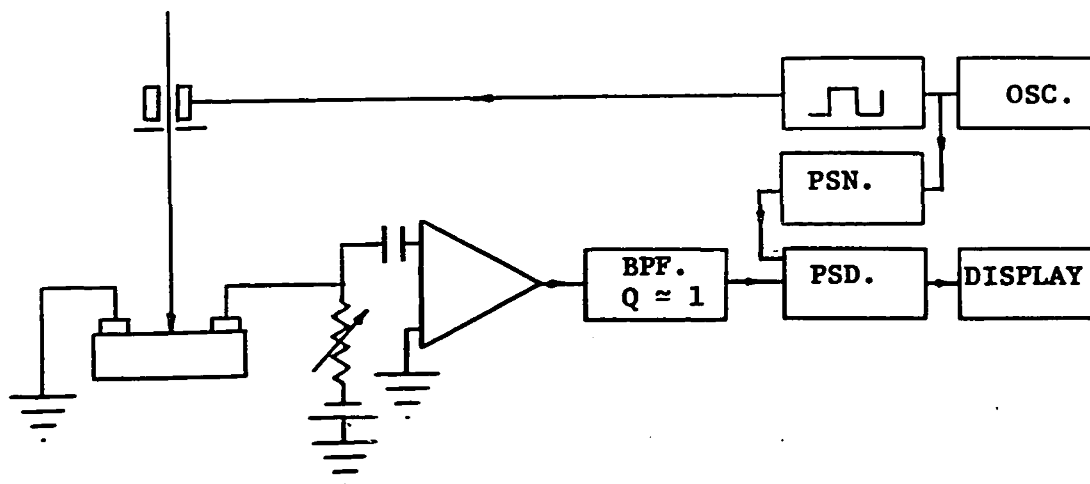

Fig. 12 Block diagram of the measuring system using the phase sensitive detector.

The system used in the experimental work included a minor modification. The modulated signal was filtered in a band-pass filter before detection. This improves the signal-to-noise ratio in the presence of a wide-band noise source.

The signal is modulated by chopping the electron beam with deflection coils, which deflect the beam over an aperture. The signal is detected and amplified, then filtered and applied to the phase sensitive detector. The reference signal is obtained from the oscillator, which also determines the chopping frequency. The reference signal is then passed through a phase shift network to allow adjustment of the relative phase of the modulating and reference signals.

The phase sensitive detector system described, improves the signal to noise ratio, but limits the rise-time of the overall signal recovery system. This then, limits the scan rate possible for a given resolution. Assuming a line scan of 0.4 sec. and a required resolution of 1/8 mm. in a 10 cm. CRT display, a value of system Q and bandwidth can be found. The signal period from the above data is $\tau_s = 0.001$ sec. By the Nyquist criterion, the chopping period must satisfy the following inequality.

$$\tau_c < \tfrac{1}{2}\tau_s$$

The value $\tau_c = 0.0002$ sec. is taken. The bandwidth of the system must be sufficient to allow the risetime to be no larger than $\frac{1}{2}\tau_c$. The bandwidth risetime relation is given by:

$$\Delta f \; \tau_r \doteq 0.4 \quad (40)$$

The bandwidth for the present case is 4KHz. The modulating frequency is $1/\tau_c = 5$KHz, and the Q of the network is 1.25.

In the experimental work, values of Q near unity were used whenever the phase sensitive detector was used in the measuring system, illustrated in Figure 13.

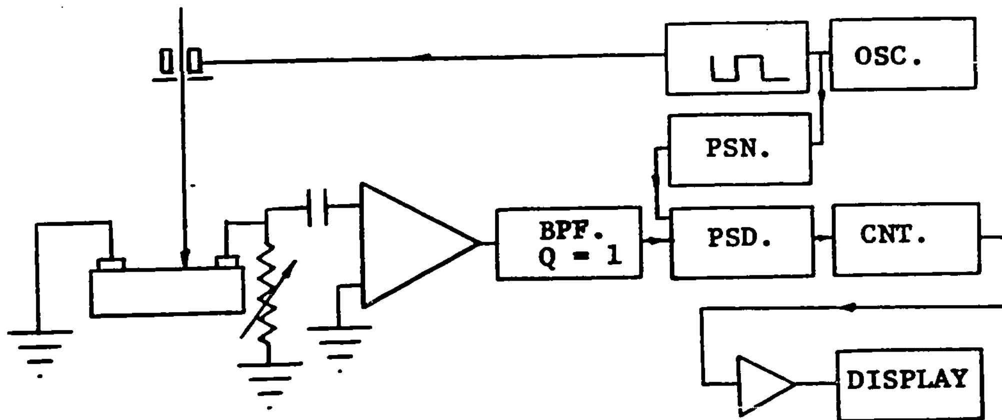

Fig. 13 The phase sensitive network system used to obtain contoured information.

3.1.5.1 Capacitively Coupled Measurements

Another use of the phase sensitive detection system described above arises in the case of capacitive coupling. Capacitive coupling of the signal refers to the situation where a stray capacitance occurs across the device, which results in differentiation of the signal. Consider the configuration illustrated below.

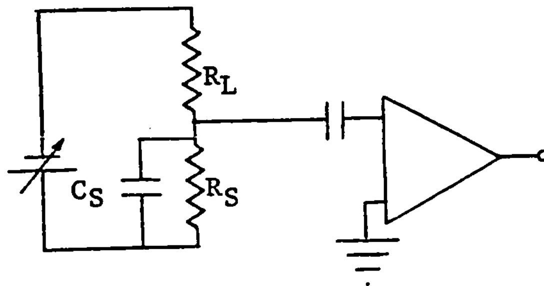

Fig. 14 Capacitively Coupled Specimen

The sample has a resistance R_S shunted by a stray capacitance C_S. If the time constant C_SR is small with respect to the time τ taken by the beam to scan one picture element, the output signal will be differentiated. It is possible to chop the electron beam at a frequency $1/\tau_s$ and recover the information from a phase sensitive detector. τ_c is the pulse width and must satisfy the following:

$\tau_s < \tau_c < RC_s$ where R is the parallel sum of resistances $(R_S//R_L)$ τ_S is the signal risetime.

The pulse width must be less than the time constant RC_S but greater than the signal risetime τ_S. If it is assumed that the signal risetime is determined by the risetime of the pulsed electron beam, then τ_S is negligibly small for practical purposes.

The waveforms shown below illustrate the possible cases for the time constant of the shunting capacitance and load resistance combination.

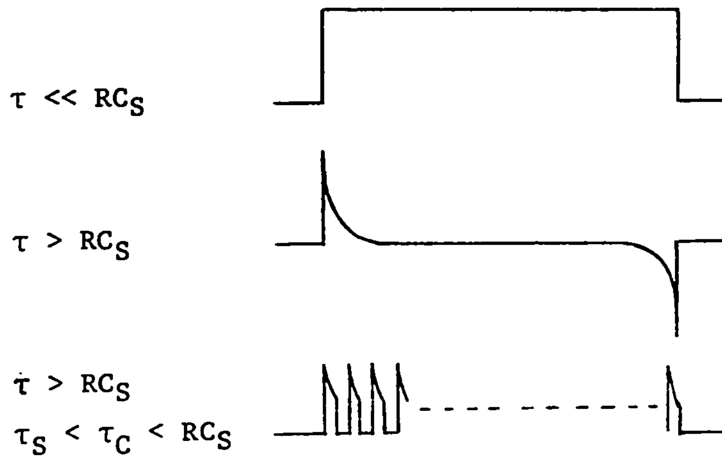

Fig. 15 Capacitive Coupling

In the first case, no difficulties with capacitive coupling arise. The second case shows the effect of differentiation while the third waveform illustrates the result of chopping the beam when differentiation occurs. This signal is the input to the phase sensitive detector which effectively integrates the signal, the output then approaches the signal of the first case.

3.1.5.2 Line Scan Measurements

The phase sensitive detector system can be used to advantage in obtaining line scans. The phase sensitive detector is used to eliminate noise from the system which would mask some of the information. The overall system is illustrated in Figure 16.

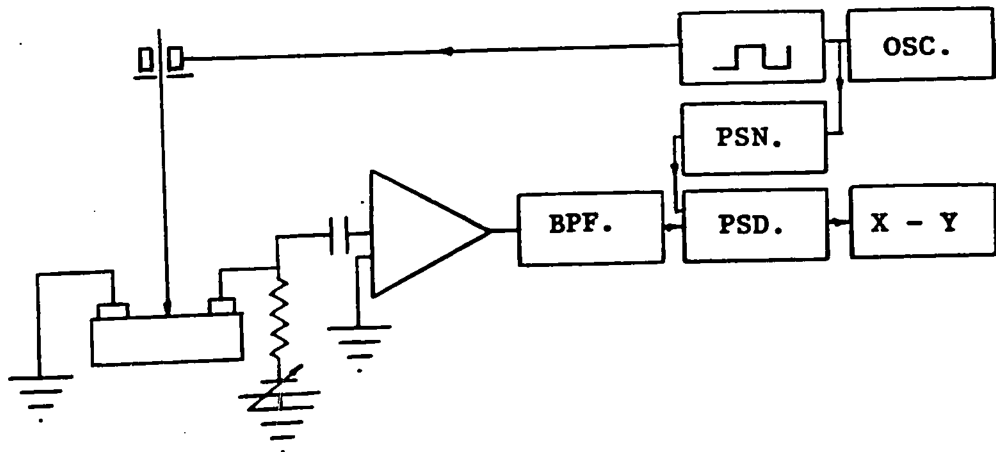

Fig. 16 Network used to obtain line scans.

It is sometimes necessary to chop the bias at a given frequency with a reduced duty cycle and comparing the results with those obtained at a 1:1 duty cycle. This technique is useful to study heating effects in the specimen. The measuring system for this case is illustrated below. Such measurements were not obtained in this work.

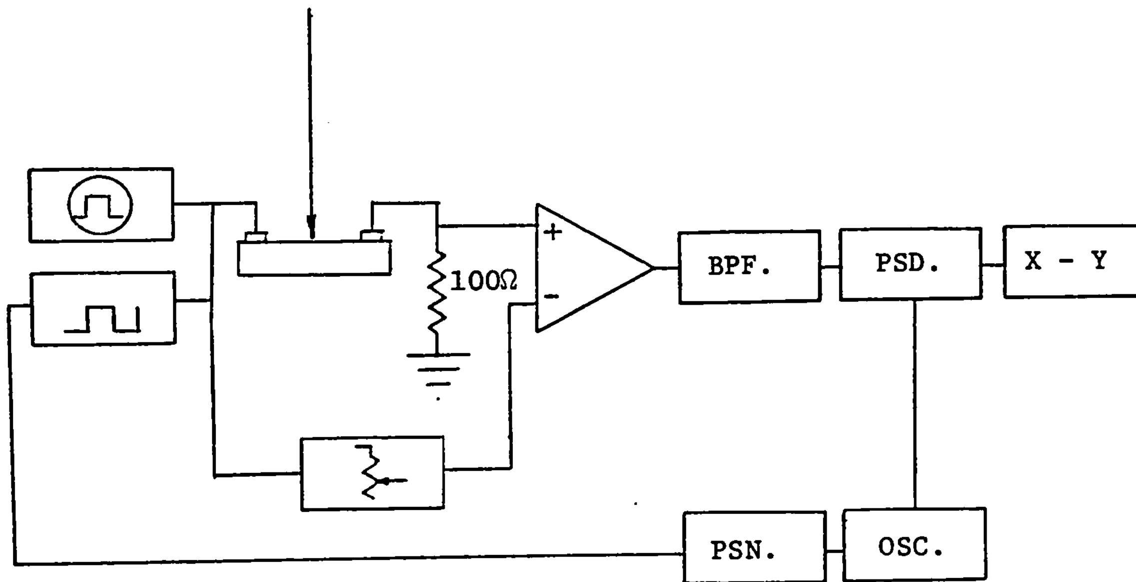

The amplifier in this case is a differential voltage amplifier.

Fig. 17 System for heating effect measurements.

3.1.6 Calibration Techniques

In the previous section, two measuring system block diagrams were given for ploting line scans. These are important since they can be calibrated and therefore serve as the basis of the quantitative measurements. A method of calibration of each of the above two measuring systems are given in Figures 18 and 19.

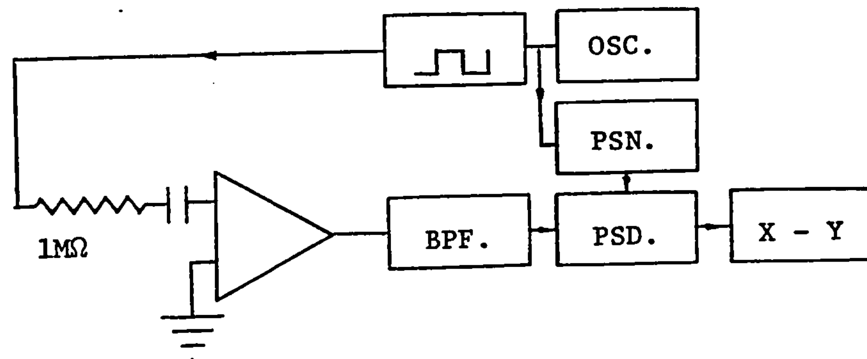

Fig. 18 Calibration of current detection system.

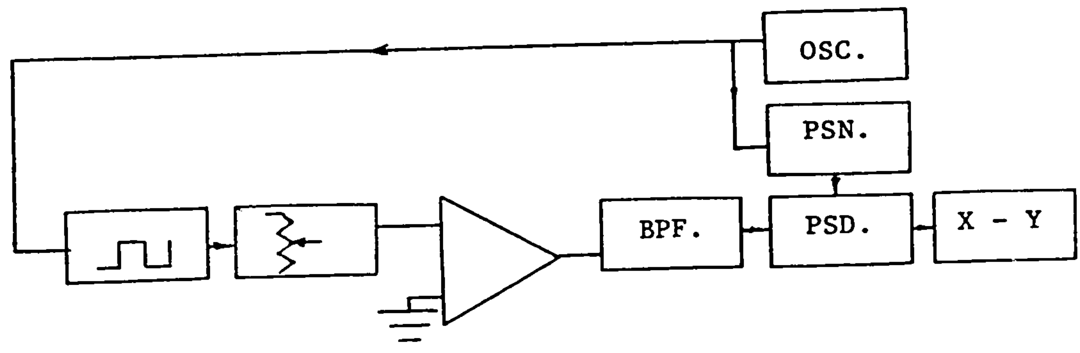

Fig. 19 Network for Voltage Calibration.

The beam current can be measured by placing a Faraday cup in the chamber and directing the beam into the cup. The cup is connected to ground through an electrometer.

3.2 Experimental Results

In Chapter I, a review of the applications of the SEM was presented. In this section, some of these applications will be investigated. Results will be given which indicate the power of the technique in material quality assessment and manufacturing process evaluation. The devices studied were transferred-electron devices, although junction devices can also be studied.

3.2.1 Devices Investigated

The devices studied in the experimental work are Gallium Arsenide Gunn-Effect diodes. Two types were considered. The first type are planar devices where the contacts and active region are co-planar. The active region is in an epitaxial layer of Gallium Arsenide (GaAs) on a semi-insulating GaAs substrate, and the contacts are strips of gold alloy on the surface of the epitaxial layer. These

devices are labelled as the R-series. The R-200 and R-450 devices have active gap widths of 20 and 45μ-m respectively. The second type of device is shaped as a small bar with tin dots at each end which serve as contacts. One face of the bar is coated with an epitaxial layer of GaAs, the bar itself is semi-insulating. These devices are labelled as the F-series and have a length of approximately 1 mm. between contacts.

The specifications of the two devices are tabulated below.

	R DEVICES	F DEVICES
Layer Thickness	5.5μ-m	10μ-m
Carrier Concentration	3.1×10^{15}	$\sim 10^{12}$
Resistivity	0.32Ω-m	
Substrate	Fe doped	High p concentration
Gap Length	20 and 45μ-m	~1 mm.

3.2.2 Measurement Results

The devices described above will be examined in the three basic modes of operation. Line scans of beam induced current will also be taken. Each mode of operation is expected to give different information. The emissive mode will

give surface information such as the presence of scratches and contact defects. The luminescent mode will give the location of dislocations, and the relative concentration of impurities among specimens. The conductive mode will give information of variation of potential and impurity variation in the specimen. The information expected from each mode is tabulated below.

MODE	INFORMATION EXPECTED
1. Emissive	Surface information: - presence of scratches - bond damage - metallization damage - etch pits
2. Luminescent	Surface and bulk information: - presence of dislocations - surface scratches - variation of impurity concentration
3. Conductive	Bulk information: - variation of impurity concentration Conductive line scans: - occurrence of current multiplication

In addition to the SEM results, electrical data and thermal plots are given for the devices.

3.2.2.1 The Use of Multiple Modes to Examine Semiconductor Devies

The R-200 Devices

The utility of the Scanning Electron Microscope is illustrated by the series of micrographs in Fig. 20(a) - 20(i), which show an R-200 series Gunn diode before and after catastrophic failure.

Emissive Micrographs

The general appearance of the device is given by the emissive micrographs in Fig. 20(a) and 20(b), where Fig. 20(a) was taken initially and 20(b) after failure. The emissive micrograph is used as a general frame of reference for the micrograph taken under other modes of operation and to locate gross faults. In this example, it illustrates how the device failed as a result of electromigration of the metallizing material, causing a short circuit between the electrodes.

Luminescent Micrographs

The epitaxial material can be examined using the cathodoluminescent mode (Fig. 20(c) and 20(d)). The first

micrograph shows the device at a slightly lower magnification than the emissive micrographs. The dark areas are regions of low luminescence efficiency and indicate faults or regions of damage. A region of damage between the electrodes can be identified on the emissive micrograph (Fig. 20a) as mechanical damage, probably incurred during the bonding operation. It may be observed that the eventual failure of the device was not related to this damage.

A section of the substrate away from the device itself is shown at a higher magnification in Fig. 20(d). The dark areas represent dislocations, the spots could be points at which edge dislocations meet the surface. The row of regularly spaced dots indicates a series of related dislocations, usually called a low-angle tilt boundary[41].

The cathodoluminescence of GaAs has been studied by several researchers whose work allows a tentative explanation of the above results. A discussion follows which explains the variation of luminescence efficiency of the device in Fig. 20(c) and 20(d).

The cathodoluminescent signal intensity in GaAs is proportional to the impurity concentration at low doping levels. At high doping concentrations ($>10^{18} cm^{-3}$)

Fig. 20(a) Emissive micrograph showing the device R-204 before failure.

Fig. 20(b) Emissive micrograph showing the device R-204 after failure.

Fig. 20(c) Luminscent micrograph of device R-204.

DC Amp. Transfer Impedance: 50 MΩ
DC Amp. Phase: Invert
Beam Accelerating potential: 20kV

Fig. 20(d) Luminescent micrograph of device R-204

DC Amp. Transfer Impedance: 100 MΩ
DC Amp. Phase: Invert
Beam Accelerating potential: 20kV

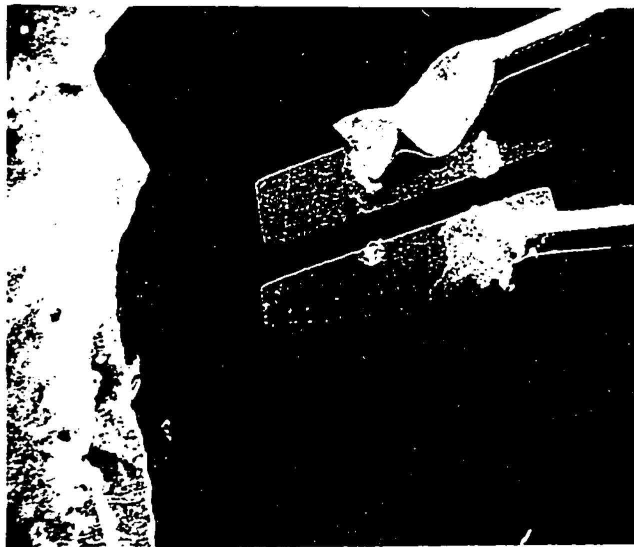

(a) 150X 70μ

(b) 150X 70μ

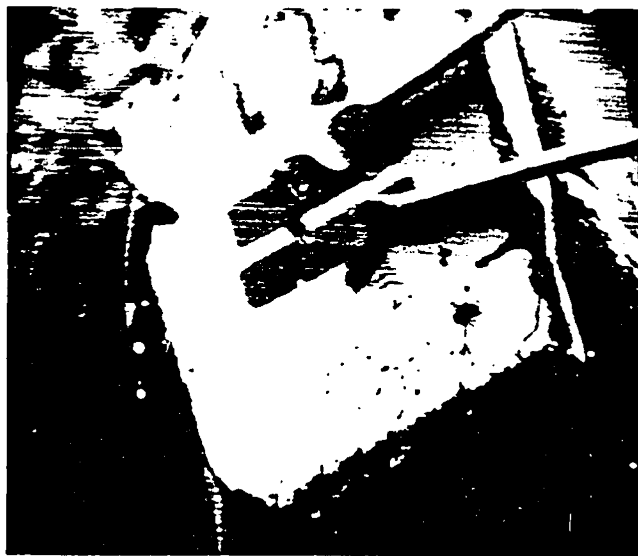

(c) 130X 75μ

(d) 1KX 10μ

Fig. [20(a) - (d)] Emissive and Cathodoluminescent Micrographs of Device R-204.

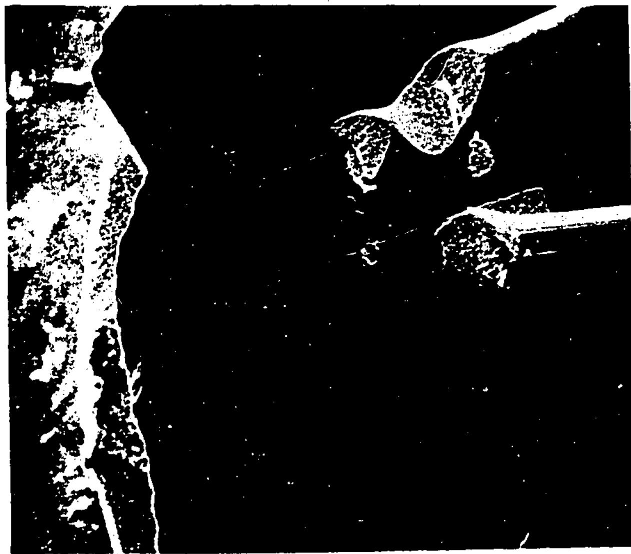

(a) 150X 70μ

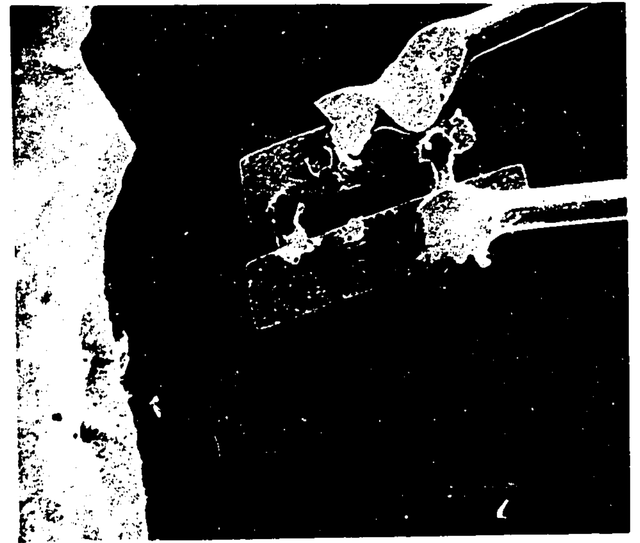

(b) 150X 70μ

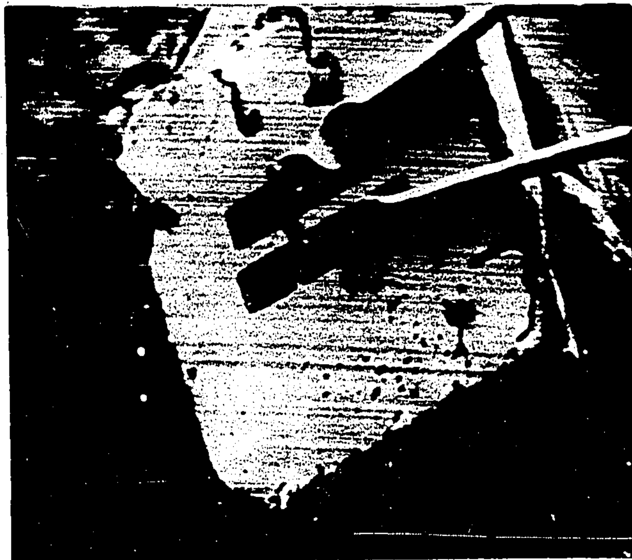

(c) 130X 75μ

(d) 1KX 10μ

Fig. [20(a) - (d)] Emissive and Cathodoluminescent Micrographs of Device R-204.

(a) 150X 70μ

(b) 150X 70..

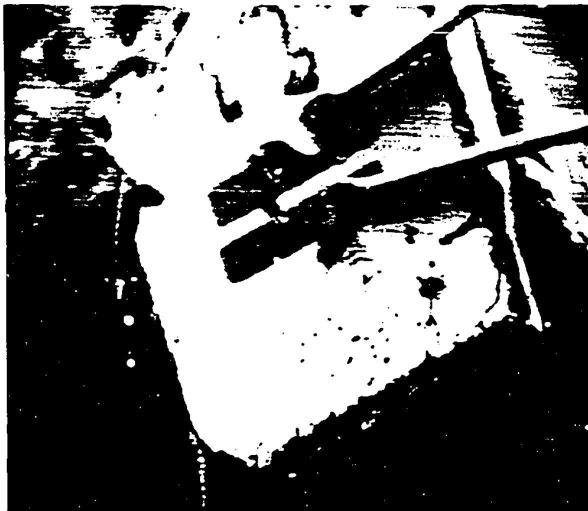

(c) 130X 75μ

(d) 1KX 10..

Fig. [20(a) - (d)] Emissive and Cathodoluminescent Micrographs of Device R-204.

the luminescent signal decreases with increasing impurity concentration[42]. Since segregation of impurities occurs at dislocations[43], the luminescent efficiency can increase in the region of dislocations if the overall impurity concentration is low. The dislocations themselves have the effect of reducing carrier lifetime[44]. The dislocations are therefore, expected to be regions of low luminescent efficiency and may be surrounded by regions of higher luminescent efficiency[45,43]. Surface scratches also add trapping centers which leads to reduced luminescent efficiency, if these are present.

Conductive Micrographs

The micrographs of Fig. 20(e) to 20(i) are all in the conductive mode. Fig. 20(e) shows a general conductive view of the device. The dark areas between the electrodes can be related with the dark areas of the cathodoluminescent micrograph of Fig. 20(c). Fig. 20(f) shows the gap at greater magnification and Fig. 20(g) a contoured version under the same conditions. The contoured version yields better Z component resolution, amplitude in this case, and produces much the same information in two dimensions as does a line scan (see below)

Fig. 20(e) Conductive micrograph of device R-204.

AC Amp. Transfer Impedance: 400 KΩ
AC Amp. Phase: Non-Inverting
Bias: 0.05V $-V_e$ on 1 Signal taken from same tab as that of applied bias
R_L: 10 K
Beam Accelerating potential: 20kV

Fig. 20(f) Conductive micrograph of device R-204.

AC Amp. Transfer Impedance: 20 KΩ
AC Amp. Phase: Inverting
Bias: 1.26V $+ V_e$ on 1 (6.85ma)
R_L: 10 K
Beam Accelerating potential: 20kV

Fig. 20(g) Contoured conductive micrograph of device R-204.

AC Amp. Transfer Impedance: 40 KΩ
AC Amp. Phase: Inverting
Bias: 1.26V $+ V_e$ on 1 (7.35ma)
R_L: 10 K
Beam Accelerating potential: 20kV
Contour circuit gain: 10
Contour circuit phase: Invert

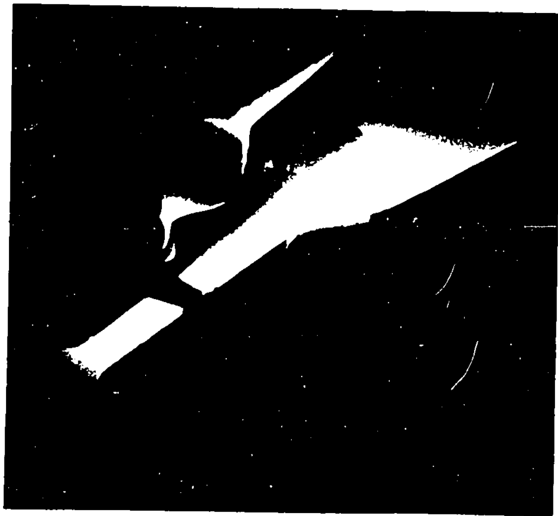

(e)

X200

50μ

(f)

X1000

10μ

(g)

X1000

10μ

Fig. [[illegible](e) – (g)]

[illegible] and [illegible]contoured [illegible] Micrographs [illegible]

in one dimension. Note that the contoured micrograph by itself indicates increments only, and an uncontoured micrograph is required for its interpretation.

Mechanisms which occurred during the failure of the device can be inferred from a comparison of the contoured micrograph of Fig. 20(h) taken immediately before failure with the electron emissive micrograph of Fig. 20(i) taken immediately after. Note that conductive information is not available after the device has shorted. It can be seen that the short circuit occurred at a region of minimum conduction indicating that the material transport, which caused the short circuit, resulted from majority carrier current flow as distinct from the minority carrier current of the conductive image.

The above series of micrographs was taken of a non-typical device. Micrographs of a more typical device of the same series are shown in Fig. 21(a) and 21(b). The first is an emissive micrograph and the second a contoured conductive micrograph. The device is quite good but has a small flaw between the bonds which may be attributed to the bonding process. This micrograph was taken with the use of the phase sensitive detector and shows a definite reduction in noise. The VI characteristic is given in Fig. 22 and shows the current saturation characteristic which is expected from such a

Fig. 20(h) Contoured Conductive Micrograph of Device R-204

Ac Amp. Transfer Impedance:	40 KΩ
Ac Amp. Phase:	Invert
Bias:	6.9 V + V_e on 1 (27.9 ma)
R_L:	10 KΩ
Beam Accelerating Potential:	20 KV
Contour Circuit Gain:	10
Contour Circuit Phase:	Invert

Fig. 20(i) Emissive Micrograph of Device R-204 after failure.

This micrograph helps to relate the failure area with the resistivity variation.

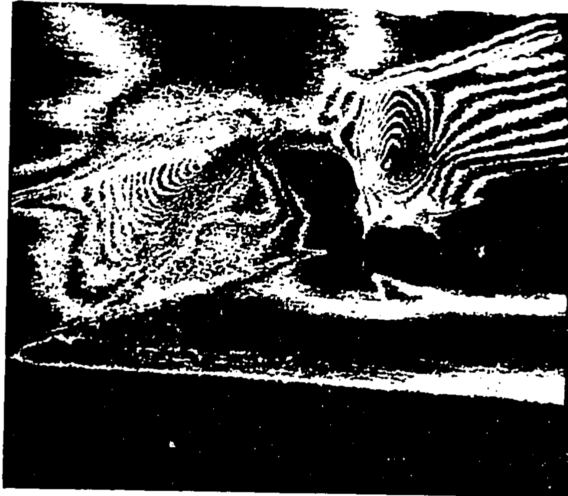

(h) X1000 10μ

(i) X1000 10μ

Fig. [20(h) - (i)] Contoured Conductive and Emissive Micrographs of Device .P-204.

Fig. 21(a) Emissive Micrograph of Device R-205.

Fig. 21(b) Contoured Conductive Micrograph of Device R-205.

Ac Amp. Transfer Impedance:	400 KΩ	
Ac Amp. Phase:	Invert	
Bias:	0.05 V	#2 pos.
RL:	10 KΩ	
Beam Accelerating Potential:	20 KV	
Contour Circuit Gain:	10	
Contour Circuit Phase:	Norm	
Beam Chopping Frequency:	10 kHz	

(a) X500 20μ

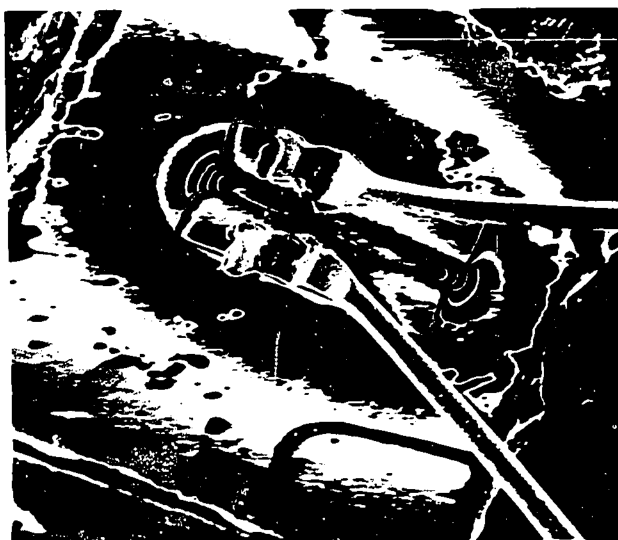

(b) X500 20μ

Fig. [21(a) - (b)] Emissive and Contoured Conductive Micrograph of Device R-205.

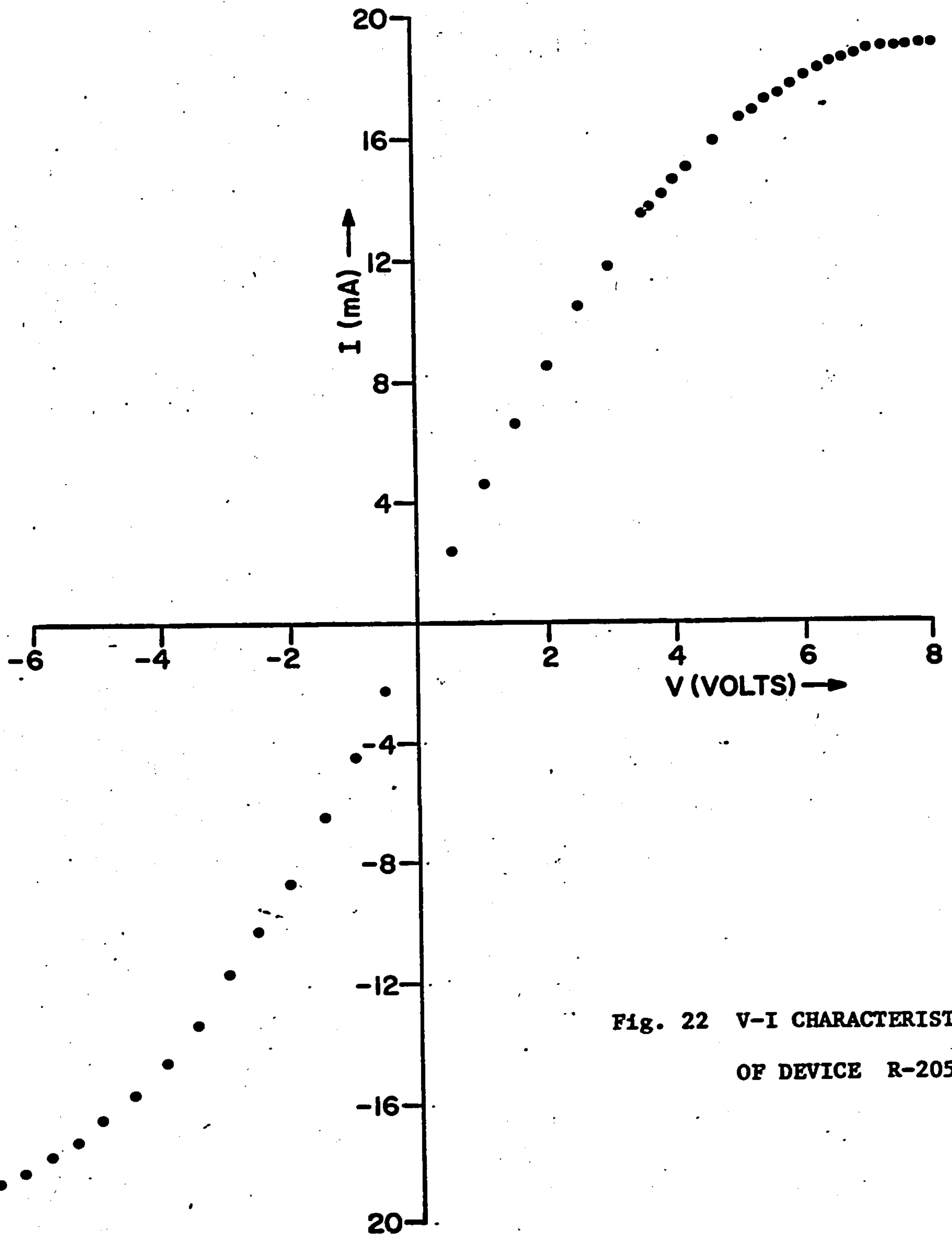

Fig. 22 V-I CHARACTERISTIC OF DEVICE R-205

device[46].

3.2.2.2 The R-450 Devices

The micrographs of the R-450 devices show similar information to that of the R-200 devices. The devices will therefore, be discussed briefly, with emphasis on details of particular interest.

Device R-451

The micrographs of Fig. 23(a) to 23(e), the effects of dislocations can be seen in all modes of operation. Fig. 23(a) and 23(b) are emissive micrographs showing etch pits at the surface of the epitaxial layer. Fig. 23(c) and 23(d) are luminescent and specimen current micrographs both of which show the above dislocations and others which do not appear at the surface. These dislocation patterns affect the conductive signals and are clearly evident in the contoured conductive micrograph in Fig 23(e).

A comparison of the micrographs in Fig. 23(c) and 23(d) shows that the same information can be obtained from the specimen current and the luminescent micrographs. These two modes of operation cannot always

Fig. 23(a,b) Emissive Micrographs of Device R-451 showing dislocation etch pits on the surface of the device.

Fig. 23(c) Luminescent Micrograph of Device R-451 showing dislocations.

DC Amp. Transfer Impedance:	50 MΩ
DC Amp. Phase:	Invert
Device Resistance:	313 Ω
Beam Accelerating Potential:	20 kV

(a)

X200

50μ

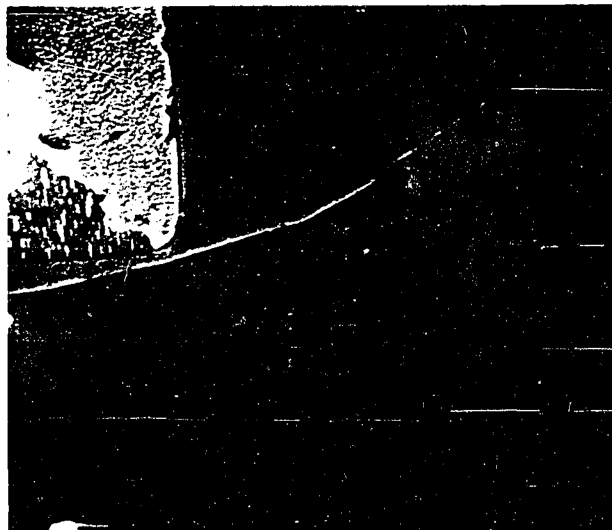

(b)

X1200

8μ

(c)

X200

50μ

Fig. [23 (a) - (c)]

Emissive and Luminescent Micrographs of Device P-451.

(a)

X200

50μ

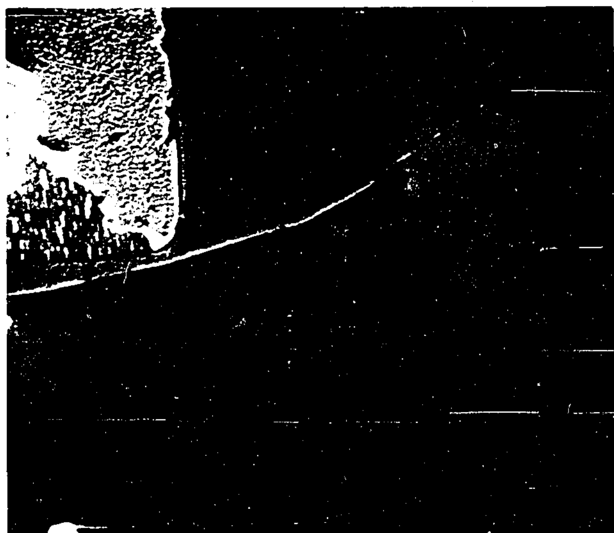

(b)

X1200

8μ

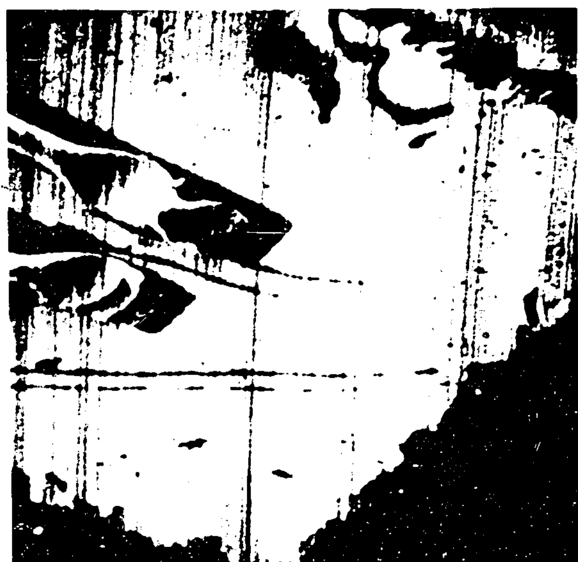

(c)

X200

50μ

Fig. [23 (a) - (c)]
Emissive and Luminescent
Micrographs of Device R-451.

Fig. 23(d) Specimen Current Micrograph of Device R-451.

Ac Amp. Transfer Impedance:	4 MΩ
Ac Amp. Phase:	Invert

Fig. 23(e) Contoured Conductive Micrograph of Device R-451

Ac Amp. Transfer Impedance:	400 KΩ
Ac Amp. Phase:	Invert
Bias:	0.1 V #2 pos. (0.3 ma)
R_L:	10 KΩ
Beam Accelerating Potential:	20 KV
Contour Circuit Gain:	10
Contour Circuit Phase:	Non-Inverting
Beam Chopping Frequency:	10 kHz

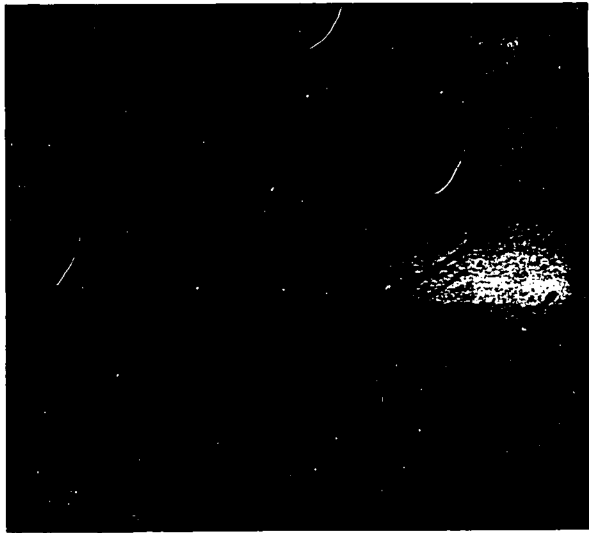

(d) X200 50μ

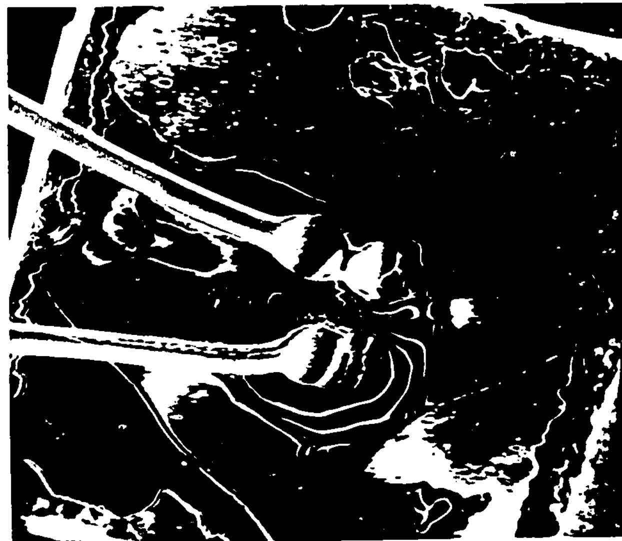

(e) X200 50μ

Fig. [23(d) - (e)] Conductive and Contoured Conductive Micrographs of Device R-451.

be used. If the impurity concentration is very low, the luminescence efficiency is also low, making this mode of operation impractical. The specimen current mode cannot be used in a specimen containing p-n junctions, since the charge collection efficiency is very high at the junctions. When both signals can be detected, the luminescent mode is preferable, since no contacts are required.

The specimen current micrograph (Fig. 23c) was taken with the a.c. amplifier giving phase inversion. The areas of mechanical damage and the dislocation patterns are dark in this micrograph. Since the total back-scattering coefficient is less than unity at high beam energies[37], an electron current flows into the amplifier (see section 1.1.2). This implies that at the regions of mechanical damage, the total backscattering coefficient increases.

Device R-452

The emissive micrographs of Fig. 24(a) and 24(b) show evidence of electromigration. The electromigration effect is the transport of metal ions under the influence of the electric field or the momentum transfer from

Fig. 24(a,b) Emissive Micrographs of Device R-452 showing electromigration effects.

Fig. 24(a) X200

Fig. 24(b) X2000

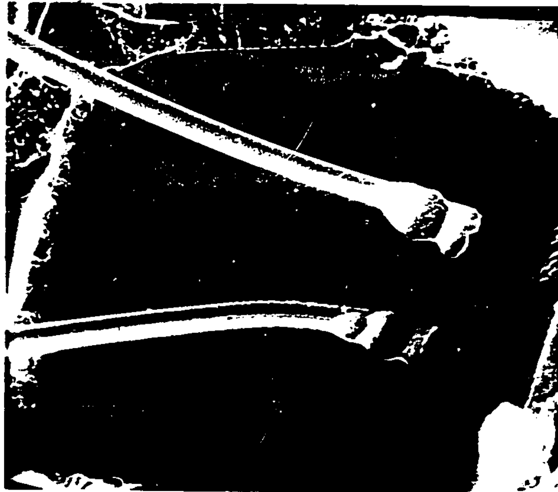

(a) X200 50µ

(b) X2000 5µ

Fig. [24(a) - (b)] Emissive Micrographs of Device R-452.

the electrons to the ions. If the electric field is high with low electron momentum transfer, as in poor electron conductors, the ions may move toward the cathode. If the momentum transfer is the more important factor, then the ions will migrate towards the anode[47,48,49]. The migration in this case was from the anode to the cathode which could be an indication that momentum transfer is not an important factor in these devices.

Device R-453

The specimen current micrograph of Fig. 25(a) shows the presence of a large area of material damage at the top of the micrograph and between the contacts. The contact metallization on the right of the micrograph is nearly broken completely across.

The contoured conductive micrograph in Fig. 25(b) shows symmetry only at the bottom of the micrograph, where the bonds and material are free of faults.

The VI characteristic is shown in Fig. 26, and is typical of devices with contacts which are damaged.

Device R-454

This device shows some characteristics of a good device. The metallization of the contacts is poor

Fig. 25(a) Specimen Current Micrograph of Device R-453.

Ac Amp. Transfer Impedance:	10 MΩ
Ac Amp. Phase:	Inverting
Device R:	295 Ω

Fig. 25(b) Contoured Conductive Micrograph of Device R-453.

Ac Amp. Transfer Impedance:	100 KΩ
Ac Amp. Phase:	Inverting
Bias:	0.2 V #1 + $V_{\acute{e}}$ (0.85 ma)
R_L:	10 KΩ
Beam Accelerating Potential:	20 kV
Contour Circuit Gain:	10
Contour Circuit Phase:	Non-Inverting
Beam Chopping Frequency:	10 kHz.

(a) X100 100μ

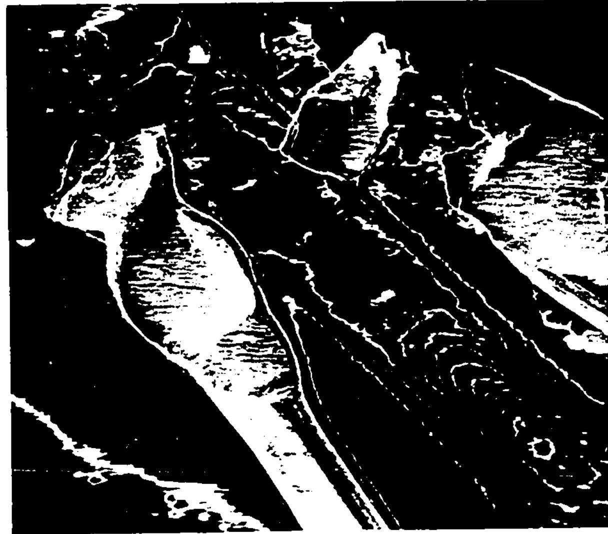

(b) X500 20μ

Fig. [25(a) - (b)] Conductive and Contoured Conductive Micrographs of Device R-453.

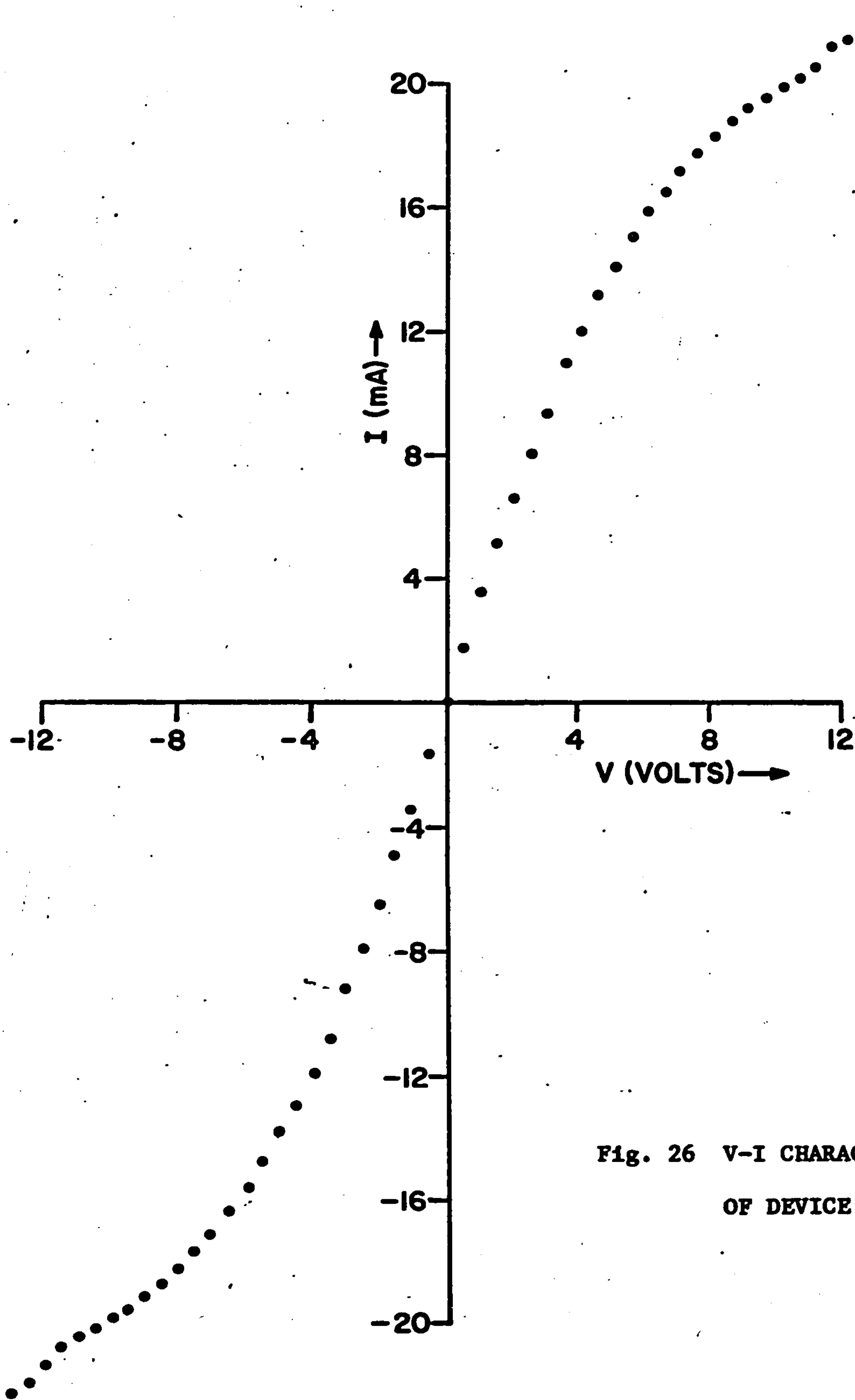

Fig. 26 V-I CHARACTERISTIC OF DEVICE R-453

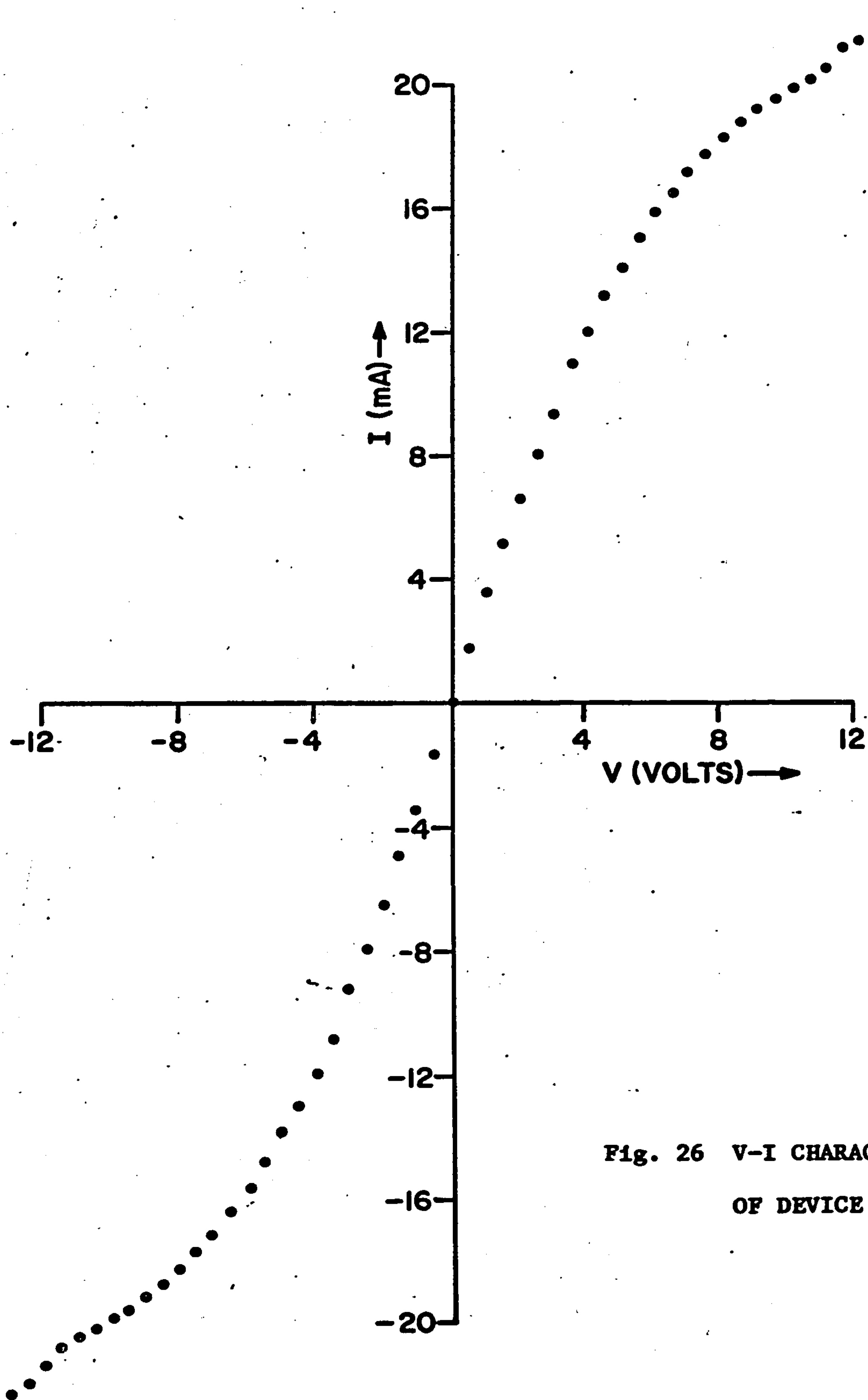

Fig. 26 V-I CHARACTERISTIC
OF DEVICE R-453

(Fig. 27a), but the material is free from major faults (Fig. 27b). The contoured conductive micrograph (Fig. 27c) shows a high degree of symmetry. The temperature profile of Fig. 28 shows a similar high degree of symmetry.

Device R-455

The specimen current micrograph, (Fig. 29a), shows many small material faults between the bonds of the device. The conductive and contoured conductive micrographs of Fig. 29(b) and 29(c) reveal a region of high signal on the left side of the micrographs. The temperatures distribution in the surface of the device is given in Fig. 30 and 31. The region of maximum heating lies in the region of lowest conductive signal in Fig. 29(b) and 29(c). This information substantiates previous evidence that the conductive signal can be related to the variation of minority carrier current, while the majority carrier current is responsible for device heating and failure (see 3.2.2.1 Conductive Micrographs).

Fig. 27(a) Emissive Micrograph of Device R-454

Fig. 27(b) Specimen Current Micrograph of Device R-454

Ac Amp. Transfer Impedance:	10 MΩ
Ac Amp. Phase:	Inverting

Fig. 27(c) Contoured Conductive Micrograph of Device R-454

Ac Amp. Transfer Impedance:	40 KΩ
Ac Amp. Phase:	Inverting
Bias:	0.46 V #2 pos. (2112 ma)
R_L:	10 KΩ
Beam Accelerating Potential:	20 kV
Contour Circuit Gain:	10
Contour Circuit Phase:	Non-Inverting
Beam Chopping Frequency:	10 kHz.

(a)

X200

50..

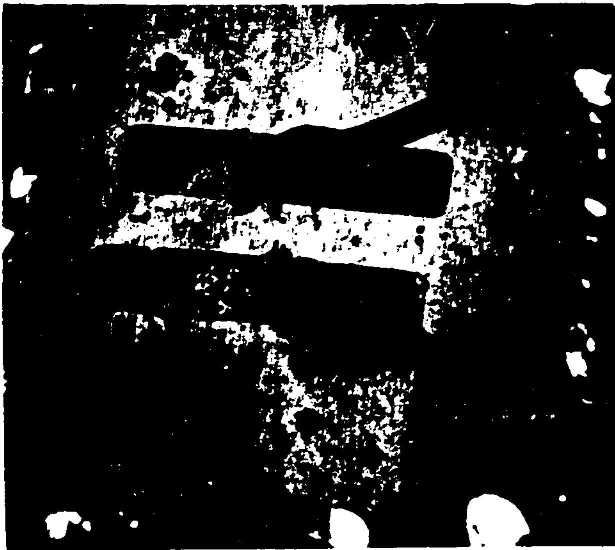

(b)

X200

50..

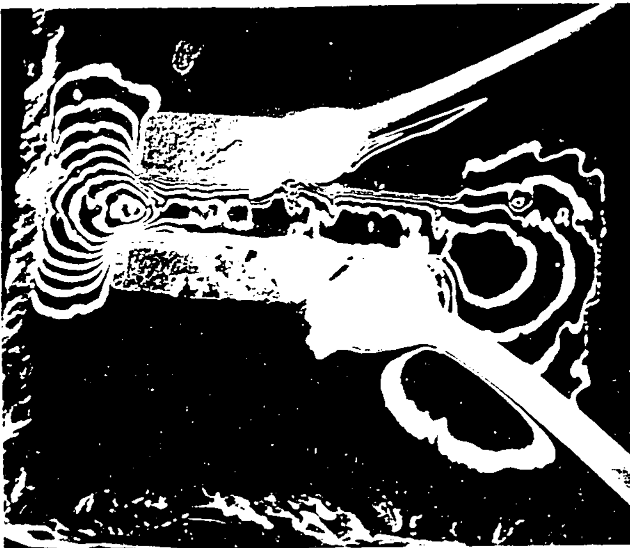

Fig. 28 Temperature Distribution in the Device R-454

Bias Voltage:	10 V
Bias Current:	25 ma

Contours of relative radiance are plotted.

Radiance given in milliwatts Steradians^{-1} cm^{-2}

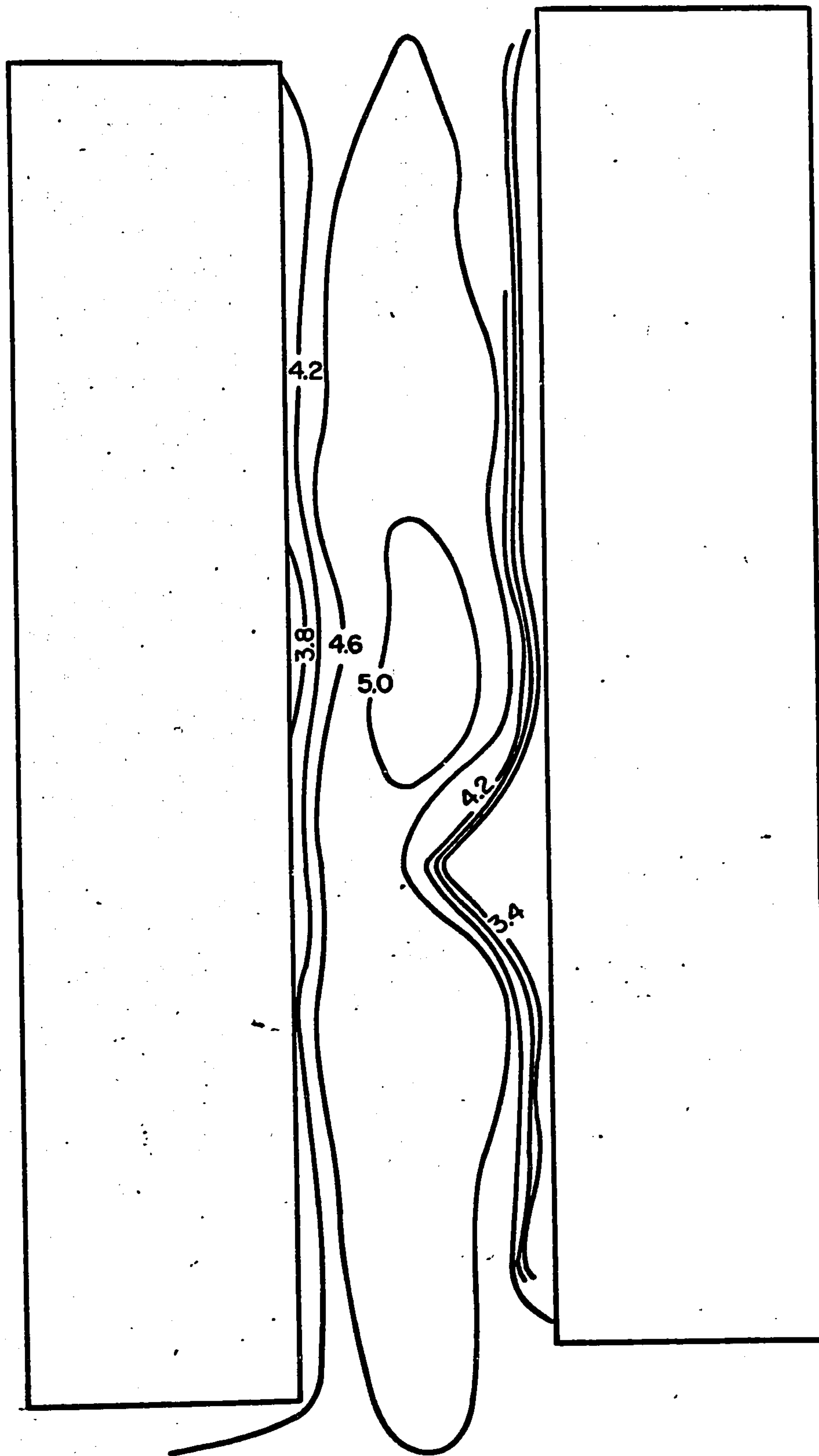

Fig. 28 TEMPERATURE DISTRIBUTION IN THE DEVICE R-454

Fig. 29(a) Specimen Current Micrograph of Device R-455

Ac Amp. Transfer Impedance:	10 MΩ
Ac Amp. Phase:	Inverting

Fig. 29(b) Conductive Micrograph of Device R-455

Ac Amp. Transfer Impedance:	4 MΩ
Ac Amp. Phase:	Inverting
Bias:	0.01 V

Fig. 29(c) Contoured Conductive Micrographs of Device R-455

Ac Amp. Transfer Impedance:	200 KΩ
Ac Amp. Phase:	Inverting
Bias:	0.2 V #1 pos. (0169)
R_L:	10 KΩ
Beam Accelerating Potential:	20 kV
Contour Circuit Gain:	10
Contour Circuit Phase:	Non-Inverting
Beam Chopping Frequency:	10 kHz

(a)

X500

20μ

(b)

X500

20μ

(c)

X500

20μ

Fig. [29(a) - (c)]

Conductive and Contoured Conductive Micrographs of Device P-455.

Fig. 30 Temperature Distribution in the Device R-455

Bias Voltage: 13.5 V
Bias Current: 18.5 ma

Radiance given in milliwatts steradians^{-1} cm^{-2}

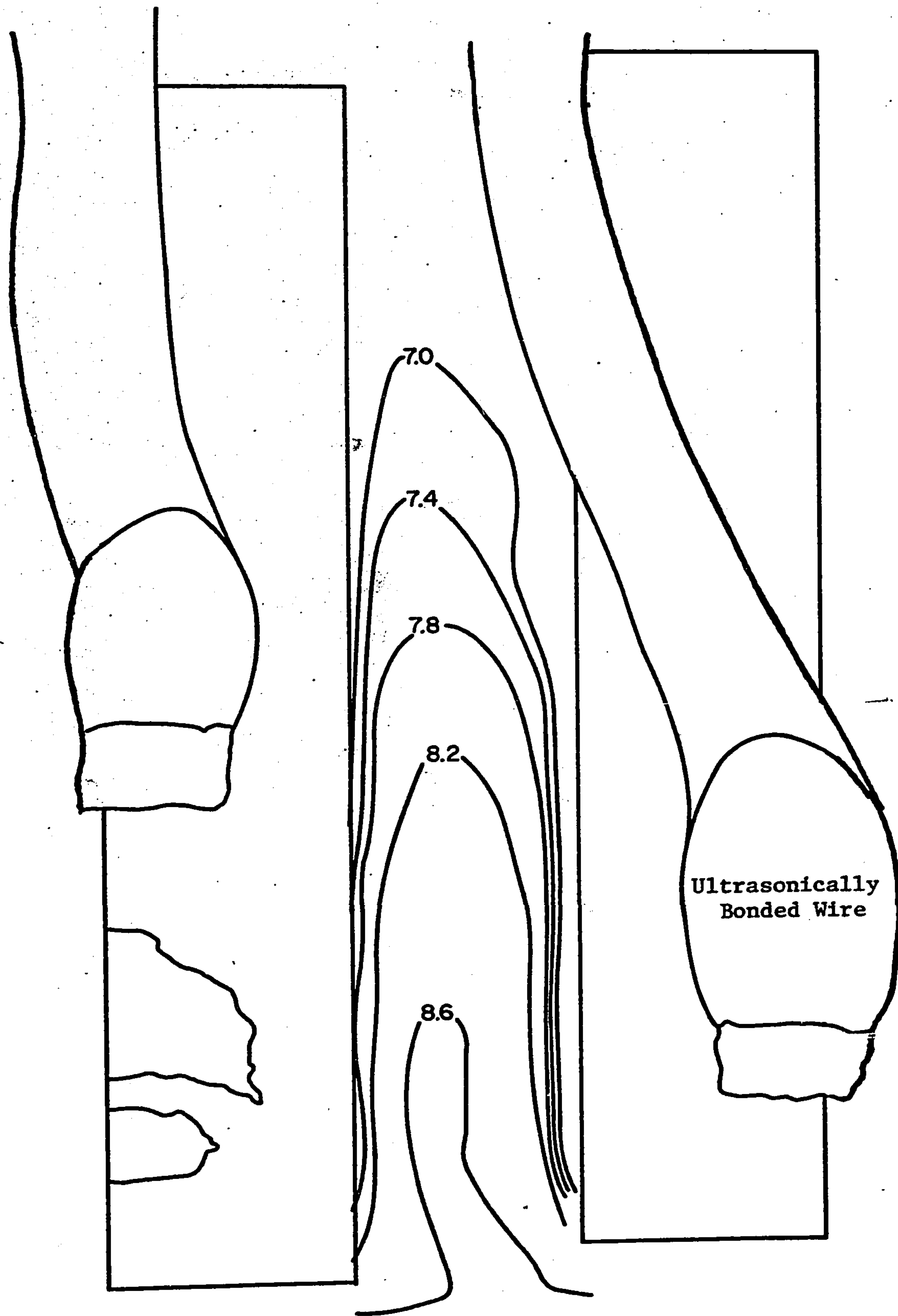

Fig. 30 TEMPERATURE DISTRIBUTION IN THE DEVICE R-455

Fig. 31 Temperature Distribution in the Device R-455

Bias Voltage:	13.5 V
Bias Current:	18.5 ma

Radiance given in milliwatts steradians^{-1} cm^{-2}

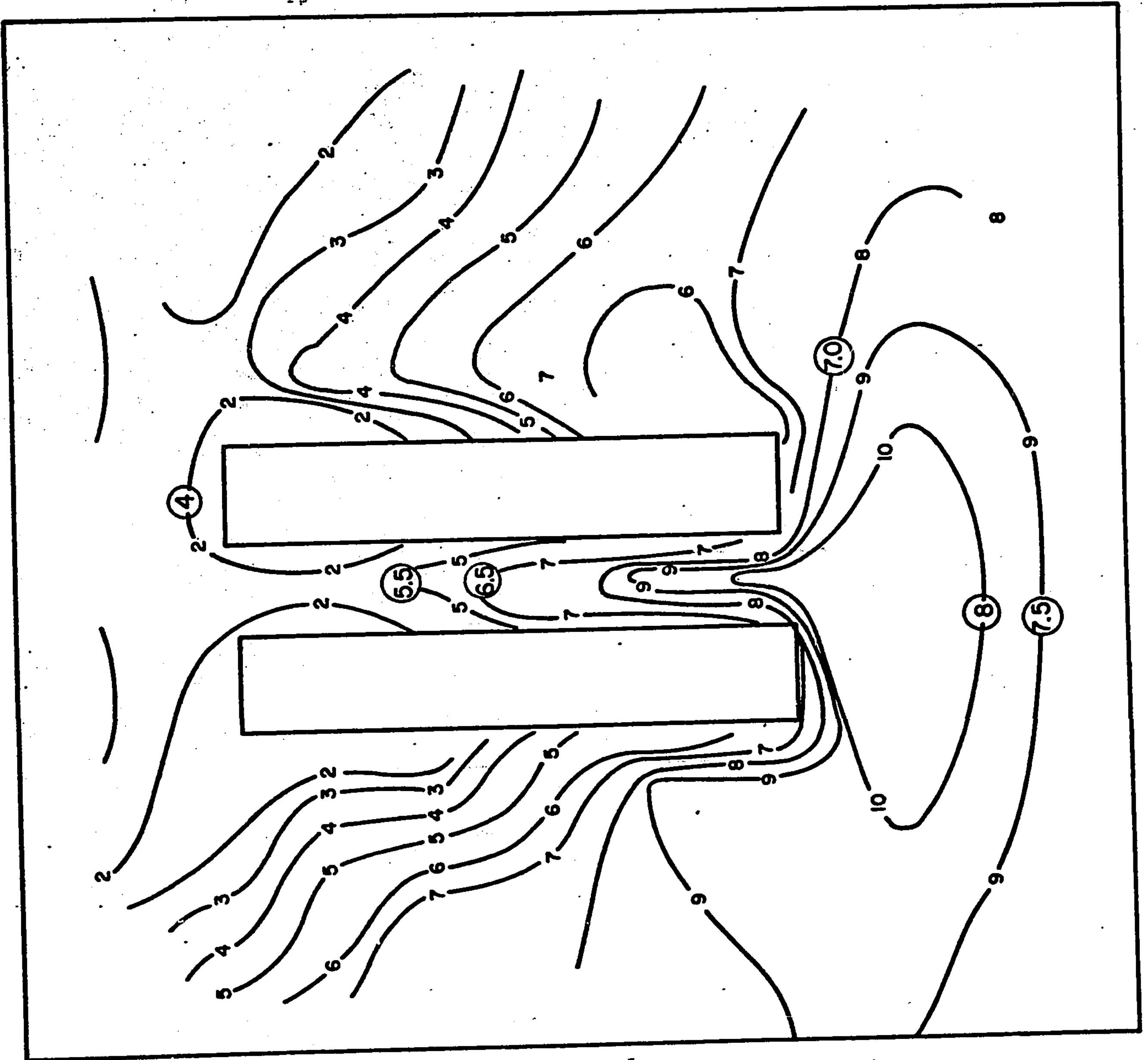

(x) Radiance Value

Fig. 31 TEMPERATURE DISTRIBUTION IN THE DEVICE R-455

3.2.2.3 The F-216 Devices

The F-216 series are transferred electron devices having a completely different geometry and contact configuration. The electrical characteristics of these devices are substantially different and the results of the SEM observations show interesting effects not present in the previous series.

Device F-216(a)

The results will be listed under the headings of the modes of operation. Emphasis will be placed on those results which differ from those given above.

Emissive Micrographs

Figures 32(a) and (b) are emissive micrographs of the device showing evidence of surface scratches. The first micrograph was taken at a low value of beam-current while the second was taken at a higher current. The dark areas at the two contacts could be contamination of the surface occurring during the bonding process.

Fig. 32(a,b) Emissive Micrographs of Device F-216a.

32(a) Taken at low beam current

32(b) Taken at high beam current

Fig. 32(c) Luminescent Micrograph of Device F-216a.

Dc Amp. Transfer Impedance:	2 MΩ
Dc Amp. Phase:	Invert
Beam Accelerating Potential:	20 kV
Beam Chopping Frequency:	10 kHz
Device Resistance:	$10^7 - 10^8$ Ω

(a)

X100

100μ

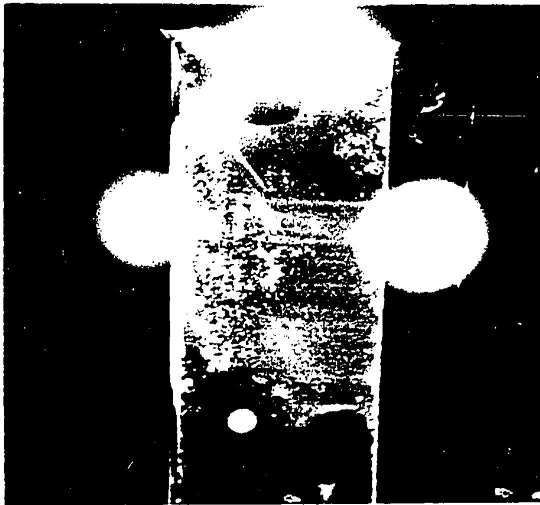

(b)

X100

100μ

Luminescent Micrograph

The luminescent micrograph of Fig. 32(c) was taken with a phase sensitive detector. The signal was too small to obtain a good micrograph otherwise. The amplifier inverted the phase of the signal so that a dark area on the micrograph corresponds to a low luminescent efficiency at the specimen. A low efficiency region results in a decreased electron current generated in the photomultiplier and a decrease in output voltage of the current amplifier (transfer impedance). The scratches in the surface resulted in a decrease in luminescence.

Conductive Micrographs

The micrographs in figures 33(a) to 33(g) show the variation in the beam induced current as a function of bias. Figure 33(a) is taken at zero bias, Figs. 33(b) to 33(d) are taken with increasing positive bias and Figs. 33(e) to 33(g) are taken with increasing negative bias. In each case, the top of the micrograph represents the biased end of the device. In this series of micrographs, the a.c. amplifier produced phase inversion. An increasing white signal represents an increasing

Fig. 33 Conductive Micrographs of Device F-216a.

(a)

Bias: 0 Volts
Ac Amp. Transfer Impedance: 4MΩ
Ac Amp. phase: Inverting

(b)

Bias: + 200mV (top contact +Vc)
Ac Amp. Transfer Impedance: 4MΩ
Ac Amp. phase: Inverting

(c)

Bias: + 9.68V
Ac Amp. Transfer Impedance: 2MΩ
Ac Amp. phase: Inverting

(d)

Bias: + BV (0.8 a)
Ac Amp. Transfer Impedance: 1MΩ
Ac Amp. phase: Inverting

(a) X90 110

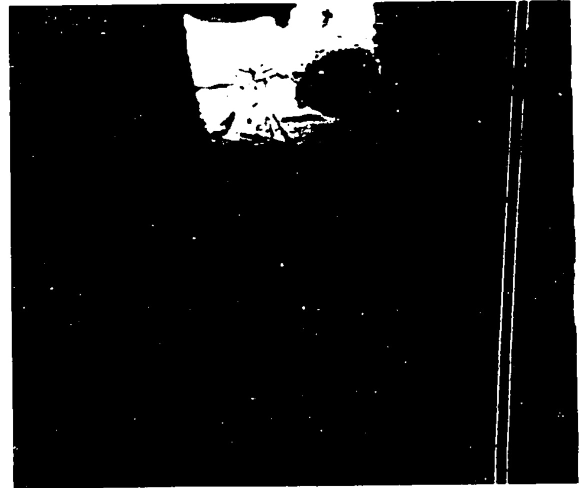

(b) X90 110

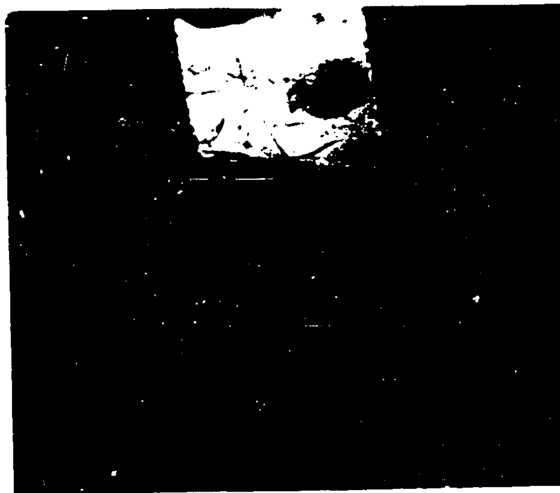

(c) X90 110

(d) X90 [illegible]

Fig. [illegible]

Fig. 33 Conductive Micrographs of Device F-216a.

(e)

Bias:	-250 mv (neg. on top contact)
Ac Amp. Transfer Impedance:	4 MΩ
Ac Amp. Phase:	Inverting

(f)

Bias:	-9.65 V
Ac Amp. Transfer Impedance:	2 MΩ
Ac Amp. Phase:	Inverting

(g)

Bias:	-13 V
Ac Amp. Transfer Impedance:	1 MΩ
Ac Amp. Phase:	Inverting

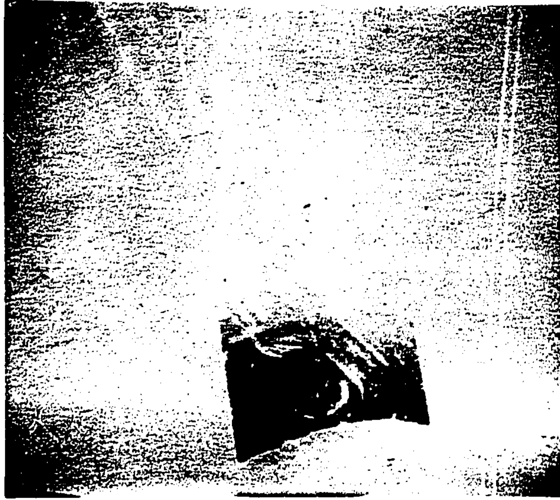

(e)

X90

110μ

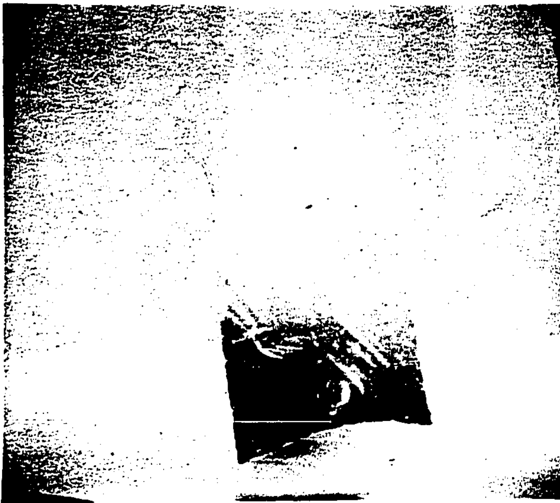

(f)

X90

110μ

(g)

X90

110μ

Fig. [33(e) - (g)]

Conductive Micrographs of Device F-216a.

electron current collected by the amplifier. Fig. 25(a) is the measuring circuit used to obtain this information.

The results in Figures 33(a) to (c) may be interpreted to mean that the minority carriers are electrons and that these drift to the positive contact under the influence of the applied field. The largest beam-induced current is then detected when the beam is close to the positive contact. Similar arguments can be applied to the case where the polarity of bias is changed. In this case, the minority electron current is toward the bottom contact which corresponds to a flow of electrons from the amplifier into the top contact. This produces a negative going output signal due to the phase inversion of the amplifier. The micrograph, therefore, appears black in the region of highest signal.

The behaviour of this device can also be analysed using conductive line scans obtained using the measuring network of Fig. 16. The line scans obtained for the positive bias applied to the top contact is shown in Fig. 34. The Fig. 35 shows the behaviour of the conductive signal for negative bias. In both cases

Fig. 34 Line Scans of Beam-Induced Current with Position of the Beam

	(a)	(b)	(c)
Ac Amp. Transfer Impedance:	10 MΩ	10 MΩ	4 MΩ
Ac Amp. Phase:	Inverting		
Bias:	0 V	+0.15 V	+2 V
R_L:	10 KΩ		
Beam Accelerating Potential:	20 kV		
Beam Current	6.0×10^{-10} Amps.		
Magnification:	140X		
Beam Chopping Frequency:	10 kHz		
PSD Time Constant:	10 mSec.		
X-Y Amplifier Sensitivity:	~500 mV/in.		
Device R:	$10^7 - 10^8$ Ω		

NOTE: Bias is applied to the top contact, signal is taken from the top contact.

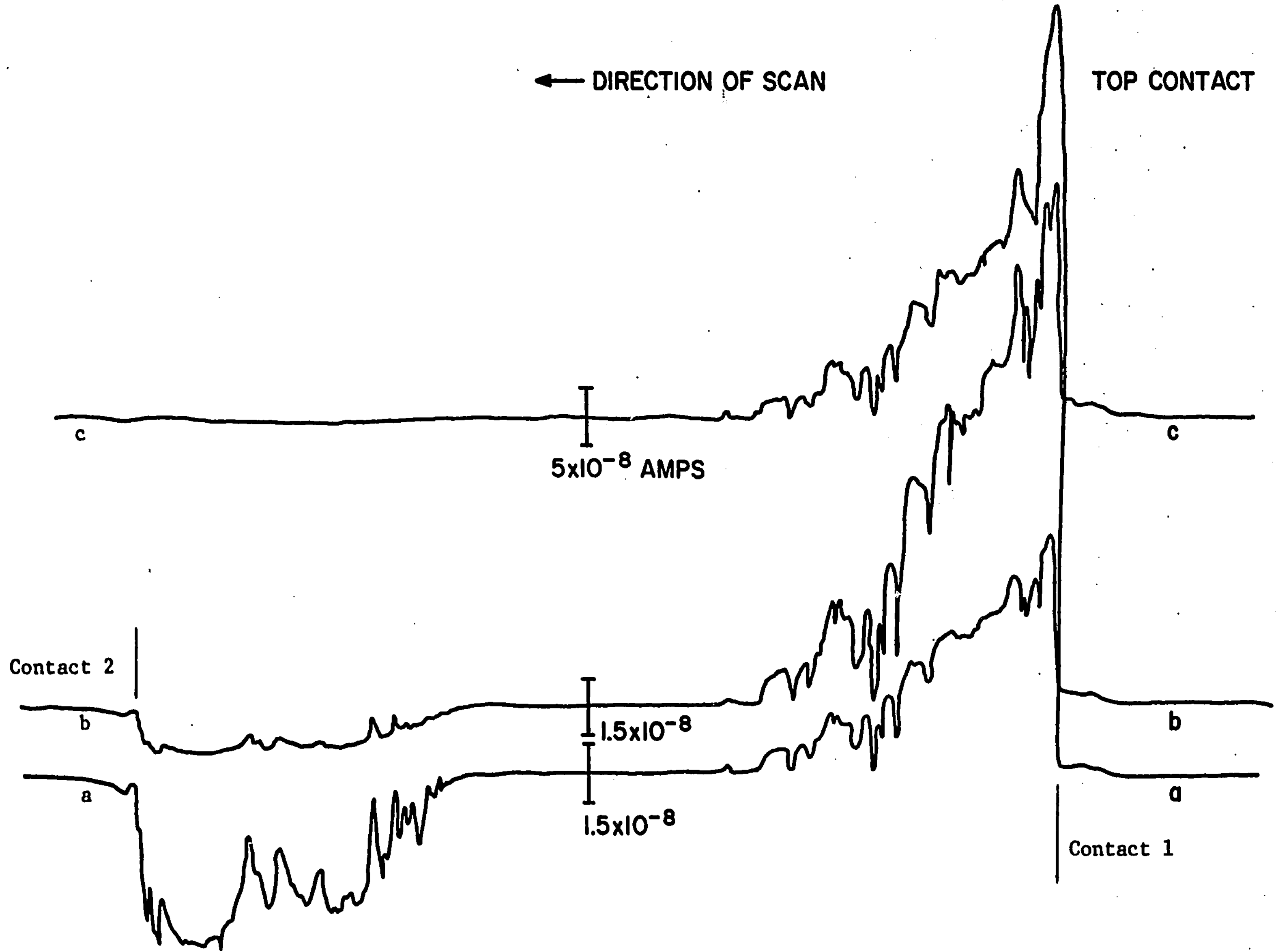

Fig. 34 LINE SCANS OF BEAM INDUCED CURRENT WITH POSITION OF BEAM

Fig. 35 Line Scans of Beam-Induced Current with Position of the Beam

	(a)	(b)	(c)
Ac Amp. Transfer Impedance:	10 MΩ	10 MΩ	4 MΩ
Ac Amp. Phase:	Inverting		
Bias:	0 V	-0.12 V	-3.0 V
R_L:	10 KΩ		
Beam Accelerating Potential:	20 kV		
Beam Current:	4×10^{-10} amps.		
Magnification:	140X		
Beam Chopping Frequency:	10 kHz		
PSD Time Constant:	10 mSec.		
X-Y Amplifier Sensitivity:	~500 mV/in.		
Device R:	$10^7 - 10^8\ \Omega$		

NOTE: Bias is applied to the top contact. Signal is taken from the top contact.

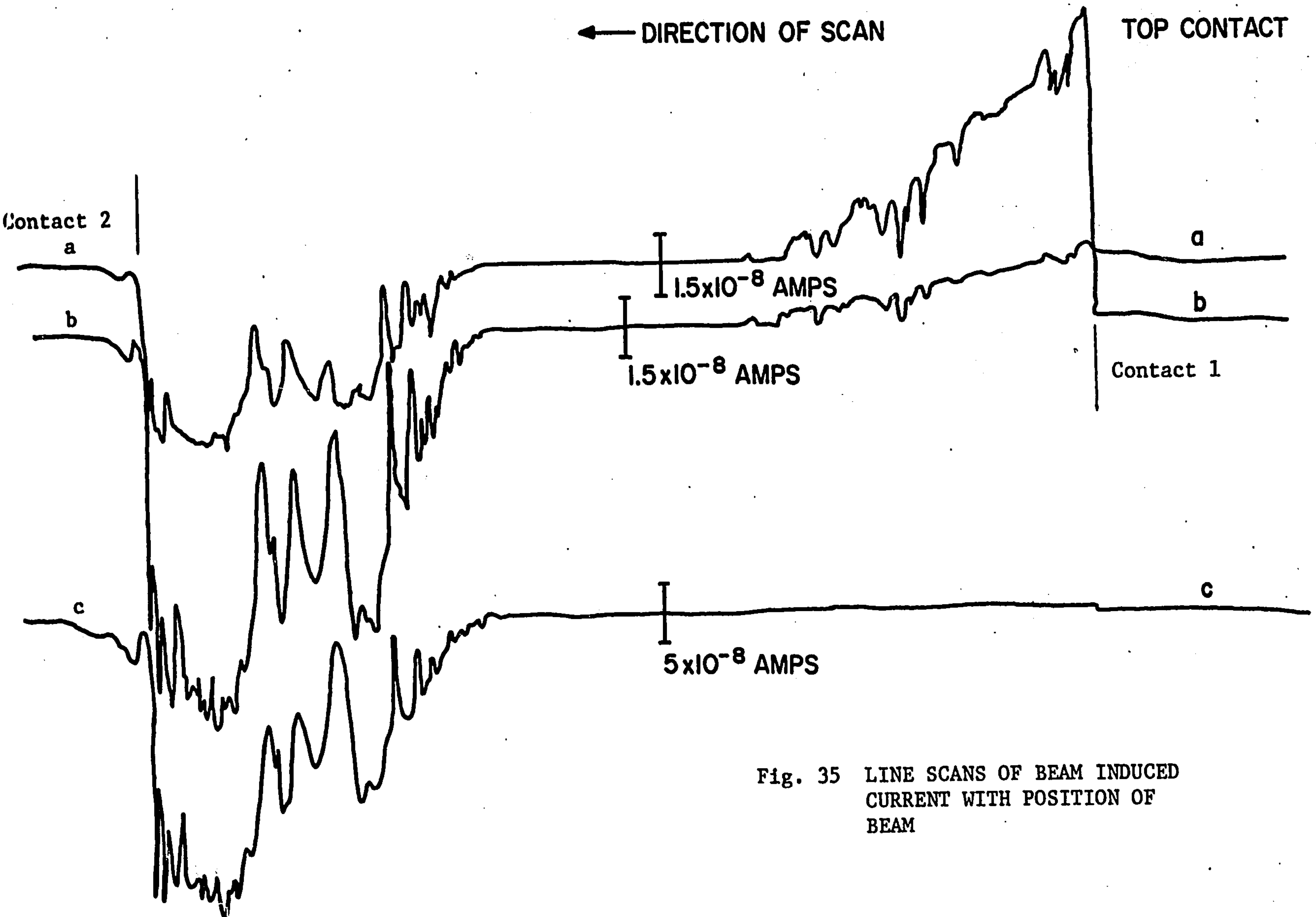

Fig. 35 LINE SCANS OF BEAM INDUCED CURRENT WITH POSITION OF BEAM

the beam is scanned from the contact #1 to which bias is applied, across the device to contact #2.

Device F-216(b)

Emissive and Luminescent Micrographs

The emissive micrograph in Fig. 36(a) shows no evidence of surface scratches or dislocation networks in the specimen surface, however, many such flaws are evident in the luminescent micrograph in Fig. 36(b). The dark regions in Fig. 36(b) corresponds to regions of low luminescence efficiency. The drying stains at the surface cause a reduction in luminescence efficiency which may be attributed to the presence of surface traps which reduces carrier lifetime.

Conductive Micrographs

The micrographs in Figs. 37(a), (b), and (c) show the variation of beam induced current as a function of bias. The a.c. amplifier does not invert the phase in this set of micrographs. The results are substantially different than those obtained for the

Fig. 36(a) Emissive Micrograph of Device F-216b.

Fig. 36(b) Luminescence Micrograph of Device F-216b.

Dc Amp. Transfer Impedance:	50 MΩ
Dc Amp. Phase:	Inverting
Beam Accelerating Voltage:	20 KV
Device Resistance:	4.5×10^5 Ω

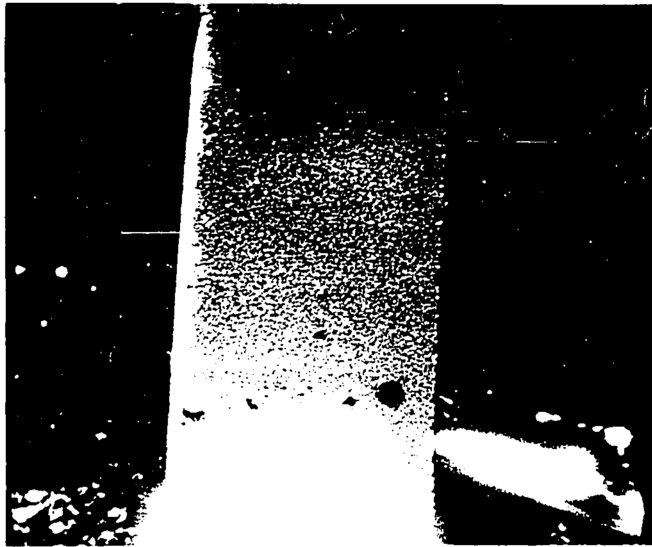

(a) X125 80μ

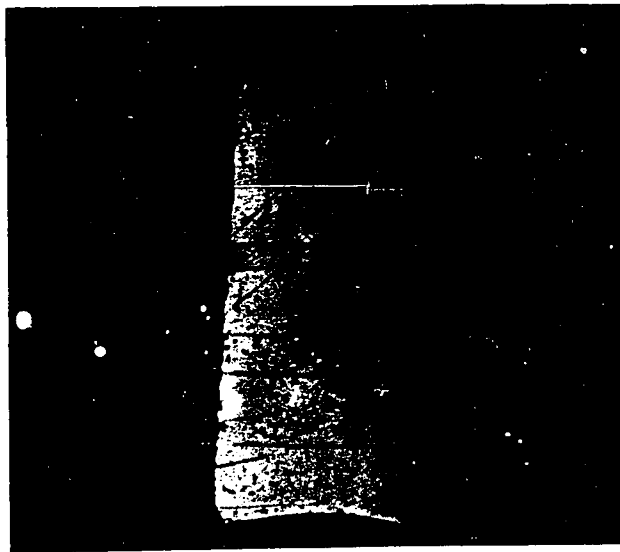

(b) X125 80μ

Fig. [36(a) - (b)] Emissive and Luminescent Micrographs of Device F-216b.

Fig. 37 Conductive Micrographs of Device F-216b.

(a)

Ac Amp. Transfer Impedance:	400 KΩ
Ac Amp. Phase:	Non-Inverting
Bias:	+2 V (Top contact + V_e)
R_L:	10 KΩ
Beam Accelerating Voltage:	20 kV
Beam Chopping Frequency:	5 kHz

(b)

Ac Amp. Transfer Impedance:	10 MΩ
Ac Amp. Phase:	Non-Inverting
Bias:	0 Volts
R_L:	10 KΩ
Beam Accelerating Voltage:	20 kV
Beam Chopping Frequency:	5 kHz

(c)

Ac Amp. Transfer Impedance:	400 KΩ
Ac Amp. Phase:	Non-Inverting
Bias:	-2 V (Top contact - V_e)
R_L:	10 KΩ
Beam Accelerating Voltage:	20 kV
Beam Chopping Frequency:	5 kHz

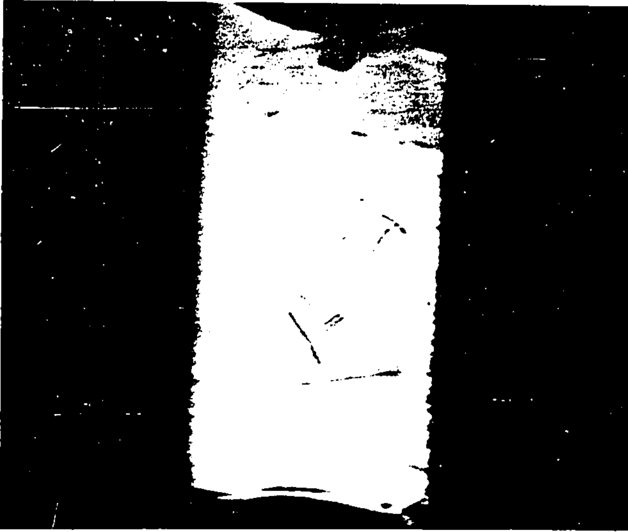

(a)

X125

80μ

(b)

X125

80μ

(c)

X125

80μ

Fig. [37(a) - (c)]

Conductive Micrographs of Device F-216b.

devices F-216(a). The line scans in Figs. 38 and 39 also show the variation of beam induced current with bias. The mechanisms responsible for these results are not understood.

3.3 Results of Computer Analysis

In the preceding sections, experimental results were given. These results illustrate, primarily, the type of qualitative information which can be obtained from an SEM. This section will present the results of the computer model, developed in Chapter II, for the interpretation of the quantitative measurements.

The results to be discussed below, are obtained for an analysis of the beam-induced voltage or current in the special case of small resistivity modulation, as discussed in section 2.1. The continuity equation has been solved to obtain the distribution of generated carriers from which the photovoltage (beam-induced voltage) was calculated. The photovoltage was obtained for two assumed specimen resistivity variations. The details of the solution are given in sections 2.2.4 to 2.2.6.

Fig. 38 Line Scan of Beam-Induced Current with Position of the Beam

	(a)	(b)	(c)
Ac Amp. Transfer Impedance:	1 MΩ	1 MΩ	1 MΩ
Ac Amp. Phase:	Non-Inverting		
Bias:	0 V	0.52 V	2.0 V
R_L:	10 KΩ		
Beam Accelerating Potential:	20 kV		
Beam Current:	8.4×10^{-9} Amps.		
Magnification:	X125		
Beam Chopping Frequency:	10 kHz		
PSD Time Constant:	1 mS		
X-Y Amplifier Sensitivity:	~500 mV/in.		
Device R	4.5×10^{5} Ω		

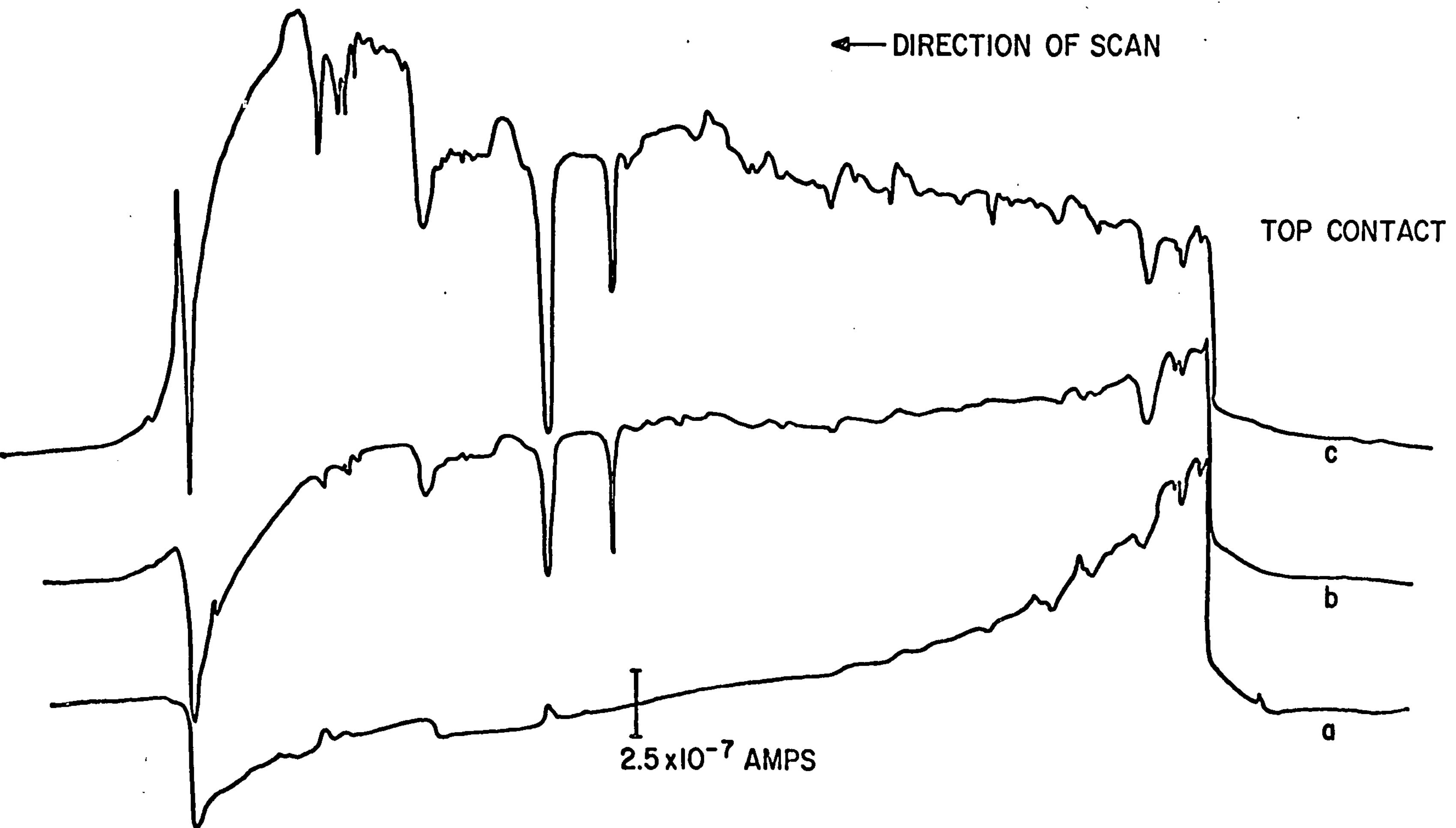

Fig. 38 LINE SCAN OF BEAM INDUCED CURRENT WITH POSITION OF BEAM

Fig. 39 Line Scan of Beam-Induced Current with Position of the Beam

	(a)	(b)	(c)
Ac Amp. Transfer Impedance:	1 MΩ	1 MΩ	400 KΩ
Ac Amp. Phase:	Non-Inverting		
Bias:	0 V	-0.52	-3.0
R_L:	10 KΩ		
Beam Accelerating Potential:	20 kV		
Magnification:	X125		
Beam Chopping Frequency:	10 kHz		
PSD Time Constant:	1 mSec.		
X-Y Amplifier Sensitivity:	~500 mV/in.		
Device R:	4.5×10^5 Ω		

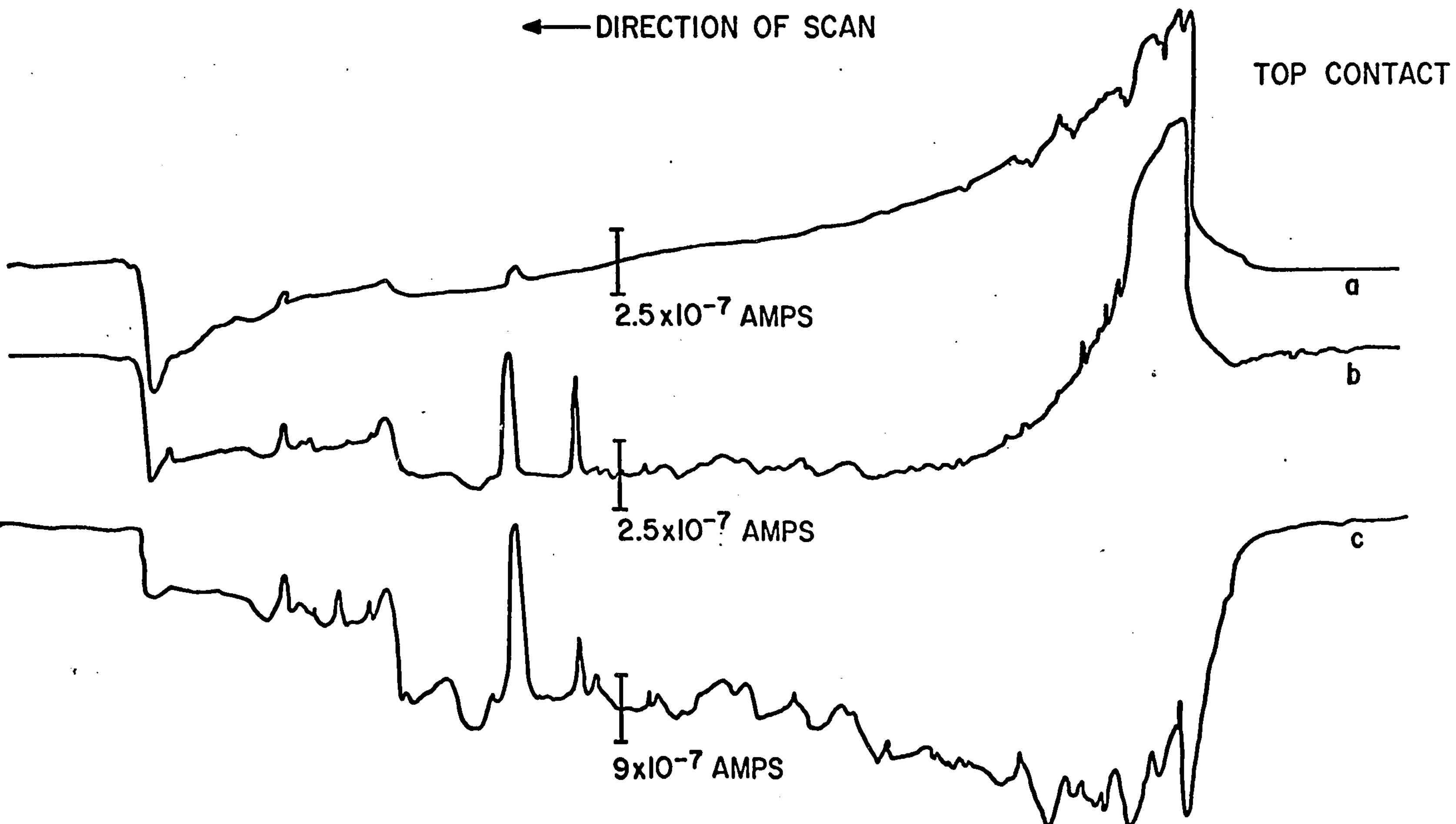

Fig. 39 LINE SCANS OF BEAM INDUCED CURRENT WITH POSITION OF BEAM

In this analysis, a one dimensional geometry was assumed. This is equivalent to the assumption that the specimen width is small with respect to the diffusion length.

The first part of the analysis consists of obtaining the distribution of the generated carriers as a function of beam position. The Fig. 40 shows the distribution of generated carriers when the beam is at the centre of the specimen. The curves show the effect of an applied electric field in the negative x direction. At zero field, the distribution is symmetrical, but as an electric field is applied, the distribution becomes assymmetrical. The minority carriers, holes in this analysis, are subject to a force in the negative x direction. The effect of the electric field may be minor in the given case, when the beam is in the central region. However, the device length was taken to be 100μ (see section 2.2.4) for a device with a short active region, the effect of the electric field would be important.

The results of the photovoltage calculations are given in Fig. 41 and Fig. 42. The photovoltage is obtained by integration of the minority carrier

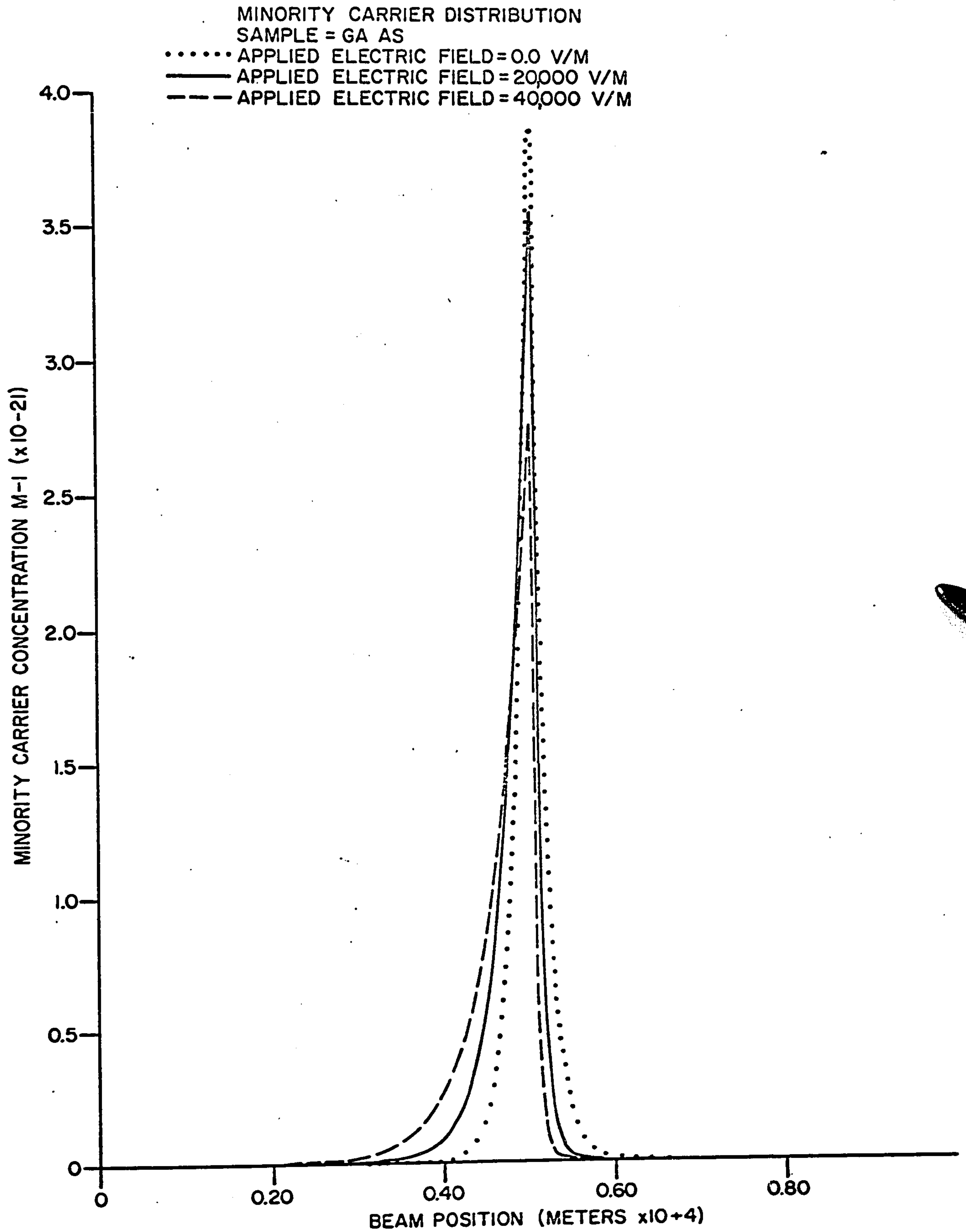

Fig. 40 MINORITY CARRIER DISTRIBUTION

distribution, multiplied by the specimen resistivity for beam positions at regular intervals along the specimen. Since the applied electric field affects the carrier distribution, the generated photovoltage is also modified. In Fig. 41, the photovoltage and the specimen resistivity are plotted as a function of electron beam position. The specimen resistivity is assumed to vary sinusoidally along the specimen. The photovoltage is expected to be proportional to the derivative of the resistivity variation (see section 2.2). The computer results show this with an error in the phase shift. The applied electric field results in a further phase shift which can be attributed to the modification of the generated carrier distribution. The photovoltage decreases in amplitude near the contacts, due to a decrease in the peak value of the generated carrier distribution.

In Fig. 42, the results of a similar analysis are given. In this case, the resistivity variation is a step function. The photovoltage approximates the derivative of the resistivity distribution of the specimen. The best approximation occurs with no applied electric field.

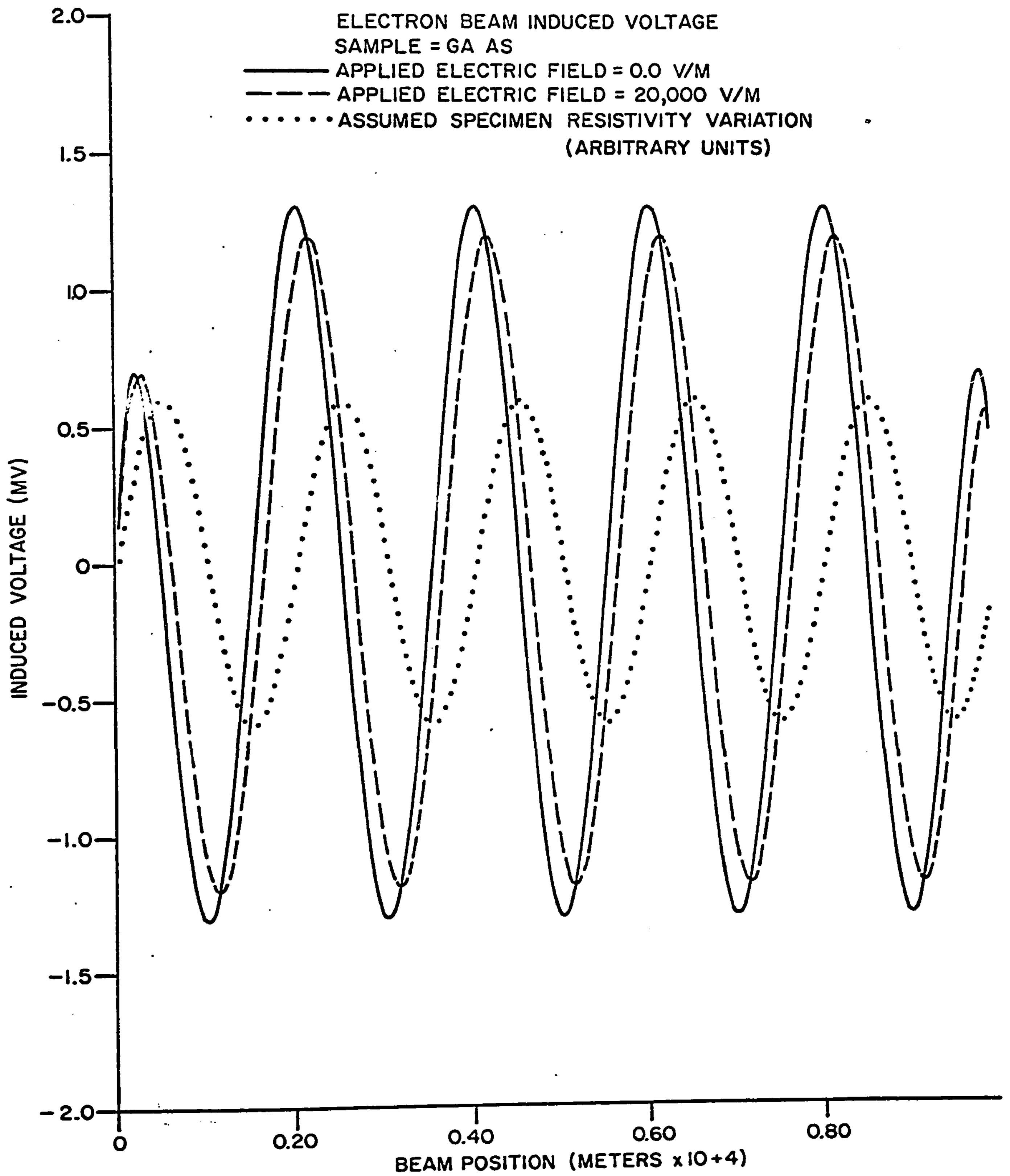

Fig. 41 ELECTRON BEAM INDUCED VOLTAGE

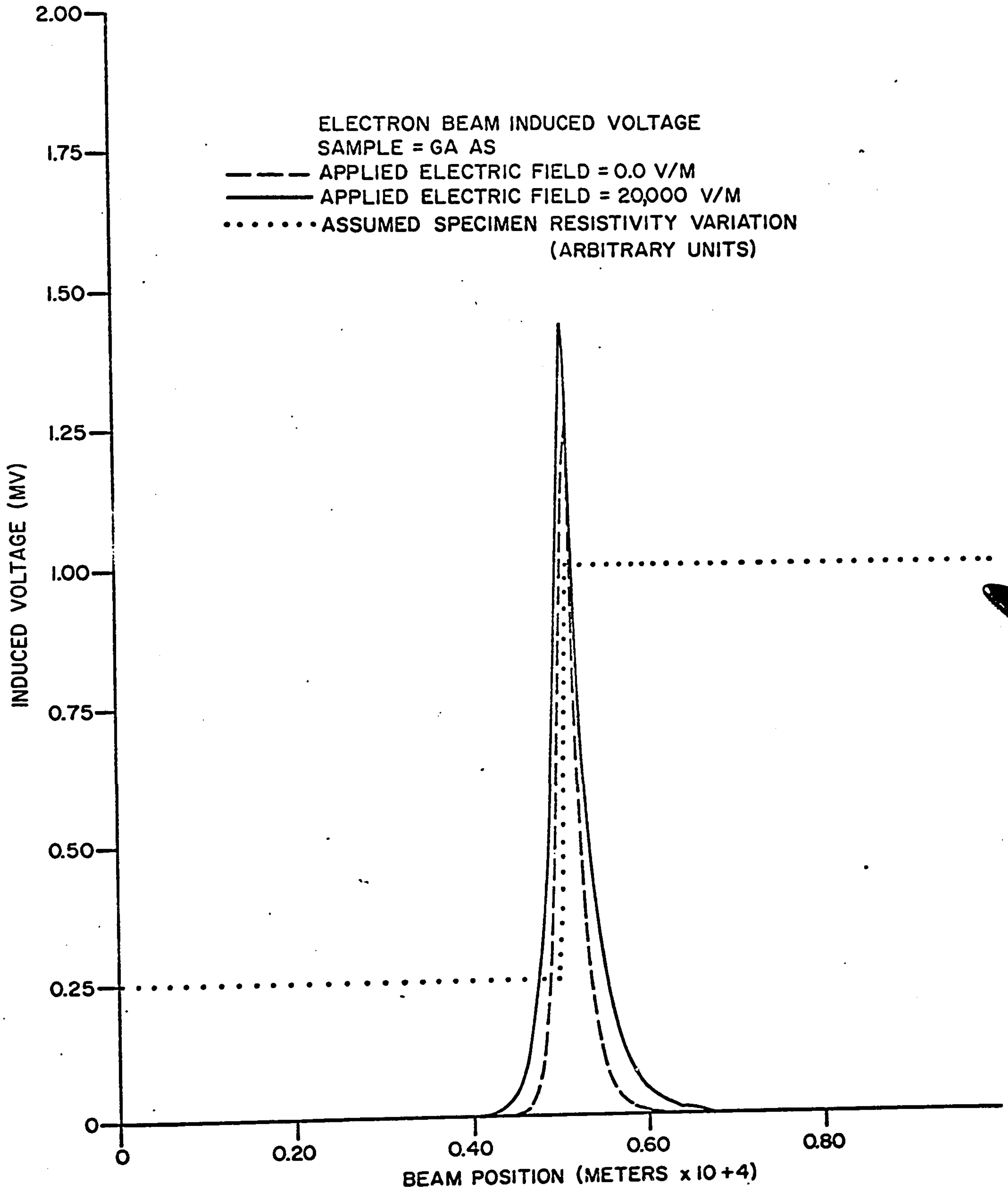

Fig. 42 ELECTRON BEAM INDUCED VOLTAGE

In both cases of sinusoidal and a step resistivity variation, the photovoltage could be integrated to obtain an approximation of the resistivity variation. The best approximation would be obtained in a region several diffusion lengths away from the contacts with no applied electric field.

In section 2.2.7, the condition for negligible internal electric field was derived. It was shown that the electric field is negligible, if the variation in impurity concentration occurs in a distance large, compared to $2L_p$. In the above discussion of the photovoltage, it was assumed that the built-in field is negligible. However, substantial built-in fields are possible in practice if the impurity gradient is large in the specimen. This occurs in specimens which contain p-n junctions.

The computer results showed that the conductive mode of operation yields the resistivity variation of a specimen. This variation showed expected deterioration at the contacts and a phase shift relative to the actual resistivity variation when an electric field is established in the specimen. However, a decrease in the amplitude of the signal with increasing electric field is predicted, which is not consistent with experimental results. The model developed for the interpretation of quantitative results is, therefore, only partially valid.

CONCLUSION

The analysis given in the previous chapters illustrates the large amount of data, both qualitative and quantitative, that can be obtained from SEM measurements. This information is obtained over a two dimensional surface and is equivalent to large numbers of point data. The micrographs of Chapter III give comparisons of impurity concentration in the cathodoluminscent mode of operation; surface information, such as metallization and bond quality are obtained in the emissive mode. The areas of high electric field are detected in the conductive mode.

The SEM is only one member of a class of electron beam instruments. Its major difference from the other instruments is its scanning feature. It yields lower resolution information than other electron beam instruments such as the transmission electron microscope, with a resolution of 5Å. However the SEM's resolution in the emissive mode is higher (100Å) and its depth of field is greater than that of an optical microscope.

In any give mode of operation, the resolution of a measurement may not be determined by the beam diameter. The phenomenon giving rise to the signal observed can be the limiting factor.

In the luminescent mode, the resolution is lower than the above, because the escape distance of generated light is larger than for electrons. In the conductive mode, the resolution is also lower than in the emissive mode because the signal originates from the plasma of electron-hole pairs.

The factors discussed above vary with the specimen because the ionization energy determines the number of collisions which an electron beam suffers before completely losing its energy. The larger the number of collisions, the larger the extent of the plasma region. Thus, in general, it is more correct to consider the resolution of the phenomenon in a given specimen rather than the resolution of the instrument in discussing the resolution of the measurement.

The versatility of the SEM can be extended by the incorporation of X-ray and Auger electron detectors and in this role becomes a microprobe analyser, making it possible to obtain a positive identification of impurities in a sample. Because of the scanning facility, the presence of a given impurity can be located over a two dimensional surface. The technique of x-ray microanalysis can detect a weight of 10^{-15} gm in a volume of $10(\mu m)^3$ assuming a density of 10 gm/cm^3.

The technique of Auger spectroscopy is applicable to elements of low atomic number and, therefore, complements x-ray microanalysis. The amplitude of Auger peaks depends on the deposition thickness and, therefore, on changes in surface coverage. A change of a few percent of a Monolayer can be detected from this variation[50].

Interpretation of Results

The above discussion illustates the versatility of the SEM. However, the main difficulty lies in the interpretation of the results.* Proposed interpretations have been based on bulk properties, and are not completely satisfactory. Three reasons for these difficulties are possible.

a) Some relevant bulk property may have been overlooked.

b) Surface properties may be responsible for the observed behaviour.

c) Because of the high resolution of electron beam measurements, the theory based on bulk phenomena, may not be valid.

* See the computer analysis results in section 3.3.

Of these three possibilities, the last two are more likely to yield an explanation of the observed results. The reason for this is that the validity of bulk theory depends on the significance of the statistical nature of the observed quantity in the volume, defined by the limits of resolution of the technique. For example, if in the volume defined by the resolution, few impurities are found, then the analysis of the beam-induced voltage to determine resistivity variation no longer applies.

A theory for dealing with the above type of problem might be developed from the hypothesis of section 2.5, where it was suggested that a field structure will exist in any lightly doped semiconductor when observed with the above resolution. However, the hypothesis was based only on the results presented in this thesis and many more data will be required for the development and testing of such a theory. Thus, this thesis shows that the Scanning Electron Microscope is an instrument which allows a new type of data to be collected about devices and materials. It is not surprising that new theory may be required for their interpretation. This thesis presents typical data and an attempt at an hypothesis.

APPENDIX I

The Photovoltage Generation in Semiconductors

From thermodynamics, the expression of photovoltage can be expressed as follows[29]:

$$V_{ph} = \frac{1}{e} \oint (t_n \, d\xi_n - t_p \, d\xi_p) \qquad (1)$$

where:

$t_n = \sigma_n/\sigma$

$t_p = \sigma_p/\sigma$

ξ_n, ξ_p = chemical potential of electrons and hole ensembles.

The following diagram gives the chemical potentials.

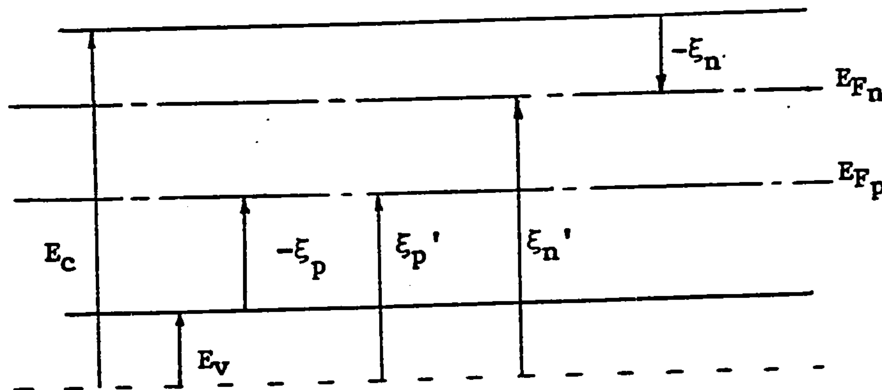

Energy notation in a homogeneous semiconductor with excess carrier concentrations under non-equilibrium conditions. E_{F_n}, E_{F_p} are Quasi Fermi levels.

Defining $\Delta\xi_n$ and $\Delta\xi_p$ as follows:

$$\Delta\xi_n = \xi_n - \xi_{no}$$

$$\Delta\xi_p = \xi_p - \xi_{po}$$

where:

ξ_{no}, ξ_{po} are the chemical potentials at equilibrium conditions of electron and hole ensembles.

The equation 1 becomes:

$$V_{ph} = \frac{1}{e} \oint (t_n \, d\Delta\xi_n - t_p \, d\Delta\xi_p) \qquad (2)$$

since:

$$d\xi_{no} = - d\xi_{po}$$

$$t_n + t_p = 1$$

The emf V_{ph} is zero when the semiconductor is not illuminated, that is $\Delta\xi_n = \Delta\xi_p = 0$. An emf exists only at non-equilibrium conditions. The emf V_{ph} is also zero when the semiconductor is homogeneous, that is:

$$\frac{d}{dx}\Delta\xi_n = \frac{d}{dx}\Delta\xi_p = 0$$

The generation of an emf depends upon the simultaneous presence of inhomogeneities and non-equilibrium carrier concentrations. The most important case of an inhomogeneity is a variation in donor and acceptor concentration along the sample.

A number of assumptions are made in the analysis of the photovoltage. These are made to simplify the derivation to follow and any analysis involving photovoltages. The assumptions are:

1. The crystal is neutral even during illumination.
2. One dimensional geometry is assumed. The thickness of the sample is small compared to the diffusion length.
3. All the impurities are ionized at room temperature.
4. The ratio of the mobilities, $b = \mu_n/\mu_p$ is a constant.
5. Classical statistics hold, even though the specimen is illuminated, that is, $n \ll N_c$ and $p \ll N_v$.

From Maxwell-Boltzmann statistics, the density of free electrons and holes can be written as follows:

$$n = N_c \exp(E_F - E_c)/kT$$

or

$$n = N_c \exp \xi_n/kT$$

$$p = N_v \exp \xi_p/kT$$

and then

$$\Delta\xi_n = \xi_n - \xi_{no} = kT \ln n/n_o$$

or

$$\Delta\xi_n = kT \ln (1 + \frac{\Delta n}{n_o})$$

$$\Delta\xi_p = kT \ln (1 + \frac{\Delta p}{p_o})$$

The rate of change of $\Delta\xi_n$ and $\Delta\xi_p$ with position are given by $\frac{d}{dx} \Delta\xi_n$ and $\frac{d}{dx} \Delta\xi_p$.

$$\frac{d}{dx} \Delta\xi_d = kT \frac{1}{1 + \frac{\Delta n}{n_o}} \cdot \frac{1}{n_o} \frac{d}{dx} \Delta n + kT \frac{1}{1 + \frac{\Delta n}{n_o}} (- \frac{\Delta n}{n_o^2}) \frac{dn_o}{dx} \tag{3}$$

$$\frac{d}{dx} \Delta\xi_p = kT \frac{1}{1 + \frac{\Delta p}{p_o}} \cdot \frac{1}{p_o} \frac{d}{dx} \Delta p + kT \frac{1}{1 + \frac{\Delta p}{p_o}} (- \frac{\Delta p}{p_o^2}) \frac{dp_o}{dx} \tag{4}$$

Substituting equations 3 and 4 into 2, the following expression is obtained:

$$V_{ph} = \frac{1}{e}\int [tn\,(-kT\,\frac{1}{1+\frac{\Delta n}{n_o}}\cdot\frac{\Delta n}{n_o^2}\frac{dn_o}{dx} + kT\,\frac{1}{1+\frac{\Delta n}{n_o}}\,\frac{1}{n_o}\,\frac{d}{dx}\,\Delta x)$$

$$+\ tp\,(kT\,\frac{1}{1+\frac{\Delta p}{p_o}}\cdot\frac{\Delta p}{p_o^2}\,\frac{dp_o}{dx} - kT\,\frac{1}{1+\frac{\Delta p}{p_o}}\,\frac{1}{p_o}\,\frac{d\Delta p}{dx})]\,dx \qquad (5)$$

However:

$$t_n = \frac{\sigma n}{\sigma} = (\frac{\mu_n n}{\mu_n n + \mu_p p})$$

$$t_p = \frac{\sigma p}{\sigma} = (\frac{\mu_p p}{\mu_n n + \mu_p p})$$

$$n = n_o + \Delta n \quad , \quad \Delta n < n_o$$

$$p = p_o + \Delta n \quad , \quad \Delta p < p_o$$

Substituting these relations into equation 5, the following expression is obtained:

$$V_{ph} = \frac{kT}{e}\int [-\frac{\mu_n}{\mu_n n + \mu_p p}\,\frac{\Delta n}{n_o}\,\frac{dn_o}{dx} + \frac{\mu_n}{\mu_n n + \mu_p p}\,\frac{d\Delta n}{dx}$$

$$+\ \frac{\mu_p}{\mu_n n + \mu_p p}\,\frac{\Delta n}{p_o}\,\frac{dp_o}{dx} - \frac{\mu_p}{\mu_n n + \mu_p p}\,\frac{d\Delta x}{dx}]\,dx \qquad (6)$$

From the relation $n_o p_o = n_i^2$ the equilibrium hole concentration p_o can be eliminated, and the equation 6 becomes:

$$V_{ph} = -\frac{kT}{e}\int \frac{\mu_n + \mu_p}{\mu_n n + \mu_p p}\,\frac{\Delta n}{n_o}\,\frac{dn_o}{dx}\,dx + \frac{kT}{e}\int \frac{\mu_n - \mu_p}{\mu_n n + \mu_p p}\,\frac{d\Delta n}{dx}\,dx \tag{7}$$

This equation applies for n-type material, a similar expression for p-type material can be obtained by eliminating n_o from equation 6. The first term is V_c, the second is V_d.

V_c is the chemical potential

V_d is the diffusion potential (Dember emf.).

Further simplification is possible for the case of weak illumination. In this case, the change in conductivity is small relative to the equilibrium conductivity.

$$\Delta\sigma < \sigma_o$$

also

$$n_i^2 < n_o^2$$

From 7 V_c can be written as follows:

$$V_c = -\frac{kT}{e}\int \frac{(\mu_n + \mu_p)\,\Delta n}{\mu_n n_o^2 + \mu_p n_i^2 + \Delta n\, n_o(\mu_n + \mu_p)}\,\frac{dn_o}{dx}\,dx$$

which becomes:

$$V_c = -\frac{kT}{e} \int \frac{\Delta\sigma}{\sigma_o^2} \frac{d\sigma_o}{dx} \, dx \tag{8}$$

but

$$\sigma_o = 1/\rho_o$$

hence

$$V_c = \frac{kT}{e} \int \Delta\sigma \frac{d\rho_o}{dx} \, dx \tag{9}$$

From equation 7, V_d can be written as follows:

$$V_d = \frac{kT}{e} \frac{\mu_n - \mu_p}{\mu_n + \mu_p} \int \frac{(\mu_n + \mu_p)}{\mu_n n + \mu_p p} \frac{d}{dx} \Delta n \, dx$$

or

$$V_d = -\frac{kT}{e} \frac{\mu_n - \mu_p}{\mu_n + \mu_p} \int \Delta\sigma \frac{d\rho_o}{dx} \, dx \tag{10}$$

The photovoltage can be written from equations 9 and 10 as follows:

$$V_{ph} = V_c + V_d$$

$$V_{ph} = 2 \frac{kT}{e} \left(\frac{1}{1 + b}\right) \int \Delta\sigma \frac{d\rho_o}{dx} \, dx \tag{11}$$

This equation holds for n-type materials. For p-type materials:

$$V_{ph} = -2 \frac{kT}{e} \frac{b}{1 + b} \int \Delta\sigma \frac{d\rho_o}{dx} \, dx \tag{12}$$

Equations 11 and 12 express the photovoltage for the case of weak illumination and are the basis of the analysis of Chapter II.

APPENDIX II

The Computer Program

The flow chart given below describes the program written for the calculation of the photovoltage. The sample is assumed to have a sinusoidal resistivity variation.

The main program calculates the distribution of minority carriers for a given beam position and finds the photovoltage generated for this beam position. The photovoltage is computed for 200 positions along the specimen, and these calculations are repeated for three values of applied electric field.

Two subroutines are called in the main program. The first is a Gauss elimination to solve a family of six linear equations in six unknowns. These are the constants in the solutions of the continuity equation. The second subroutine is an IBM numerical quadrature program from the system 360SSP package. This subroutine evaluates the integral to obtain the photovoltage from the product of carrier distribution and the first derivative of the specimen resistivity.

MAIN PROGRAM

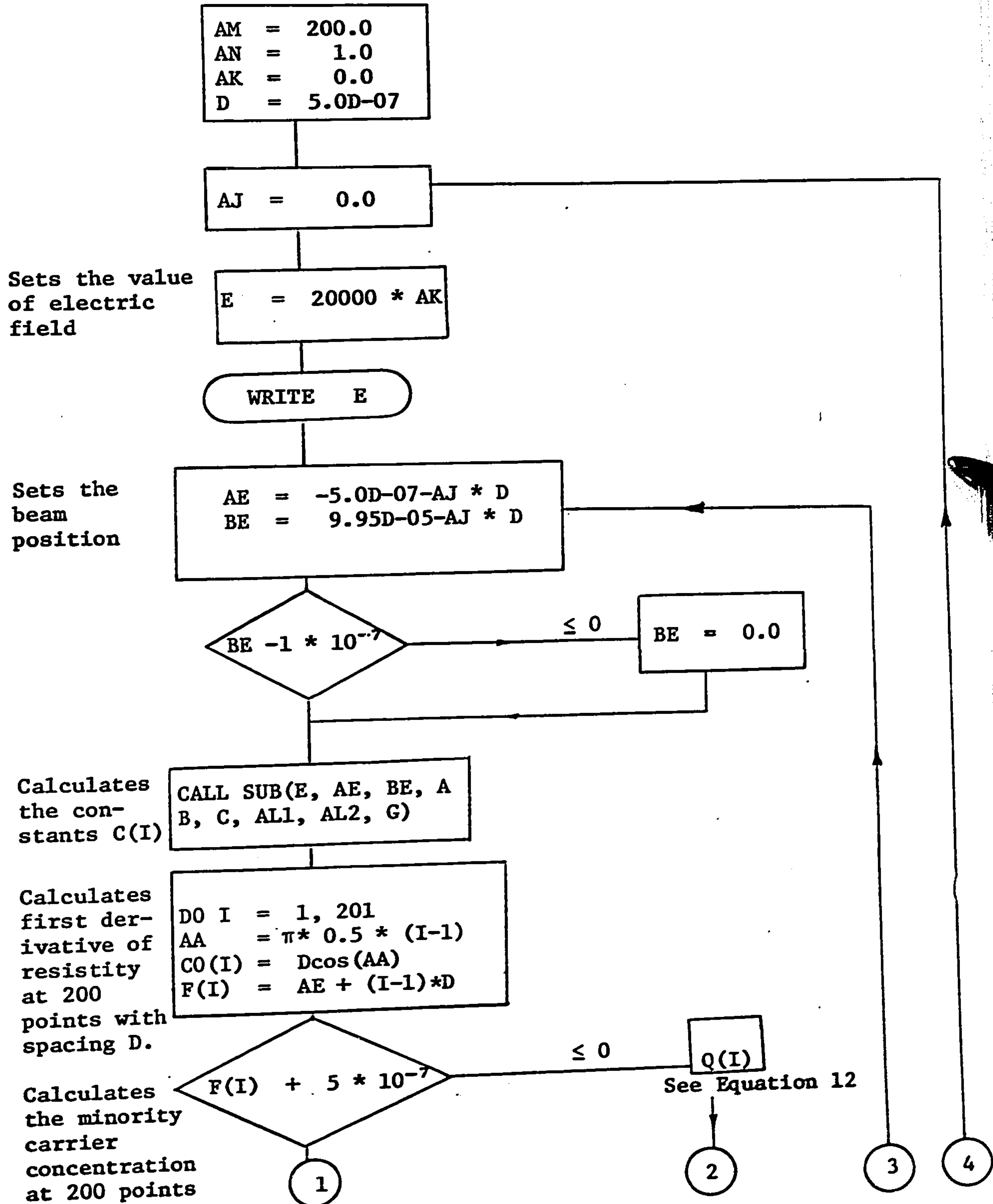

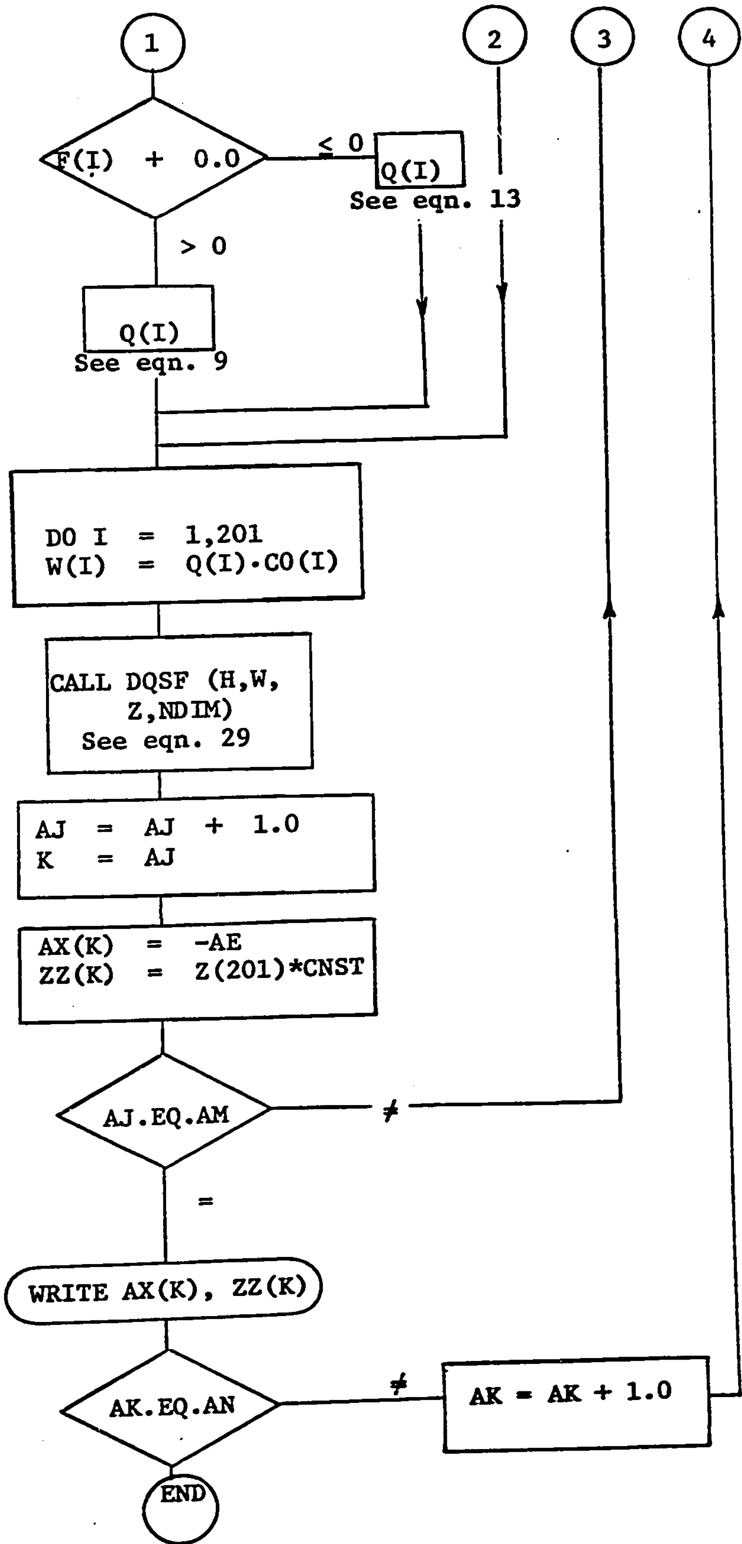

Calculate the photovoltage for one position of the electron beam. (Integration routine from the IBM 360 SSP).

Repeat the calculations for 200 beam positions.

Repeat all the calculations for three values of electric field.

The Subroutine SUB(E,AE,BE,A,B,C,AL1,AL2,G)

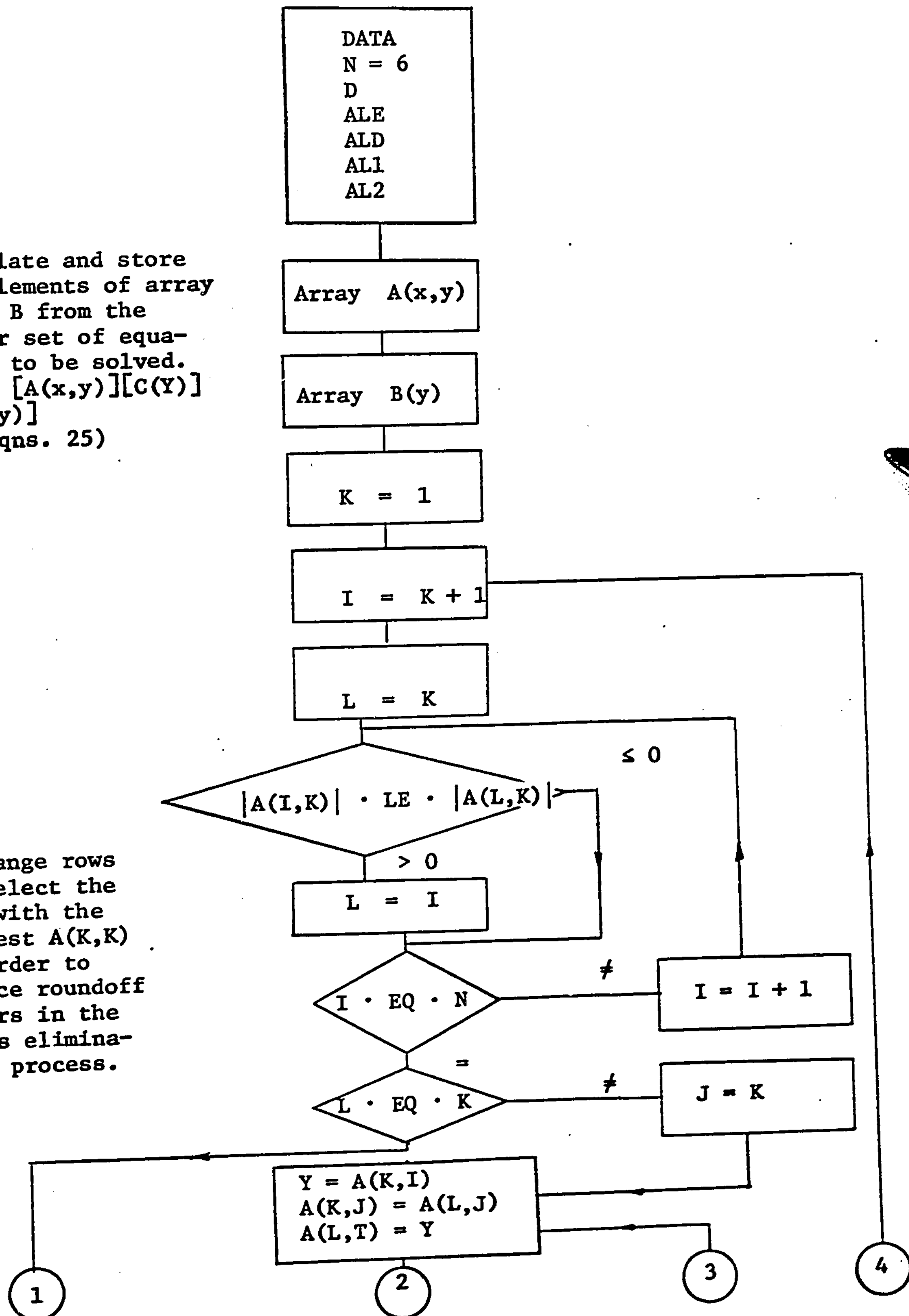

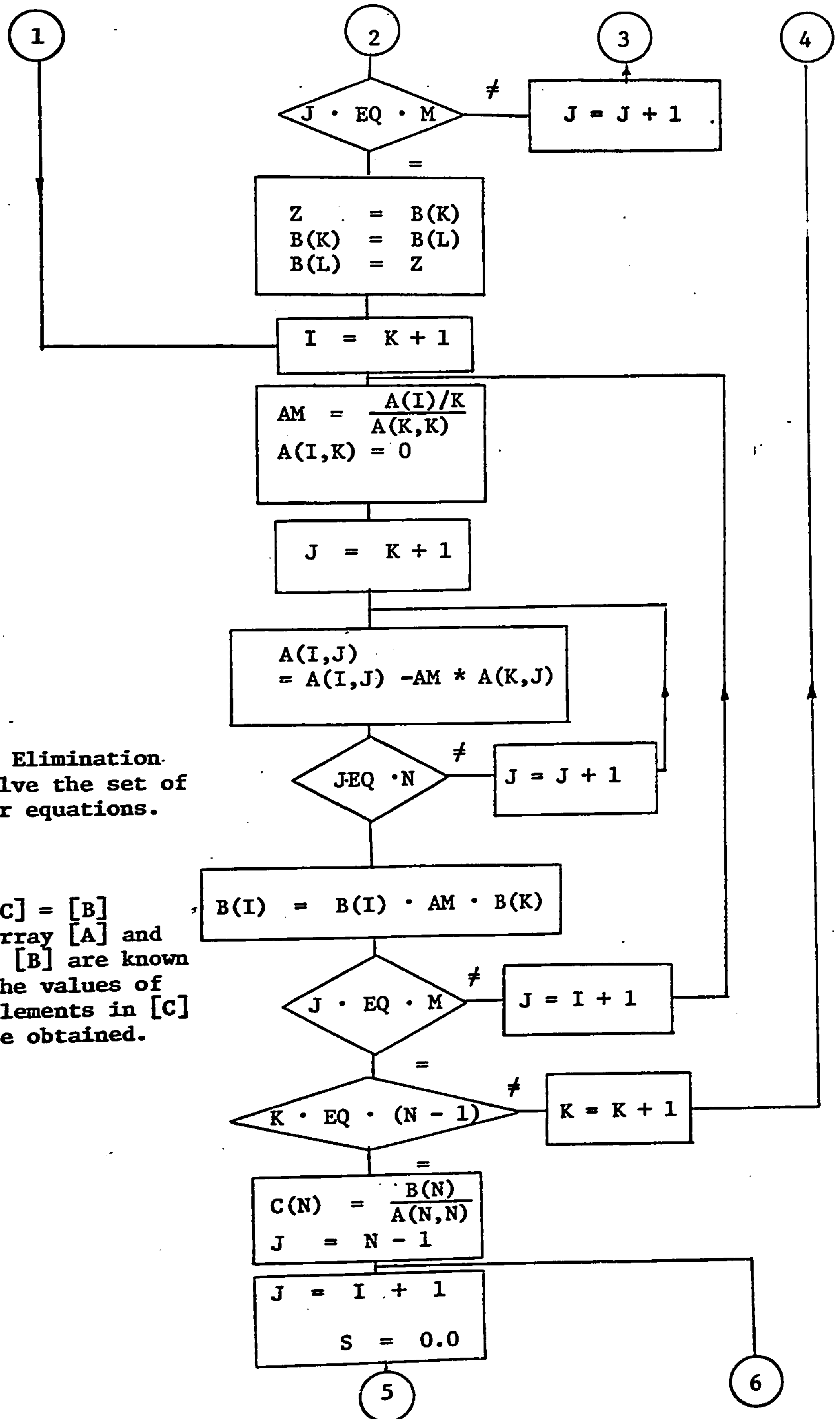

Gauss Elimination to solve the set of linear equations.

[A] [C] = [B]
The array [A] and array [B] are known and the values of the elements in [C] can be obtained.

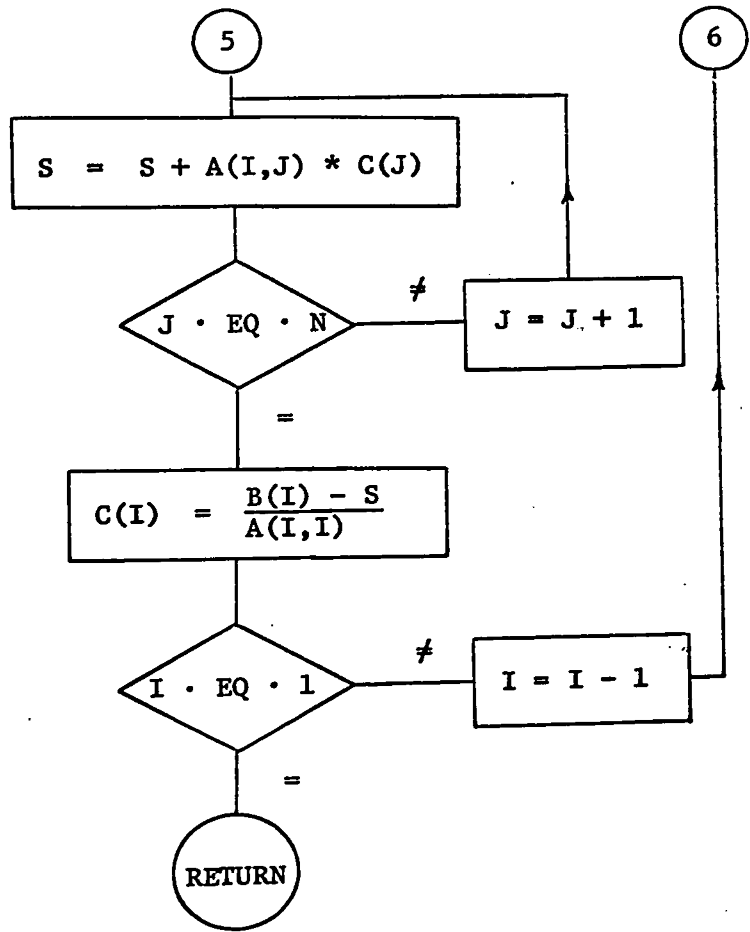
5
6
S = S + A(I,J) * C(J)
J · EQ · N
≠
J = J + 1
=
C(I) = B(I) - S / A(I,I)
I · EQ · 1
≠
I = I - 1
=
RETURN

REFERENCES

1. Kenneth R. Shoulders, "Microelectronics", Advances in Computers, Vol. 2, pp. 137-293, ed. Franz L. Alt, Acad. Press, N. Y., 1961.

2. G. Glinski et al., "The Multipurpose Integrated Electronic Processor", Proc. IEEE, Vol. 52, pp. 1475-1478, Dec. 1964.

3. W. R. Samaroo, "The Multipurpose Microelectronic Processor", Ph.D. Thesis, Dept. Of Elect. Engg., Univ. of Ottawa, 1965.

4. G. Glinski and W. R. Samaroo, "Methods of Bending a Pulsed Beam of Charged Particles", Tech. Report No. 63-15, Dept. of Elect. Engg., Univ. of Ottawa, 1963.

5. W. J. Jirafe, "A duoplasmatron Ion Sources for Ion Beam Deposition", Tech. Report No. 66-15, Dept. of Elect. Engg., Univ. of Ottawa, 1966.

6. C. C. Tsai, "An Analysis of a Duoplasmatron Ion Source for Ion Beam Deposition", M.Sc. Thesis, Dept. of Elect. Engg., Univ. of Ottawa, 1966.

7. P. V. Ramana, "Study of Semiconductor Detectors for Scanning Electron Microscope", M.Sc. Thesis, Dept. of Elect. Engg., Univ. of Ottawa, 1966.

8. R. E. Hayes, "A Feasibility Study of the Application of Ion and Electron Beams to Semiconductor Device Fabrication", M.Sc. Thesis, Univ. of Ottawa, 1970.

9. V. Caloia, "Power and Noise as Physical Size Limitations to Microelectronic Elements", M.Sc. Thesis, Dept. of Elect. Engg., Univ. of Ottawa, 1967.

10. T. E. Everhart et al., "Factors Affecting Contrast and Resolution in the Scanning Electron Microscope", J. Electron. and Control, Vol. 7, pp. 97-111, 1959.

11. P. A. Redhead et al., "The Physical Basis of Ultrahigh Vacuum", Chapman and Hall, London, 1968, pp. 160.

12. P. R. Thornton, "Scanning Electron Microscopy", Chapman and Hall, London, 1968, p. 205.

13. D. McMullan, "An Improved Scanning Electron Microscope for Opaque Specimens", Proc. IEE, Vol. 100B, p. 245, 1953.

14. N.F.B. Neve et al., "The Scanning Electron Microscope as a Means of Investigating "Second Breakdown" and Similar Phenomena", IEEE Trans. Electron Devices, Vol. ED-13, pp. 639-642, Aug. 1966.

15. D. A. Shaw et al., "Simultaneous Observation of Surface Detail and Cathodoluminescence in the Scanning Electron Microscope", J. Appl. Phys., Vol. 38, pp. 887-888, Feb. 1967.

16. D. B. Wittry and D. F. Kyser, "Cathodoluminescence at p-n Junctions in GaAs", J. Appl. Phys., Vol. 36, pp. 1387-1389, April 1965.

17. J. P. Flemming, "The Display of Information from Scanned Measuring Systems by Contour Mapping", J. Sci. Instrum., Vol. 2 (Ser. 2), pp. 93-95, 1969.

18. P. R. Thornton et al., "Scanning Electron Microscopy in Device Diagnostics and Reliability Physics", IEEE Trans. Electron Devices, Vol. ED-16, pp. 360-371, April 1969.

19. P. R. Thornton et al., "Quantitative Measurements by Scanning Electron Microscopy - I. The use of Conductivity Maps", Microelectron and Reliab., Vol. 5, pp. 291-298, Nov. 1966.

20. N. C. MacDonald and T. E. Everhart, "Direct Measurement of the Depletion Layer Width Variation vs. Applied Bias for a p-n Junction", Appl. Phys. Lett., Vol. 7, pp. 267-269, Nov. 1965.

21. K. C. A. Smith and C. W. Oatley, "The Scanning Electron Microscope and its Field of Application", Brit. J.A.P., Vol. 6, pp. 373-376, Nov. 1955.

22. I. M. Mackintosh, "Applications of the Scanning Electron Microscope to Solid State Devices", Proc. IEEE, Vol. 53, pp. 370-377, April 1965.

23. T. E. Everhart et al., "A Novel Method of Semiconductor Device Measurements", Proc. IEEE, Vol. 52, Dec. 1964.

24. T. E. Everhart et al., "Evaluation of Passivated Integrated Circuits Using the Scanning Electron Microscope", J. Electrochem. Soc., Vol. 111, pp. 929-936, August, 1964.

25. Y. Tarui et al., "Electron Beam Exposure System for Integrated Circuits", Microelectron. and Reliab., Vol. 8, pp. 101-111, May 1969.

26. A. B. El-Kareh, "An Electron-Beam Machine", RCA Rev., Vol. 24, pp. 5-46, March 1963.

27. P. R. Thornton et al., "Device Failure Analysis by Scanning Electron Microscopy", Microelectron. and Reliab., Vol. 8, pp. 33-53, Feb., 1969.

28. Richard H. Bube, "Photoconductivity of Solids", John Wiley & Sons, Inc., N. Y., 1960, p. 376.

29. Jan Tauc, "Photo and Thermoelectric Effects in Semiconductors", Pergamon Press, N. Y., 1962.

30. S. M. Ryvkin, "Photoelectric Effects in Semiconductors", Consultants Bureau, New York, 1964, pp. 269-276.

31. Chusuke Munakata, "On the Voltage Induced by an Electron Beam in a Bulk Semiconductor Crystal", Jap. J. Appl. Phys., Vol. 5, pp. 756-763, Sept. 1966.

32. C. Munakata, "Detection of Resistivity Variation in a Semiconductor Pellet with an Electron Beam", Microelectron, Reliab., Vol. 6, pp. 27-33, 1967.

33. C. Hilsum, "Semiconductors and Semimetals", Vol. 1, "Some Key Features of III-V Compounds", Acad. Press, N. Y., 1966, p. 16.

34. Donald Long, Semiconductors and Semimetals, Vol. 1, Acad. Press, N. Y., 1966, p. 148.

35. T. S. Moss, "Semiconductors and Semimetals", Vol. 2, Acad. Press, N. Y., 1967, p. 238.

36. Chusuke Munakata and Hiroshi Watanabe, "Measurement of Resistance by Means of Electron Beam - II -", Jap. J. Appl. Phys., Vol. 5, pp. 1157-1160, Dec. 1966.

37. P. R. Thornton, "Scanning Electron Microscopy", Chapman and Hall, London, 1968, p. 111.

38. W. R. Patterson, "Effect of Ohmic Contacts on the Dember Voltage", J. Appl. Phys., Vol. 38, pp. 4034-4035, Feb. 1967.

39. J. P. Flemming, "The Display of Information from Scanned Measuring Systems by Contour Mapping", J. Phys. E. Sci. Instrum., Vol. 2, pp. 93-95, 1969.

40. J. D. Ryder, "Electronic Fundamentals and Applications", Prentice-Hall, N. J., 1964, p. 300.

41. T. S. Hutchison and D. C. Baird, "The Physics of Engineering Solids", John Wiley & Sons, N. Y., 1963, p. 106.

42. D. A. Cusano, "Radiative Recombination From GaAs Directly Excited by Electron Beams", Solid State Communs., Vol. 2, pp. 353-358, 1964.

43. D. A. Shaw, P. R. Thornton, "Cathodoluminescent Studies of Laser Quality GaAs", J. Mat. Sci., Vol. 3, pp. 507-518, 1967.

44. N. Czaja, "Detection of Partial Dislocations in Silicon with the Scanning Electron Beam Technique", J. Appl. Phys., Vol. 37, pp. 918-919, Feb. 1966.

45. H. C. Casey, Jr., "Investigation of Inhomogeneities in GaAs by Electron-Beam Excitation", J. Electrochem. Soc., Vol. 114, pp. 153-158, Feb. 1967.

46. Toshiya Hayashi, Michiyuki Uenohara, "Tin-Gold Contacts for Planar Bulk GaAs Devices", J. Phys. Soc. Japan, Vol. 24, pp. 110-114, Jan. 1968.

47. James R. Black, "Electromigration - A Brief Survey and Some Recent Results", IEEE Trans. Electron Devices, Vol. ED-16, pp. 338-347, April 1969.

48. Thomas E. Hartman and James C. Blair, "Electromigration in Thin Gold Films", IEEE Trans. Electron Devices, Vol. ED-16, pp. 407-410, April 1969.

49. I. A. Blech and E. S. Meieran, "Electromigration in Thin Aℓ Films", J. Appl. Phys., Vol. 40, pp. 485-491, Feb. 1969.

50. A. V. MacRae, K. Müller, J. J. Lander and J. Morrison, "An Electron Diffraction Study of Cesium Adsorption on Tungsten", Surface Sci., Vol. 15, pp. 483-497, 1969.

V I T A

NAME:	Robert Philippe Beaulieu
BORN:	February 27, 1941
	Ottawa, Ontario
EDUCATED:	
Pre-University:	Ottawa Technical High School
	Ottawa, Ontario
	Eastern Ontario Institute of Technology
	Ottawa, Ontario
University:	University of Ottawa
	Ottawa, Ontario
COURSE:	Electrical Engineering
DEGREES:	B.A. Sc. (Ottawa)